NPS ARCHIVE
1967
KAAG, W.

A CASE STUDY OF THE SPACE AND TIME CONTINUITY OF NUMERICAL FRONTAL ANALYSIS

WILLIAM CARROLL KAAG

LIBRARY
NAVAL POSTGRADUATE SCHOOL

5

A CASE STUDY OF THE SPACE AND TIME CONTINUITY OF NUMERICAL FRONTAL ANALYSIS

by

William Carroll Kaag
Lieutenant Commander, United States Navy
M.A., Memphis State University, 1961

Submitted in partial fulfillment
for the degree of

MASTER OF SCIENCE IN METEOROLOGY

from the

NAVAL POSTGRADUATE SCHOOL
September 1967

NPS ARCHIVE
1967
KRAG, W.

ABSTRACT

The space and time continuity of numerical fronts as operationally produced by the Fleet Numerical Weather Facility, Monterey, California (FNWF), are investigated at 1000, 850, 700, 500, and 300 mbs for the four-day period January 25-28, 1967. Front locations, intensities, movements and slopes are examined over North America and compared with those from other analysis centers. Vertical structures of baroclinic zones and their changes with time are also investigated. Finally, a study is made of the FNWF computer-processed temperature fields compared to manually analyzed temperatures.

Results indicate reasonable vertical consistency of frontal information in the central and eastern United States below the 700-mb level. Time continuity is best maintained at the 700-mb surface. A fictitious displacement of numerical fronts toward the warm air is observed at each of the mandatory pressure levels considered. The temperature fields of FNWF are found to produce smoothing of thermal perturbations associated with open frontal waves while relaxing the thermal gradient which leads to widening and weakening of baroclinic zones.

LIBRARY
NAVAL POSTGRADUATE SCHOOL
MONTEREY, CALIF. 93940

TABLE OF CONTENTS

Section		Page
1.	Introduction	11
2.	Area, Data, and Charts	14
3.	Vertical Consistency	15
4.	Time Continuity	18
5.	Relative Comparison of Various Frontal Analyses	21
6.	Frontogenetical Properties	26
7.	Conclusions	26
8.	Recommendations	27
	Bibliography	29

LIST OF TABLES AND FIGURES

Table

		Page
1.	Average deviation (deg. lat.) of CAO fronts from FNWF fronts	31
2.	Average algebraic displacement to the warm/cold air (deg. lat.) of CAO fronts from FNWF fronts	31
3.	Average deviation (deg. lat.) of FNWF/CAO fronts from ESSA fronts	32
4.	Average algebraic displacement to the warm/cold air (deg. lat.) of FNWF/CAO fronts from ESSA fronts	32
5.	FNWF adjusted frontal positions versus CAO fronts. Deviations and algebraic displacements in degrees latitude	33
6.	FNWF adjusted frontal positions versus ESSA fronts. Deviations and algebraic displacements in degrees latitude	34

Figure

1.	Illustrative example of the relationship between θ, $\lvert\nabla\theta\rvert$ and GGθ. (a) Field of θ (^{o}A) and derived frontal parameters. Troughs in GGθ field are shown by dashed lines; ridges by dashed lines with superposed symbols. (b) $\lvert\nabla\theta\rvert$ in ^{o}C/(100 km) and derived frontal parameters. Ridges and troughs in $\lvert\nabla\theta\rvert$ field shown by dotted line. Other lines as in (a). (c) Field of GGθ in ^{o}C/(100 km)^{2}. Other lines as in (a). (d) Cross-sectional view of θ, $\lvert\nabla\theta\rvert$ and GGθ taken along line N in (a), (b) and (c). (Figure 3, (11)).	35
2.	ESSA surface chart 1200 GCT 25 January 1967	36
3.	ESSA surface chart 0000 GCT 26 January 1967	37
4.	ESSA surface chart 1200 GCT 26 January 1967	38
5.	ESSA surface chart 0000 GCT 27 January 1967	39
6.	ESSA surface chart 1200 GCT 27 January 1967	40
7.	ESSA surface chart 0000 GCT 28 January 1967	41
8.	Composite ESSA, FNWF, and IMGUB surface frontal analysis at 1200 GCT 25 January 1967	42

9. Composite of ESSA, FNWF and IMGUB surface frontal analysis at 1200 GCT 26 January 1967 43

10. Composite of ESSA, FNWF and IMGUB surface frontal analysis at 1200 GCT 27 January 1967 44

11. Plots of selected vertical cross-sections through hyper-baroclinic zones: Group A. Solid-line profile to right represents GGθ ridge; left profile, GGθ trough. Dashed curve represents ESSA frontal profile. Values at labeled pressure levels indicate θ (°A) and width of baroclinic zone (° lat.). Numbers between labeled levels are slope values (° lat/5000 feet). Each cross-section is identified by number (see Figures 16-21), date and time. Example: 1/12Z/25 on Figure 11 indicates cross-section 1 of 1200 GCT 25 January 1967 45

12. Plots of selected vertical cross sections through hyper-baroclinic zones: Group B. Legend same as Figure 11. 46

13. Plots of selected vertical cross-sections through hyper-baroclinic zones: Group C. Legend same as Figure 11. 47

14. Plots of selected vertical cross sections through hyper-baroclinic zones: Group D. Legend same as Figure 11. 48

15. Plots of selected vertical cross sections through hyper-baroclinic zones: Group E. Legend same as Figure 11. 49

16. Composite of FNWF GGθ ridges at selected levels at 1200 GCT 25 January 1967. Cross section slices indicated by numbered solid lines 50

17. Composite of FNWF GGθ ridges at selected levels at 0000 GCT 26 January 1967. Cross-section slices indicated by numbered solid lines. 51

18. Composite of FNWF GGθ ridges at selected levels at 1200 GCT 26 January 1967. Cross section slices indicated by numbered solid lines. 52

19. Composite of FNWF GGθ ridges at selected levels at 0000 GCT 27 January 1967. Cross section slices indicated by numbered solid lines. 53

20. Composite of FNWF GGθ ridges at selected levels at 1200 GCT 27 January 1967. Cross-section slices indicated by numbered solid lines. 54

21. Composite of FNWF GGθ ridges at selected levels at 0000 GCT 28 January 1967. Cross section slices indicated by numbered solid lines. 55

22. Composite of centers of positive GGθ at selected levels at 1200 GCT 25 January 1967. 56

23. Composite of centers of positive GGθ at selected levels at 0000 GCT 26 January 1967 57

24. Composite of centers of positive GGθ at selected levels at 1200 GCT 26 January 1967 58

25. Composite of centers of positive GGθ at selected levels at 0000 GCT 27 January 1967 59

26. Composite of centers of positive GGθ at selected levels at 1200 GCT 27 January 1967 60

27. Composite of centers of positive GGθ at selected levels at 0000 GCT 28 January 1967 61

28. Composite of FNWF 1000-mb frontal positions from 1200 GCT 25 January to 0000 GCT 27 January 1967 62

29. Composite of FNWF 1000-mb frontal positions from 0000 GCT 27 Janaury to 0000 GCT 28 January 1967 63

30. Composite of FNWF 850-mb frontal positions from 1200 GCT 25 January to 0000 GCT 27 January 1967 64

31. Composite of FNWF 850-mb frontal positions from 0000 GCT 27 January to 0000 GCT 28 January 1967 65

32. Composite of FNWF 700-mb frontal positions from 1200 GCT 25 January to 0000 GCT 27 January 1967 66

33. Composite of FNWF 700-mb frontal positions from 0000 GCT 27 January to 0000 GCT 28 January 1967 67

34. Composite of FNWF 500-mb frontal positions from 1200 GCT 25 January to 0000 GCT 27 January 1967 68

35. Composite of FNWF 500-mb frontal positions from 0000 GCT 27 January to 0000 GCT 28 January 1967 69

36. Composite of FNWF 300-mb frontal positions from 1200 GCT 25 January to 0000 GCT 27 January 1967 70

37. Composite of FNWF 300-mb frontal positions from 0000 GCT 27 January to 0000 GCT 28 January 1967 71

38. Composite of 1000-mb centers of positive GGθ from 1200 GCT 25 January to 0000 GCT 28 January 1967 72

39. Composite of 850-mb centers of positive GGθ from 1200 GCT 25 January to 0000 GCT 28 January 1967 73

40. Composite of 700-mb centers of positive GGθ from 1200 GCT 25 January to 0000 GCT 28 January 1967 74

41. Composite of 500-mb centers of positive GGθ from 1200 GCT 25 January to 0000 GCT 28 January 1967 75

42. Composite of 300-mb centers of positive GGθ from 1200 GCT 25 January to 0000 GCT 28 January 1967 76

43. Schematic temperature profiles as a function of "grid point" data. Simulated computations of $|\nabla\theta|$ and GGθ are shown at grid points. Solid arrow indicates true frontal position and dashed arrow indicates likely position from FNWF GGθ program. 77

44. Composite of FNWF potential virtual temperature and ESSA potential temperature fields at 850 mbs, 1200 GCT 26 January 1967 78

45. Composite of FNWF potential virtual temperature and ESSA potential temperature fields at 850 mbs, 0000 GCT 27 January 1967 79

46. Composite of FNWF potential virtual temperature and ESSA potential temperature fields at 850 mbs, 1200 GCT 27 January 1967 80

LIST OF SYMBOLS AND ABBREVIATIONS

A	Absolute temperature
C	Centigrade temperature
CAO	Central Analysis Office, Meteorological Branch, Department of Transport, Montreal, Canada
ESSA	Environmental Sciences Services Administration
FG	Frontogenesis = $-\nabla(\vec{V}_g \cdot \vec{n}_\theta) \cdot \nabla\theta$
FNWF	Navy Fleet Numerical Weather Facility, Monterey, California
GGθ	Frontal parameter = $-\nabla\lvert\nabla\theta\rvert \cdot \vec{n}_\theta$
IMGUB	Institute for Meteorology and Geophysics of the Free University of Berlin, Germany
K	Kelvin temperature
km	Kilometer
mb	Millibar
θ	Potential virtual temperature
$\vec{V}_g$	Geostrophic wind
$\vec{n}_\theta$	Unit vector in the direction of $\nabla\theta$ on a constant pressure surface
$\nabla\theta$	Horizontal gradient of potential virtual temperature on a constant pressure surface

ACKNOWLEDGEMENTS

The author wishes to express his sincere appreciation to Associate Professor Robert J. Renard, Department of Meteorology and Oceanography, Naval Postgraduate School for his advice, patience and assistance in the preparation of this paper. A special thanks is also extended to Mr. Leo Clarke and the staff of the Navy Fleet Numerical Weather Facility for the time and effort spent in obtaining the numerical data necessary for this thesis study.

A CASE STUDY OF THE SPACE AND TIME CONTINUITY OF NUMERICAL FRONTAL ANALYSIS

1. Introduction

The need for a numerical method of frontal analysis has been recognized for some time. In the search for a front-location parameter to which numerical techniques could be applied, Renard and Clarke (11) chose potential virtual temperature (θ). Specifically, the parameter is defined as the directional derivative of the gradient of potential virtual temperature along its gradient on a constant pressure surface, hereafter symbolized as GGθ. Thus,

$$GG\theta = -\frac{\nabla|\nabla\theta|\cdot\nabla\theta}{|\nabla\theta|} \equiv -\nabla|\nabla\theta|\cdot\vec{n}_\theta \tag{1}$$

where $\vec{n}_\theta$ is a unit vector in the direction of $\nabla\theta$.

Figure 1 shows the relationship of θ, $\nabla\theta$, and GGθ. Areas between lines of GGθ maxima (i.e. ridges) and minima (i.e. troughs) represent hyperbaroclinic zones.[1] The ridge line depicts the warm air boundary of the baroclinic zone and is thus the numerical analog of manually analyzed fronts.

The Navy Fleet Numerical Weather Facility, Monterey, California (FNWF), operationally computes a hemispheric field of GGθ on a twice-daily basis. The product is available to major weather centrals and facilities as an aid in frontal analysis. The Central Analysis Office, Meteorological Branch, Department of Transport, Montreal, Canada (CAO), is experimenting with a similar approach to objective frontal analysis; however, this thesis study is primarily concerned with the FNWF method.

[1]Such zones will be referred to as baroclinic zones in subsequent paragraphs.

Since θ is derived in a unique way, it is of interest at this point to summarize briefly the FNWF automatic processing technique. Surface observations and mandatory-level radiosonde data plus extrapolations from ship reports and selected aircraft observations comprise the raw data field. Using these data a static stability parameter is derived for five layers (1000-775 mbs; 775-600 mbs; 600-450 mbs; 450-300 mbs; and 300-200 mbs). The stability parameter is a constant for each of these layers at each radiosonde station, but is allowed to vary in the horizontal. Using the 1000-mb height, 1000-500-mb thickness and static stability as specified at intersections of a 63x63 linear grid, the θ's at mandatory levels may be computed. The θ's so determined (hereafter called processed θ) are the basis for calculation of GGθ in equation 1. Details of this processing technique may be found in (1).

It is the purpose of this thesis to investigate the space-time continuity of baroclinic zones as indicated by the field of GGθ and related analyses for a winter synoptic situation, 25-28 January 1967. The ultimate goal is to enhance the usefulness of the GGθ analyses and prognoses as received by the Naval Weather Service operational consumer.

The research comprises three phases of investigation and attempts to answer the specific questions posed below:

a. Vertical Consistency

(1) What is the geometric relationship of the tropospheric baroclinic zones at each of several mandatory levels?

(2) How does the orientation and slope of numerical fronts compare to their manually[2] drawn counterparts?

[2]"Manually drawn" is to be considered synonomous with "conventional" front.

(3) Is there vertical consistency in position and intensity of GGθ centers as found along the GGθ ridges?

b. Time Continuity

(1) What is the relationship of the baroclinic zone from one synoptic time to another at representative mandatory levels and how do baroclinic layers change with time?

(2) Do the position and intensity of GGθ centers exhibit time continuity?

(3) Is the movement of numerical fronts consistent with the horizontal wind field and movement of manually analyzed fronts?

(4) Is there a usable relationship between movement of pressure centers and GGθ centers?

(5) Is there diurnal variation of movement and intensity of GGθ centers?

c. Relative Comparison of Various Frontal Analyses

(1) How do FNWF frontal positions compare with CAO and the Environmental Sciences Services Administration (ESSA) locations?

(2) What are the existing and potential merits and deficiencies of the FNWF frontal analyses, the knowledge of which would aid the consumer in the operational use of GGθ charts?

As an adjunct to the primary objectives, a kinematic geostrophic expression for computing frontogenesis (10) is applied to the θ field. Employing the geostrophic wind, the working equation may be symbolized as:

$$FG = -\nabla\left(\vec{V}_g \cdot \frac{\nabla\theta}{|\nabla\theta|}\right) \cdot \nabla\theta \equiv -\nabla\left(\vec{V}_g \cdot \vec{n}_\theta\right) \cdot \nabla\theta \qquad (2)$$

Positive (negative) values indicate an instantaneous increase (decrease) in horizontal gradients of θ.

2. Area, Data, and Charts

The region studied for vertical consistency and time continuity was limited to the Northern Hemisphere south of 55° latitude and between 65° and 125° west longitude. For that portion of the investigation dealing with comparison of frontal positions the area was extended as indicated in Section 5.

Computer printouts of numerically contoured θ, $\nabla\theta$, GGθ and FG at standard tropospheric levels (1000, 850, 700, 500, and 300 mbs) for the synoptic times 1200 GCT 25 January to 0000 GCT 28 January 1967 were obtained from FNWF. Each printout is a 63 x 63 grid-point field on a polar stereographic projection with a scale of 1:30,000,000. The mesh length is 381 kms. GGθ ridges and troughs were drawn by hand. Any positive GGθ zone with less than six grid-point values equal to or greater than +0.05 C/(100 km)^2 or which did not contain one value of at least +0.15 C/(100 km)^2 was ignored as meteorologically insignificant. ESSA's Northern Hemisphere surface maps and upper air analyses for the United States and Canada were used for comparison to FNWF charts.

During the period of study an intense storm developed from a frontal perturbation located in the Texas Panhandle area 25-26 January 1967 and deepened as it moved northeastward through the central states (Figures 2-7). The situation was a classical example of a cold air injection (5) over Texas with subsequent deepening of the primary low. While hand analysis of frontal positions must of necessity be used as a basis of comparison, it was believed, apriori, that the situation east of the Rocky Mountains would show a minimum of disagreement among experienced meteorologists in locating fronts (see Figures 8-10). Frontal positions over the mountainous western United States are not nearly so

well defined and continuity of conventional frontal analyses was more difficult to maintain. For this reason the focus of attention is on the central and eastern region and it is this area which generated most of the discussion and conclusions that follow.

3. Vertical Consistency

Thirty vertical cross-sections of North American baroclinic-zone boundaries were plotted, twenty of which are shown in Figures 11-15. Vertical slices were selected in order to examine the baroclinic zone at approximately 5^{o} of latitude either side of the peak of the warm sector (as shown by the ESSA analyses). Once these positions were determined, additional sections were taken at approximately 10^{o} intervals. This interval was shortened in a few cases in order to aid in evaluation of continuity. When fronts of short horizontal distance were encountered, a position near the mid point was selected. Each vertical slice was taken in a direction perpendicular, or nearly so, to the 850-mb GGθ ridge. The selected positions are shown on Figures 16-21 by solid straight lines.

With reference to the cross-sections of baroclinic-zone boundaries (solid curves in Figures 11-15), the cold (warm) side boundary is to the left (right) in each case. The width of the baroclinic zone at each pressure level is indicated in degrees of latitude at a position between the two profiles at the particular level. Similarly, the θ values at each level considered are displayed in degrees absolute at the outer edges of the thermal zone. Values between levels represent frontal slopes coded as horizontal displacement of the frontal position (^{o} lat.) per 5000 feet change in height. Positive (negative) values represent slopes toward the cold (warm) air. Thus, 1.5 indicates a slope of approximately 1 mile/105 miles. The dashed curves are vertical plots of

ESSA fronts. The ESSA surface position is plotted at the 1000-mb level. ESSA analyzes fronts at 850 mbs but not at 700 mbs, therefore, temperature profiles along the intersection of the vertical section and the pressure surface were plotted. The point of maximum curvature of the profile was used as the 700-mb frontal position. Sections have been arranged in groups to facilitate inspection of changes in time, but for the present, consider each section individually at a particular time.

In general, the GGθ trough profiles parallel the GGθ ridges. The average width of the baroclinic zone (^{o} latitude) at each level, for all thirty sections, is given below:

1000 mbs	850 mbs	700 mbs	500 mbs	300 mbs
6.3	6.8	6.6	7.7	6.5

Potential virtual temperature is observed to increase with height. Average increases (in degrees absolute) through each layer are shown below:

1000-850 mbs	850-700 mbs	700-500 mbs	500-300 mbs
6.4	6.9	10.6	8.6

Kreitzberg (8) states that broad baroclinic zones average 600 miles in width with 8^{o}C temperature change, while the narrower, intense zones average 130 miles in width with a contrast of 5^{o}C horizontally across the zone. O'Connor (9) observed that in the cooler season the potential temperature of the polar front may increase from 298^{o}K near the surface to 302^{o}K at the 500-mbs level. The data presented above agrees reasonably well with the findings of Kreitzberg and O'Connor except that the widths of the majority of FNWF baroclinic zones appear to be biased toward the high values. The number of cases considered is insufficient to make any conclusions regarding changes in width with height, but the relatively narrow widths at 300 mbs were surprising. Inspection of the

tropopause heights during this period, however, indicates intersections with levels in the 500-300-mb layer and this makes interpretation of 300-mb frontal information more complex.

Geometrically below 700 mbs the baroclinic zone generally slopes toward the cold air or is nearly vertical, while above 700 mbs both negative and positive slopes are numerous. Although negative slopes have been found at low levels, such occurrences in the free atmosphere are to be doubted (4). FNWF frontal slopes in 39 separate layers were compared with ESSA frontal slopes. Of these, 6 were identical; 18 were within $\pm 1.0^{o}$lat./5000 feet; and 21 differed by more than $\pm 1.0^{o}$lat./5000 feet.

Figures 16-21 are composites of GGθ ridges at the standard levels for 1200 GCT 25 January to 0000 GCT 28 January 1967. Notice that over the continental United States eastward of central Texas the vertical consistency of numerical fronts is quite reasonable. Over the western United States, Mexico and Central America the slopes suggested are totally unrealistic. The frontal contours in the Gulf of Mexico region at 1200 GCT 27 January and 0000 GCT 28 January demonstrate the numerical problems encountered as frontal systems move into an area of sparse data and/or when the thermal gradient weakens, while the western United States indicates well the fictitious frontal information introduced by extrapolation of data down to sea level.

Centers of positive GGθ (i.e. GGθ maxima) at each level were plotted for each synoptic time. These plots are shown in Figures 22-27. In some instances GGθ centers at 1000 mbs can be identified with maxima at higher levels, however, for the most part, there seems to be a poor relation. All centers observed at each level over the six synoptic

times are combined in Figures 38-42 in order to study movement. A comment regarding the relative number of GGθ centers at each level is pertinent here. Total numbers observed at each level were 74, 48, 50, 40, and 61 at 1000, 850, 700, 500 and 300 mbs, respectively. The sharp decrease between 1000 and 850 mbs is probably due to the effects of surface-induced heating and cooling and extrapolation problems in 1000-mb data. The increase at 300 mbs is more difficult to explain, but may be due to the fact that the tropopause complicates matters or that intensities of many relative maxima at this level are weak so that small θ errors would produce numerous centers. Should these hypotheses be correct, many individual maxima at 1000 mbs and 300 mbs have little synoptic scale meaning and correlations with adjacent levels are not to be expected.

Intensity values of GGθ maxima decreased with height in general. Greatest observed values were 74, 61, 46, 49, and 52 $(^{o}C/(100\ km)^2$ at 1000, 850, 700, 500 and 300 mbs, respectively.

4. Time Continuity

The vertical cross-sections of Figures 11-15 have been arranged in five groups (A-E). Each plot in a group is a cross-section through a similar area of a frontal system at a different synoptic time. Thus, for example, by inspecting Group C an examination of time changes in a baroclinic zone at a position nearly fixed relative to an identifiable frontal feature can be made over a period of six synoptic times.

Consider changes occurring in time through the layer 1000-700 mbs during the period 1200 GCT 25 January to 0000 GCT 28 January 1967:

Group A - Sections in Group A were taken through a warm frontal region which became less intense with increasing time and moved from the eastern continental area to the western Atlantic Ocean after 1200 GCT

25 January. The width of the baroclinic zone appears to increase from 1200 GCT 25 January to 1200 GCT 26 January. During the period covered by Group A cross-sections, the nearest GGθ maximum decreased from 65 to 55 $(^{o}C/(100\ km)^2$ at 1000 mbs, increased from 30 to 47 at 850 mbs and showed no consistent pattern at 700 mbs. The numerical frontal slope in the layer 1000-700 mbs became steeper as did ESSA's frontal surface.

Group B - This group is from a region analyzed by ESSA as a cold front until 1200 GCT 26 January and as a stationary front at 0000 GCT 27 January. The baroclinic zone increased in intensity after 0000 GCT 26 January. ESSA's frontal slopes remained nearly constant during the period while FNWF's became steeper until 0000 GCT 27 January. The nearest GGθ centers are the same as for Group A and were discussed above.

Group C - Group C is a sequence of six different synoptic times. ESSA analyzed the frontal region as a cold front until 1200 GCT 26 January and as a warm front for the latter three synoptic times. No consistent pattern of change in width of the FNWF baroclinic zone or in the slope of ESSA or FNWF is noted. Adjacent GGθ centers fluctuated at 1000 mbs, increased steadily at 850 mbs until 0000 GCT 27 January, decreased at 1200 GCT 27 January and then increased. The intensity fluctuated irregularly at 700 mbs.

Group D - Sections in Group D were taken in an area of intense cold air advection. Winds in the cold air were on the order of 40 to 50 knots at 850 mbs and 50 to 70 knots at 700 mbs. The cold air injection was in progress at the time of the first section in the sequence. The thermal zone is narrow throughout the period. Slopes are observed to be steep.

Group E - The frontal area of these sections was similar to Group D, but displaced to the west of the intense cold air injection. The geo-

graphy of the area includes the mountains along the Texas-Mexico border and the western coast of the Gulf of Mexico. Irregularities in ESSA and FNWF frontal contours are to be noted.

Above 700 mbs large space and time variations in the slopes of all baroclinic zones occur, possibly due to upper tropospheric fronts or jet streams.

Again with reference to Figures 11-15, maximum variation of frontal θ values at specified levels, during the time intervals represented by each group, are shown in the following table (^{o}C). It is to be noted that the least change occurred at 850 mbs and through a warm front sector (Group A). The former again highlights the utility of a free atmospheric level compared to the surface (or 1000 mbs) for frontal analysis.

Level	Group A	Group B	Group C	Group D	Group E
1000 mbs	3	4	6	6	3
850 mbs	2	2	10	3	2
700 mbs	2	4	4	5	7
500 mbs	5	9	4	4	4
300 mbs	8	6	3	4	7

Composites of the numerical frontal positions in time at the mandatory levels 1000-300 mbs are included in Figures 28-37. Time continuity is maintained best at 700 mbs. Frontal patterns can be identified from one synoptic time to the next and movements are reasonable. The picture at 850 mbs is much improved over that at 1000 mbs, but some unrealistic behavior is noted, as over the Gulf of Mexico from 0000 GCT to 1200 GCT 27 January. Such movement may be due to lack of data, erroneous reports, or the sudden appearance of correct reports where such were previously absent. In any event, this example demonstrates the possibility of

unrealistic movement in sparse data areas. Deviations of numerical positions from hand drawn locations are given in Section 5, but since deviations did not increase with time, it is concluded that the average speed of FNWF fronts is consistent with that observed for conventional fronts. This is not necessarily true for individual 12-hour intervals as compared to ESSA positions. Movement evaluation based on the mean wind perpendicular to the front was attempted but the results were inconclusive. Time continuity diminishes at 500 mbs relative to the lower levels and is poor at 300 mbs.

The plots of GGθ maxima at each level considered (Figures 38-42) show that continuity is about equal at 850 and 700 mbs. In cases where GGθ center positions exhibited continuity from one synoptic time to the next, but the hand analysis did not depict a front in the area, cyclone tracks were plotted. In most cases a similarity in movement of GGθ and cyclone centers was observed but the speeds varied. Deepening of cyclones appeared to be accompanied by increases in intensity of GGθ centers but the number of cases observed was insufficient to make any conclusions.

5. Relative Comparison of Various Frontal Analyses

A comparison was made of FNWF frontal positions with those located numerically by CAO and manually by ESSA for the period 0000 GCT 26 January to 1200 GCT 27 January. The CAO method (3) uses the GGθ parameter as well as others and processing procedures differ from FNWF.

The FNWF 1000-mb GGθ analysis was not used in this portion of the study, but rather a frontal analysis derived from the mean temperature in the layer 1000-700 mbs (10/7 model). Since a number of fronts is produced by both the FNWF and CAO methods which have no counterparts in ESSA analyses or orientations were such that no meaningful comparisons

could be made in some cases, the following critera were established as basis for consideration:

(a) Length of numerical front must be at least 10^{o} of latitude.

(b) At least one point on the CAO front must be within 5^{o} of latitude of FNWF position. When comparing with ESSA analyses one point on either CAO or FNWF fronts within 5^{o} of latitude of ESSA position was sufficient for both to be compared.

(c) No comparison was made if the average orientation of a front was such as to make an angle of more than 45^{o} with its counterpart.

Deviations were measured at intervals of one grid length along and normal to the FNWF front for FNWF versus CAO, while ESSA's frontal position was similarly used as the base for the FNWF/CAO versus ESSA comparison. Deviations were measured to the nearest ½ degree of latitude. Average deviations and average algebraic displacements toward cold or warm air in degrees of latitude are given in Tables 1-4.

Deviations shown in Table 1 and 2 reflect a comparison at 850, 700, and 500 mbs only since the 1000 and 300-mb positions were not available from CAO. The area considered encompassed the west longitudes of the Northern Hemisphere. In Tables 3 and 4, FNWF's 10/7 model analyses were compared with ESSA's surface positions; here the area was the entire Northern Hemisphere. FNWF/CAO comparisons with ESSA were made only at 850 mbs and the area was the continental regions of southern Canada, the United States, northern Mexico and the adjacent coastal waters. The cumulative average deviations and algebraic displacements are based on the average at each synoptic time weighted in proportion to the number of points measured.

Table 1 indicates that FNWF-CAO deviations increase with height and

Table 2 shows that the average CAO position is displaced to the cold air side of its FNWF counterpart, the displacement increasing with height. Table 3 indicates that on the average, CAO positions are closer to the ESSA analyzed locations than are the FNWF fronts at 850 mbs. The 1000-mb and 850-mb deviations of FNWF from ESSA are equivalent, but Table 4 shows that at 850 mbs FNWF fronts have an average algebraic displacement relative to ESSA fronts of about 2.3° latitude toward the warm air. The average algebraic displacement of the FNWF 1000-mb positions and the CAO 850-mb fronts approximates the ESSA positions.

Because of the results in Tables 1-4 and since GGθ is utilized exclusively by FNWF and inclusively by CAO for frontal analysis, an examination of the FNWF processing method was undertaken to see if this feature accounts for the difference noted.

As stated earlier, the FNWF processing procedure involves the calculation of a stability parameter for specific layers which is constant through the layer. This is equivalent to obtaining an average lapse rate through the layer. Such a procedure produces deviations from the actual temperature at specified levels. The magnitude of the deviation depends on the variability in the sounding and the location of extremes (i.e. inversions) relative to the level where temperatures are desired. Such a conclusion is supported by statistics gathered by Schardt (12) who compared FNWF processed (virtual) temperatures to the observed dry-bulb temperatures at 1000, 850, 700, 500 and 300 mbs. His data showed that deviations in the range +1.0 to 2.9 and -1.0 to -2.9°C occurred at 39% of the grid points at 1000 mbs, 53% at 850 mbs, 42% at 700 mbs, 25% at 500 mbs and 46% at 300 mbs. Further, the data showed that 16%, 8%, 2.5%, 8% and 16% of the grid points at 1000, 850, 700, 500, and 300 mbs,

respectively, had processed (virtual) temperatures colder than observed dry-bulb temperatures and hence are unquestionably in error. Such errors and others not isolated in this analysis could easily produce spurious baroclinic zones or cause artificial displacements of numerical fronts. The likelihood seems more probable in regions of weak thermal gradients.

The arguments stated above do not explain the displacement of FNWF fronts toward the warm air side of hand drawn fronts using actual data on constant pressure surfaces. Figure 43 represents a simulation of the computer calculations of GGθ assuming a correct temperature field. It also assumes a situation in which $\nabla\theta$ is parallel to $\nabla|\nabla\theta|$ so that the cosine of the angle between $\nabla\theta$ and $\nabla|\nabla\theta|$ is one, when taking the dot product in the GGθ formula (equation 1). Three temperature profiles are shown, as based on "grid point" data. The solid arrow indicates the actual point of maximum curvature (GGθ maximum) and the dashed arrow shows the probable point at which the FNWF numerical method would indicate a GGθ maximum. The upper profile represents the most intense front with decreasing intensities in the lower two. Note that the numerical computations displace the GGθ maximum toward the warm air in all cases. Notice also that the numerical position would not be altered even though the dashed curve in the upper profile existed. Thus, an error in positioning the front ranges from approximately ¼ to 1 grid length (i.e. 1-3° latitude). The same feature is observed relative to the GGθ troughs except the displacement is toward the cold air. The combined result could artificially broaden the baroclinic zone by as much as six degrees of latitude.

In the two lower profiles where the change of temperature was less intense, the numerically indicated position approaches more closely the

actual position. The difference would be greater, however, if the point of maximum curvature occurred farther from the grid point.

A further attempt to examine observed versus processed temperature fields was made by converting the ESSA analyzed dry-bulb temperature field to potential temperature and superimposing the FNWF processed field. Figures 44-46 show three such examples. To be sure, moisture effects have not been taken out of the FNWF field, but it is readily apparent that perturbations of a synoptic scale (open frontal waves) are smoothed, the gradient is relaxed and regions of maximum change of gradient are displaced toward the warm air in the FNWF field.

Because of the apparent displacement of FNWF fronts toward the warm air, a search was made for a correction which could be applied to the numerical frontal analyses at the mandatory levels. An arbitrary correction toward the cold air of one-half the distance from the GGθ ridge to the $0.0^{o}C/(100\ km)^2$ GGθ isoline was made and another comparison with CAO and ESSA was undertaken. Tables 5 and 6 show the results. Notice that the deviations of FNWF from CAO positions were reduced at every level; also the FNWF position relative to ESSA locations improved. Applying the adjustment to the FNWF 10/7 model positions resulted in greater deviations than were observed without the correction and consequently are not shown here.

The 0.0 $C/(100\ kms)^2$ isoline is not computer plotted on FNWF GGθ charts, but the +0.05 $C/(100\ kms)^2$ isoline is plotted; thus a displacement of the GGθ ridge one-half the distance to the latter isoline will accomplish nearly the same result. However, such a correction should not be made to the frontal product generated by the 10/7 model.

6. Frontogenetical Properties

The applicability of equation (2) as an indicator of frontogenesis (FG) was investigated at the 850-mb and 700-mb levels in an area roughly comprising the continental United States. The average values of FG at each grid point for two consecutive map times were plotted against changes in $|\nabla\theta|$ for the same period on a scattergram. The correlation was insignificant. This supported the findings of Schardt (12); however, he suggested that a correlation might exist between negative values of FG (i.e. frontolysis) and decreases in $|\nabla\theta|$. Separate scattergrams were plotted using only negative FG values but, again, the result was inconclusive.

7. Conclusions

In mountainous and sparse data regions and above the 700-mb level in the North American area, the time-space continuity of numerical fronts was found to be poor. The conclusions stated below refer to the lower troposphere east of the Rocky Mountains:

(a) Numerical baroclinic zones slope toward the cold air or are nearly vertical with a few exceptions. Frontal θ values increase with height.

(b) Slopes of numerical fronts compare favorably with those of the ESSA analyses in some cases, but differ considerably in others. The largest deviations are in areas of weak gradient or sparse data.

(c) GGθ centers have little vertical consistency. Associations are best between 850 and 700 mbs. Centers associated with intense baroclinic zones display continuity in time. The more intense the center, the more likely it is to persist. Speed of movement was observed to be irregular; the 850 and 700-mb levels displayed the best continuity in this respect.

(d) Average movement of numerical fronts over a sequence of several map times is comparable to ESSA frontal movements, but large deviations were observed over a given 12-hour interval.

(e) Of the levels considered, continuity of frontal movement is maintained best at the 700-mb level over continental North America.

(f) FNWF frontal positions, except when the 10/7 model is used, are displaced toward the warm air side of the "true" hyperbaroclinic zone. This appears due to grid size and method of computing derivatives.

(g) The data processing method employed by FNWF tends to smooth open waves in the thermal field and contributes to the present inability of the numerical frontal scheme to display properly the occlusion process. The CAO analyses display open waves in a manner more closely resembling the conventional product.

(h) Frontal analysis at mandatory levels may be improved in accuracy by displacing the GGO ridge toward the cold air one-half the distance from the indicated position to the $+0.05^{\circ}C/(100\ km)^2$ isoline.

8. Recommendations

The problems involved with lack of data can be solved only with increased observations and are not germaine to this discussion. There are certain aspects of the numerical analysis problem, however, which may be susceptible to improvement under present data conditions. The following items are listed as suggested areas of further research:

(a) Reduce the mesh length, thereby reducing the artificial broadening of the hyperbaroclinic zones and the displacement of the numerical front toward the warm air.

(b) Investigate the feasibility of using observed dry-bulb temperature as the basic temperature field. This may aid in retaining thermal perturbations well into the occluded stage.

(c) Where frontal bands can be identified from satellite data, this information should be made available to the computer by injecting "dummy" data in the form of θ, $|\nabla\theta|$ or GGθ.

BIBLIOGRAPHY

1. Carstensen, L. P. and G. E. Lawniczak, Jr. Surface and tropospheric analysis. Technical Note No. 15, Fleet Numerical Weather Facility, Monterey, California, January 1966: 15 pp.

2. Clarke, L. C. and R. J. Renard. Objective frontal analysis. Technical Note No. 24, Fleet Numerical Weather Facility, Monterey, California, August 1966: 40 pp.

3. Creswick, W. S. Experiments in objective frontal contour analysis. Unpublished manuscript, Meteorological Branch, Department of Transport, Central Analysis Office, Montreal, Canada, 1966.

4. Duthie, W. D. Notes on the analysis of weather charts. Third edition, unpublished manuscript, Department of Meteorology and Oceanography, Naval Postgraduate School, Monterey, California, 1965.

5. George, J. J. Weather Forecasting for Aeronautics. Academic Press, New York and London, 1960.

6. Hamrick, J. M. A frontal comparison between a hand-analyzed product and a numerical product. Unpublished manuscript, Department of Meteorology and Oceanography, Naval Postgraduate School, Monterey, California, 1965: 34 pp.

7. Hamrick, J. M. Static stability as an aid in numerical baroclinic zone analysis. Masters Degree Thesis, Department of Meteorology and Oceanography, Naval Postgraduate School, Monterey, California,

8. Kreitzberg, C. W. The structure of occlusions as determined from serial ascents and vertically-directed radar. Meteorology Laboratory Project 8641, Air Force Cambridge Research Laboratories, Office of Aerospace Research, United States Air Force, January 1964: 121 pp.

9. O'Connor, J. F. Practical methods of weather analysis and prognoses. OPNAV 50-1P-502, Office of the Chief of Naval Operations, U. S. Navy, November 1952: 192 pp.

10. Petterssen, S. Weather Analysis and Forecasting, 2nd ed., v. 1, McGraw-Hill, 1956: 201-202.

11. Renard, R. J. and L. C. Clarke. Experiments in numerical objective frontal analysis. Monthly Weather Review, v. 93, 1965: 547-556.

12. Schardt, D. L. A case study of data processing and wind parameters in relation to the U. S. Navy's numerical frontal analysis scheme. Masters Degree Thesis, Department of Meteorology and Oceanography, Naval Postgraduate School, Monterey, California, May 1966: 92 pp.

13. Schiffner, R. C. Analysis of baroclinicity utilizing significant-level radiosonde data. Masters Degree Thesis, Department of Meteorology and Oceanography, Naval Postgraduate School, Monterey, California, Oct 1966: 34 pp.

TABLE 1

AVG DEVIATION OF CAO FROM FNWF

Time/date	850 mbs/No. pts.		700 mbs/No. pts.		500 mbs/No. pts.	
00Z26JAN	2.3	73	2.8	71	3.2	55
12Z26JAN	2.5	78	2.5	60	2.9	49
00Z27JAN	2.7	67	2.8	65	3.1	50
12Z27JAN	2.5	79	2.4	58	3.8	54
Avg/totals	2.5	291	2.5	254	3.3	208

TABLE 2

AVG ALGEBRAIC DISPLACEMENT OF CAO FROM FNWF TOWARD WARM/COLD AIR

Time/date	850 mbs/No. pts. in warm air		700 mbs/No. pts. in warm air		500 mbs/No. pts. in warm air	
00Z26Jan	1.8 cold	16	2.6 cold	4	3.2 cold	1
12Z26JAN	1.8 cold	12	2.0 cold	7	2.9 cold	0
00Z27JAN	1.3 cold	8	2.7 cold	2	2.9 cold	3
12Z27JAN	2.3 cold	7	1.9 cold	4	3.6 cold	3
Avg/totals	1.9 cold	43	2.3 cold	17	3.2 cold	7

TABLE 3

AVG DEVIATION OF FNWF/CAO FROM ESSA

	FNWF				CAO	
Time/date	1000 mbs/No. pts.		850 mbs/No. pts.		850 mbs/No. pts.	
00Z26JAN	1.8	51	2.3	23	2.4	27
12Z26JAN	3.2	62	4.1	21	3.2	21
00Z27JAN	3.1	70	1.8	20	1.5	20
12Z27JAN	2.4	95	2.6	25	1.1	27
Avg/totals	2.6	278	2.6	89	2.0	95

TABLE 4

AVG ALGEBRAIC DISPLACEMENT OF FNWF/CAO FROM ESSA TOWARD WARM/COLD AIR

	FNWF				CAO	
Time/date	1000 mbs/No. pts. in warm air		850 mbs/No. pts. in warm air		850 mbs/No. pts.in warm air	
00Z26JAN	0.1 warm	25	1.4 warm	18	0.9 cold	8
12Z26JAN	0.7 warm	26	4.1 warm	21	2.3 warm	16
00Z27JAN	2.4 cold	17	1.3 warm	14	0.2 cold	8
12Z27JAN	0.2 warm	49	2.6 warm	24	0.0	16
Avg/totals	0.4 cold	117	2.3 warm	77	0.2 warm	48

TABLE 5

FNWF (ADJUSTED) VS CAO

Time/date	Average Deviation	Average CAO Displacement (warm/cold)	No. CAO pts. in warm air	Total Points
		850 mbs		
00Z26JAN	1.9	0.5 cold	34	81
12Z26JAN	1.8	0.2 cold	25	75
00Z27JAN	1.3	0.8 cold	17	62
12Z27JAN	1.3	0.4 cold	21	76
Avg/totals	1.6	0.5 cold	97	294
		700 mbs		
00Z26JAN	1.7	1.2 cold	14	71
12Z26JAN	1.2	0.3 cold	15	55
00Z27JAN	1.5	0.4 cold	11	56
12Z27JAN	1.3	1.0 cold	12	64
Avg/totals	1.4	0.8 cold	52	246
		500 mbs		
00Z26JAN	1.4	0.8 cold	12	55
12Z26JAN	1.5	1.3 cold	4	49
00Z27JAN	1.6	1.1 cold	5	41
00Z27JAN	2.2	1.7 cold	7	55
Avg/totals	1.7	1.2 cold	28	200

TABLE 6

FNWF (ADJUSTED) VS ESSA

850 mbs

Time/date	Average Deviation	Average FNWF Displacement (warm/cold)	No. FNWF Pts. in warm air	Total Points
00Z26JAN	1.3	0.9 warm	13	23
12Z26JAN	3.2	2.9 warm	13	21
00Z27JAN	2.4	1.4 cold	8	27
12Z27JAN	2.4	2.4 warm	24	29
Avg/totals	2.3	1.1 warm	58	100

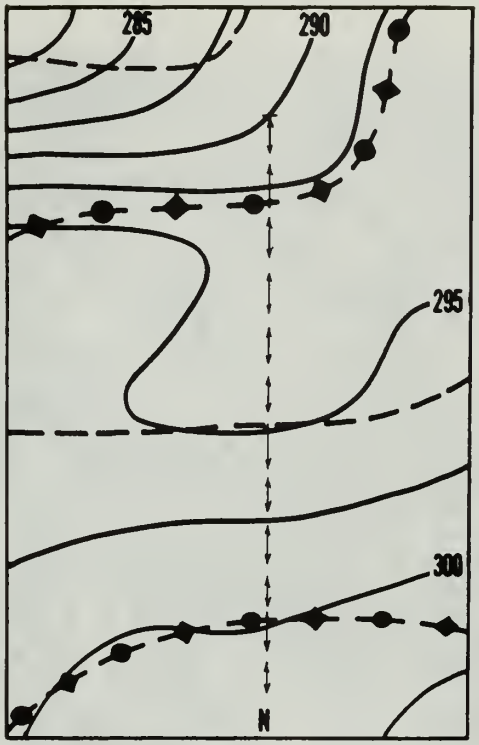
285
290
295
300
N

a

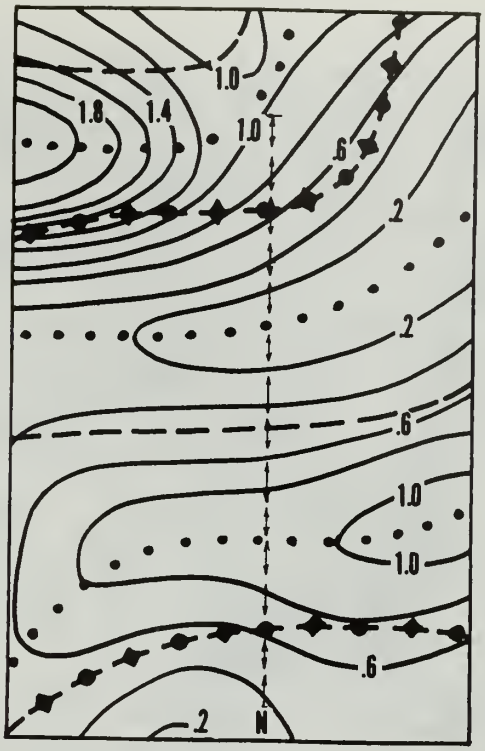
1.0
1.8
1.4
1.0
.6
.2
.2
.6
1.0
1.0
.6
.2
N

b

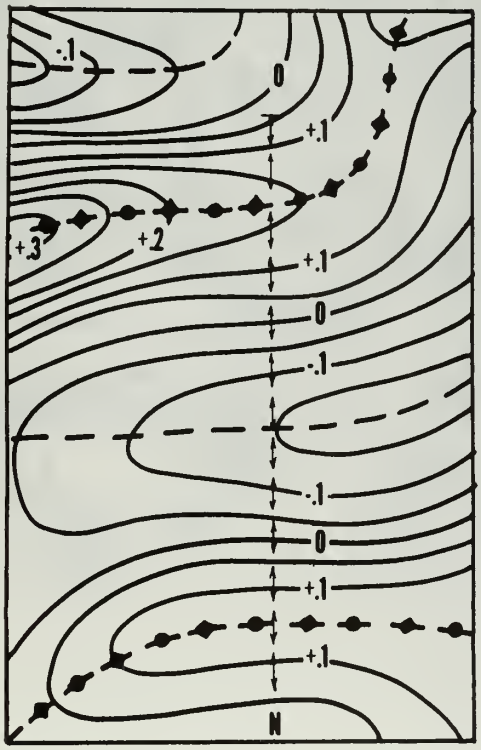
-.1
0
+.1
+.3
+.2
+.1
0
-.1
-.1
0
+.1
+.1
N

c

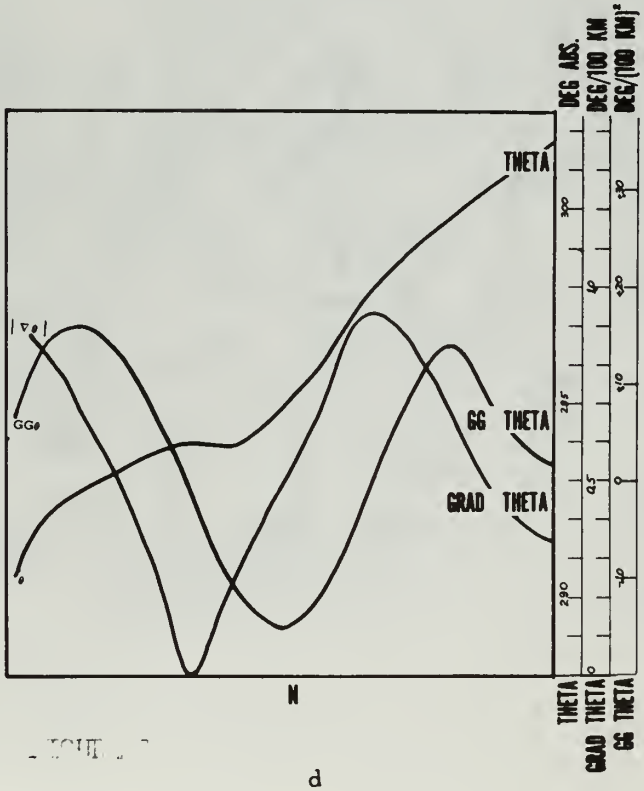
THETA
GG THETA
GRAD THETA
N
DEG ABS.
DEG/100 KM
DEG/(100 KM)²
THETA
GRAD THETA
GG THETA

d

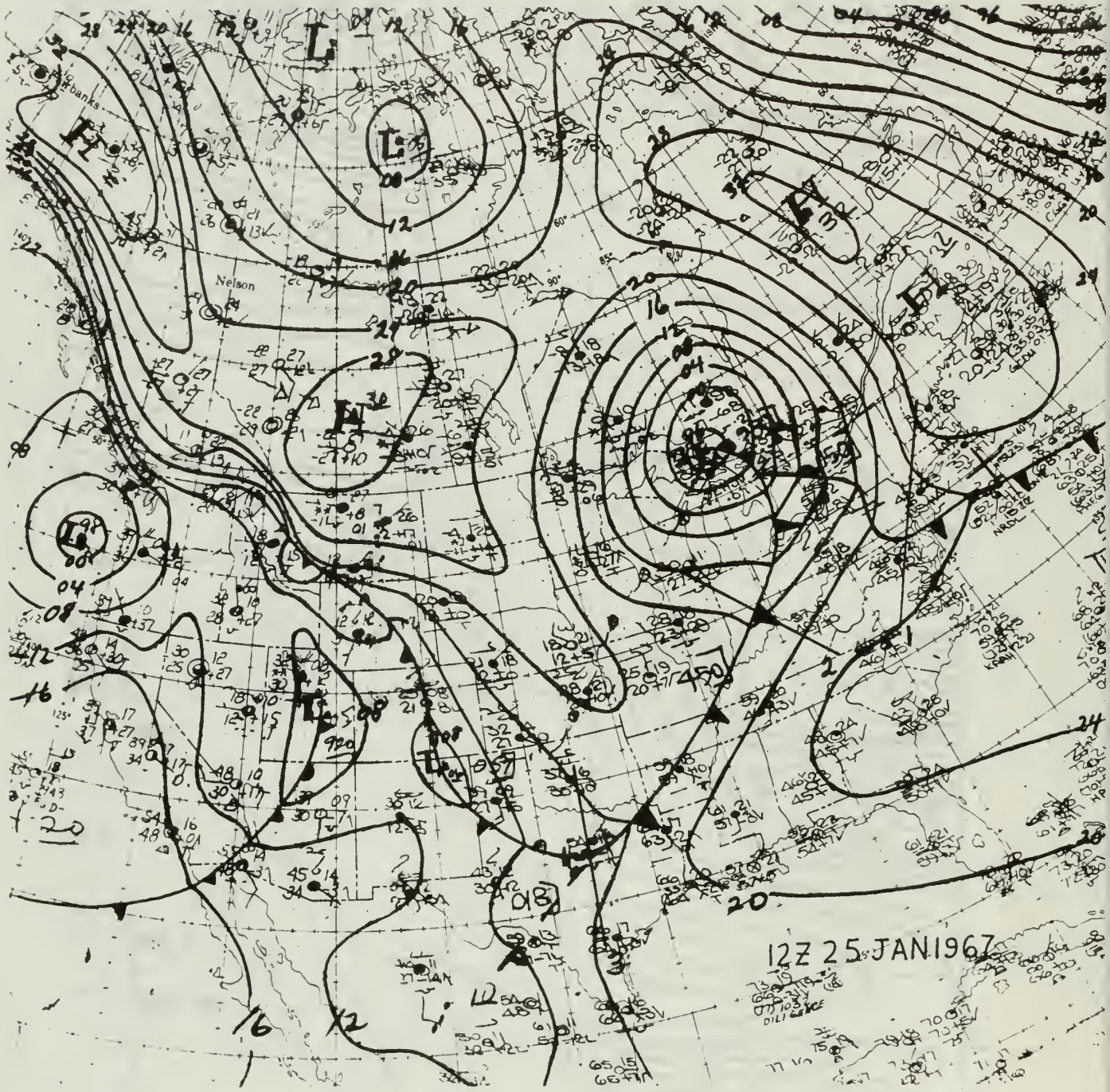

FIG. 2

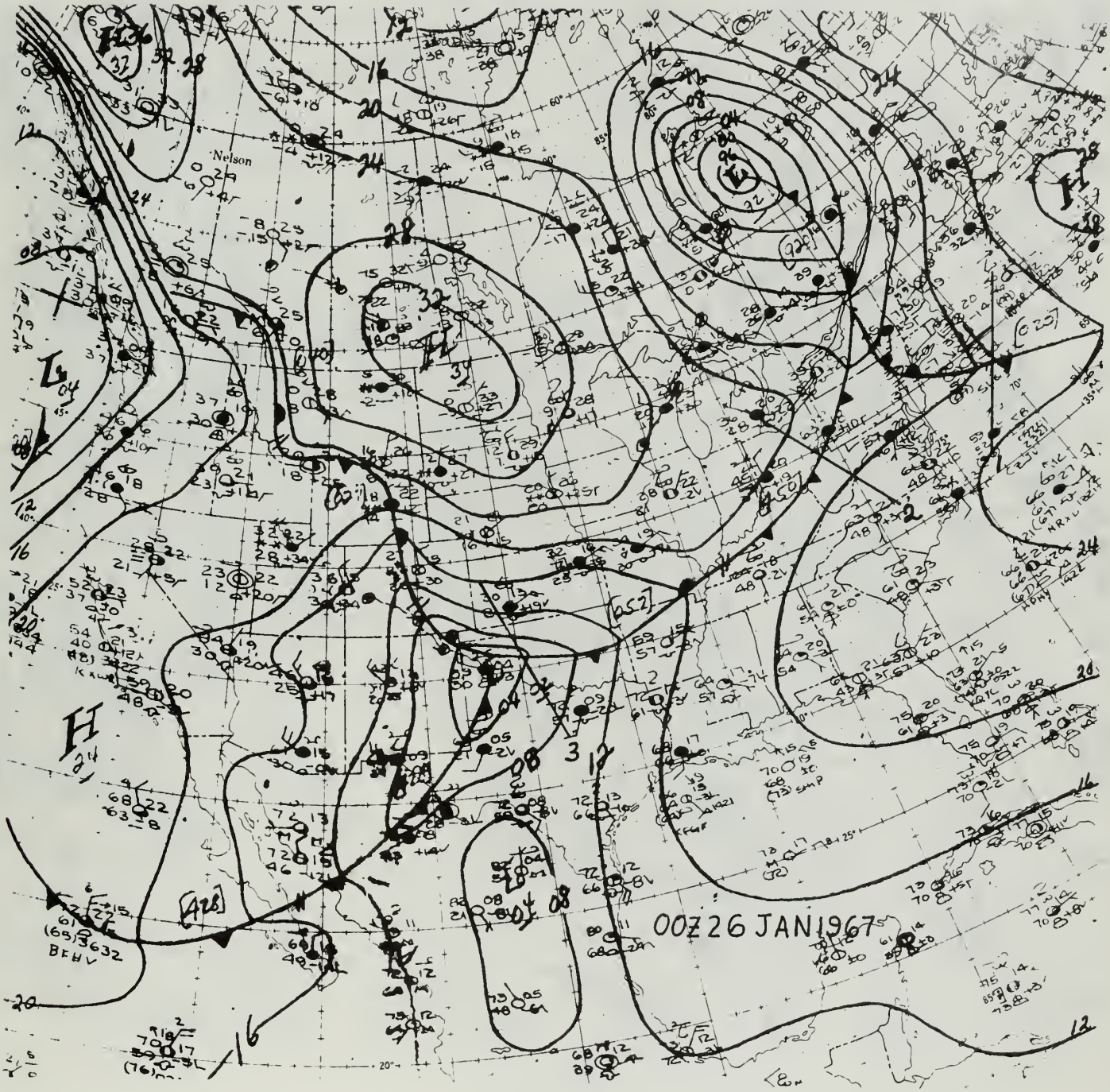

FIG. 3

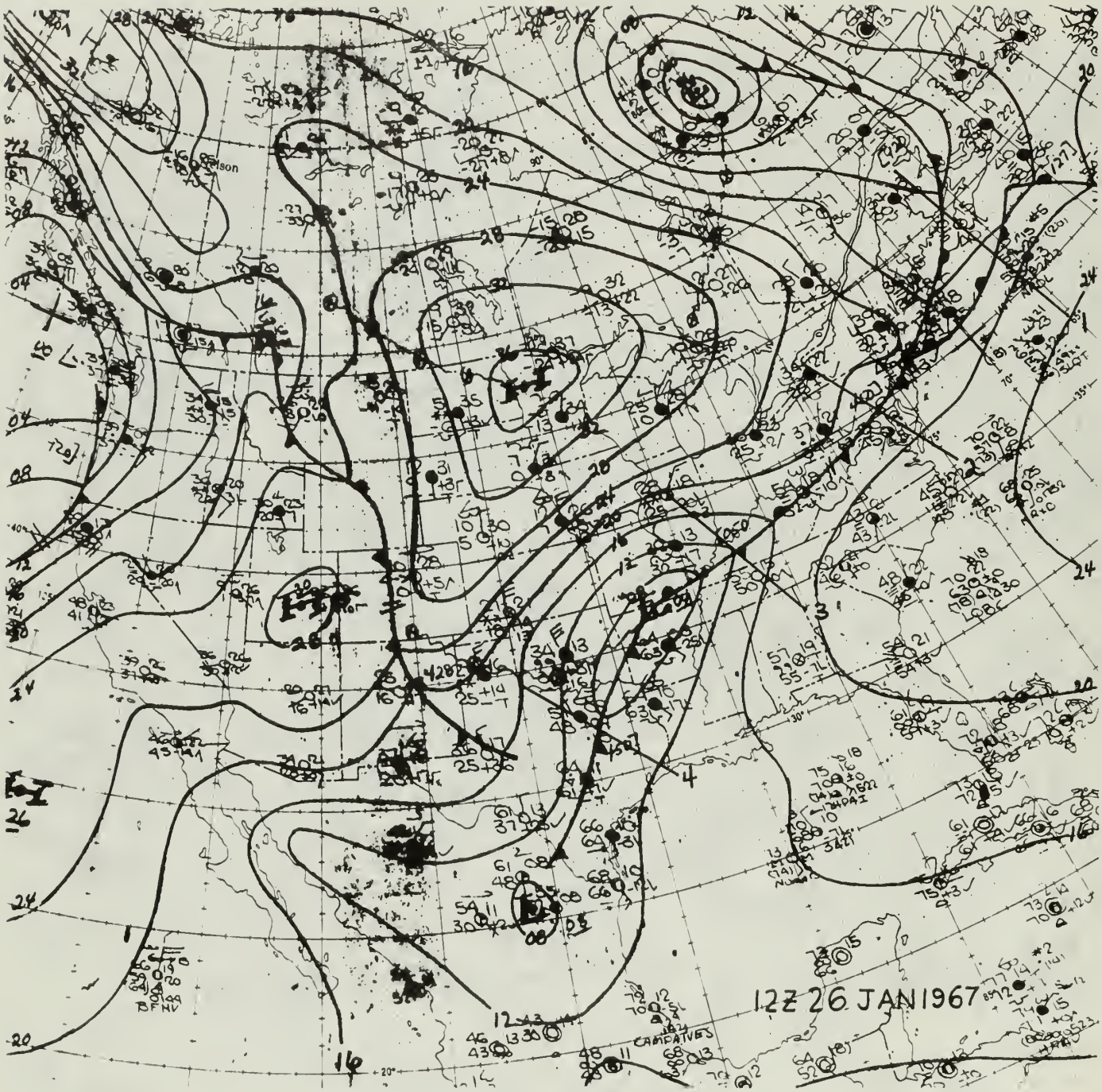

FIG. 4

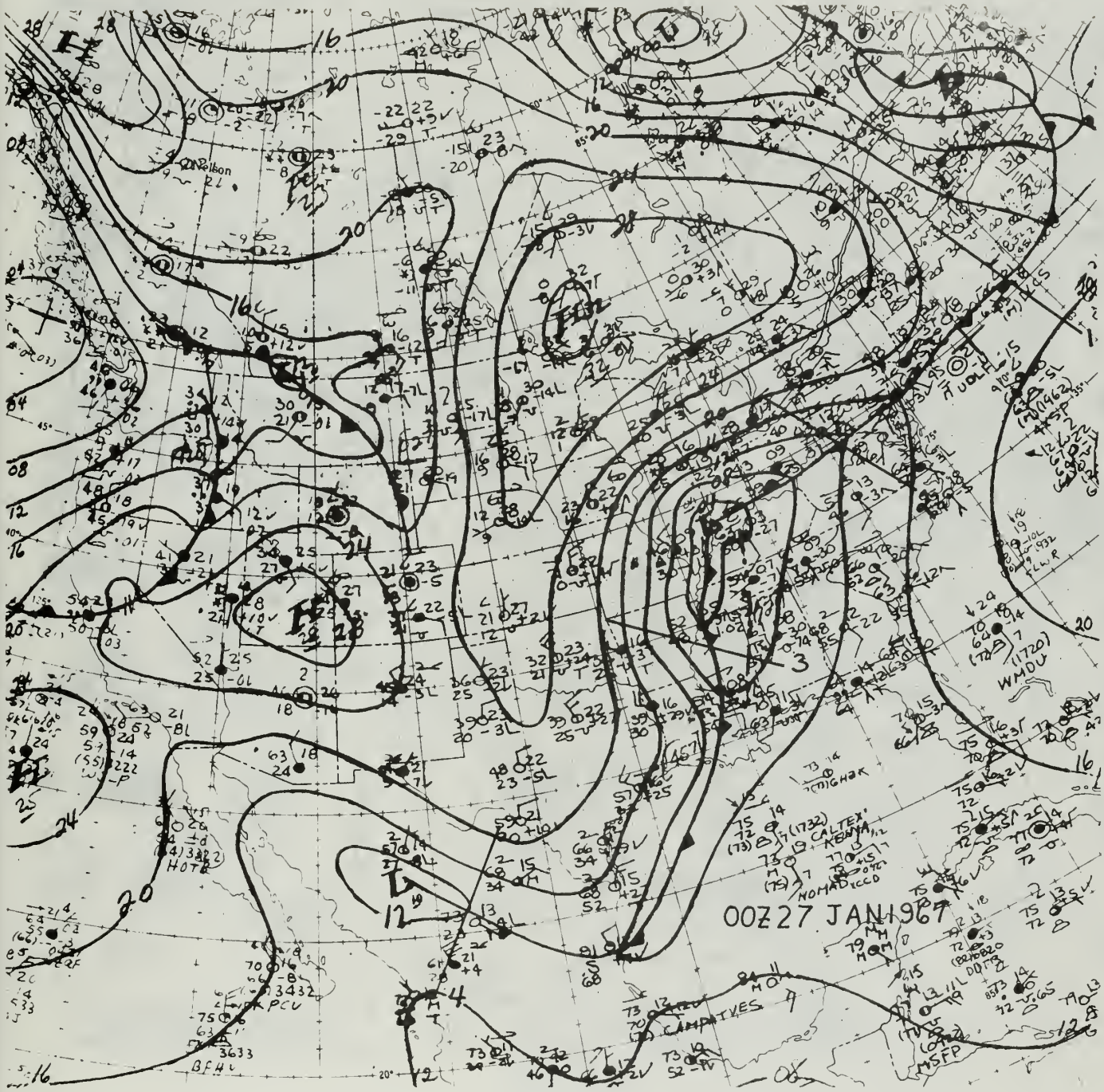

FIG. 5

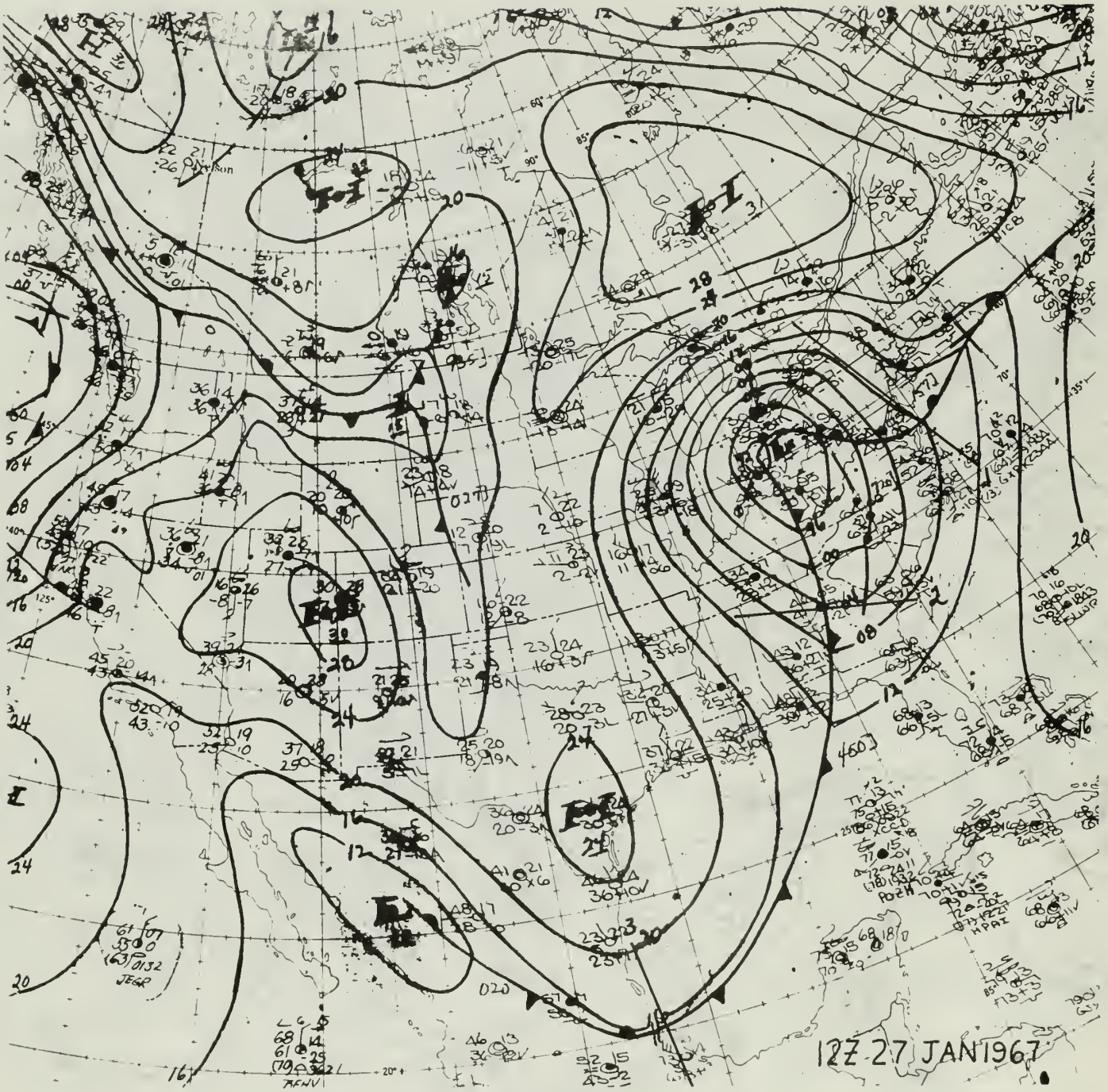

FIG. 6

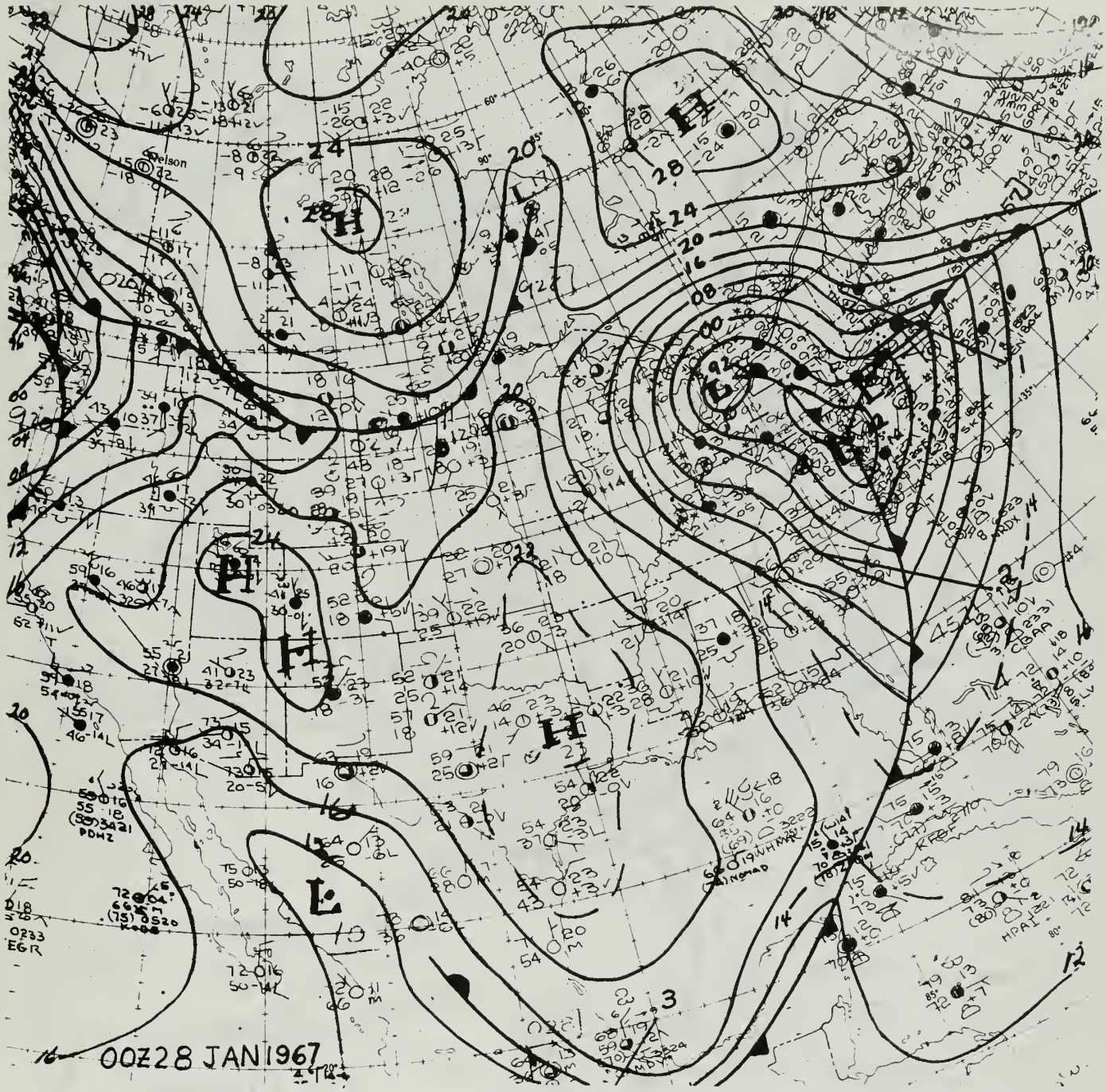

FIG. 7

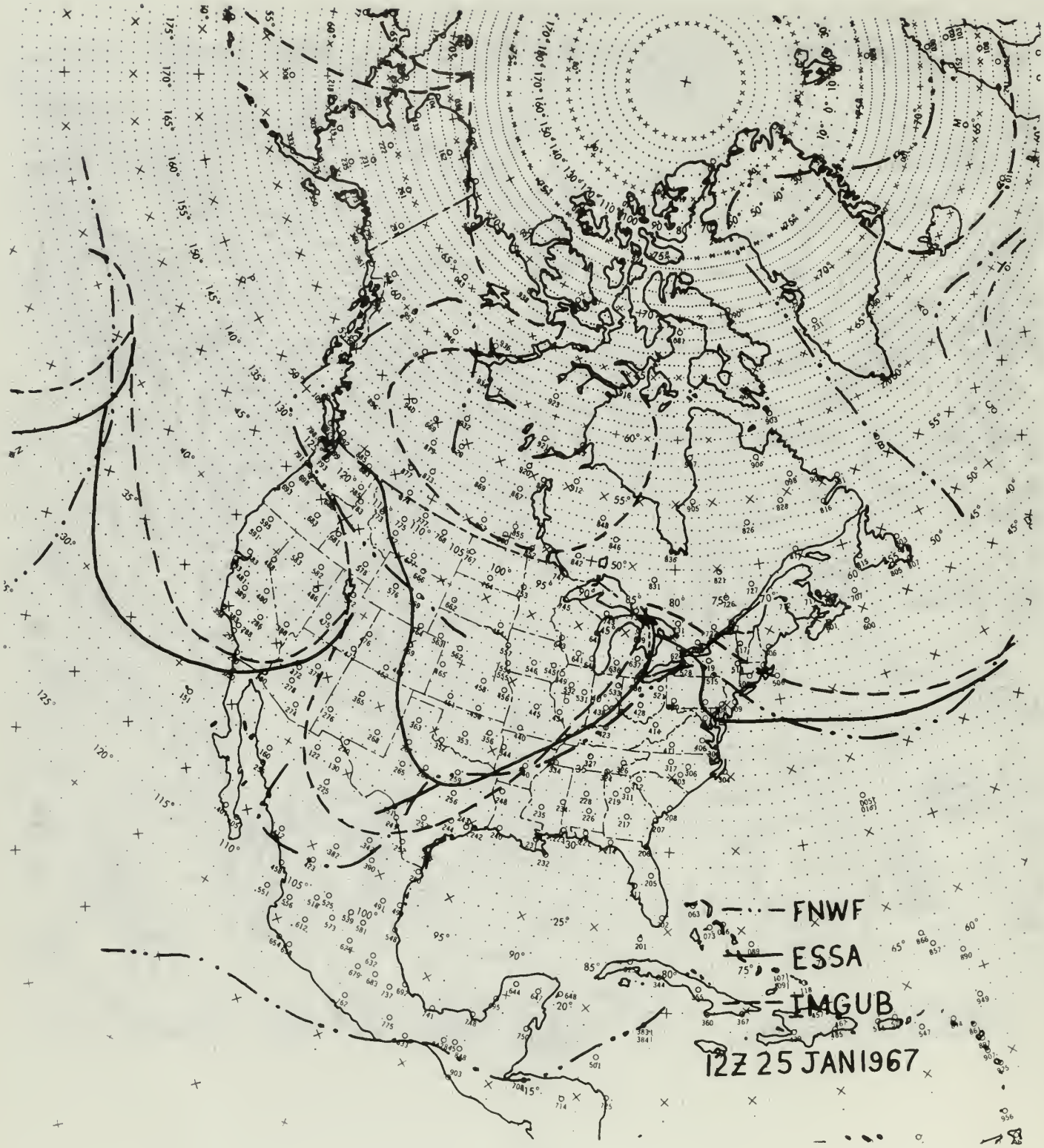

FIG. 8

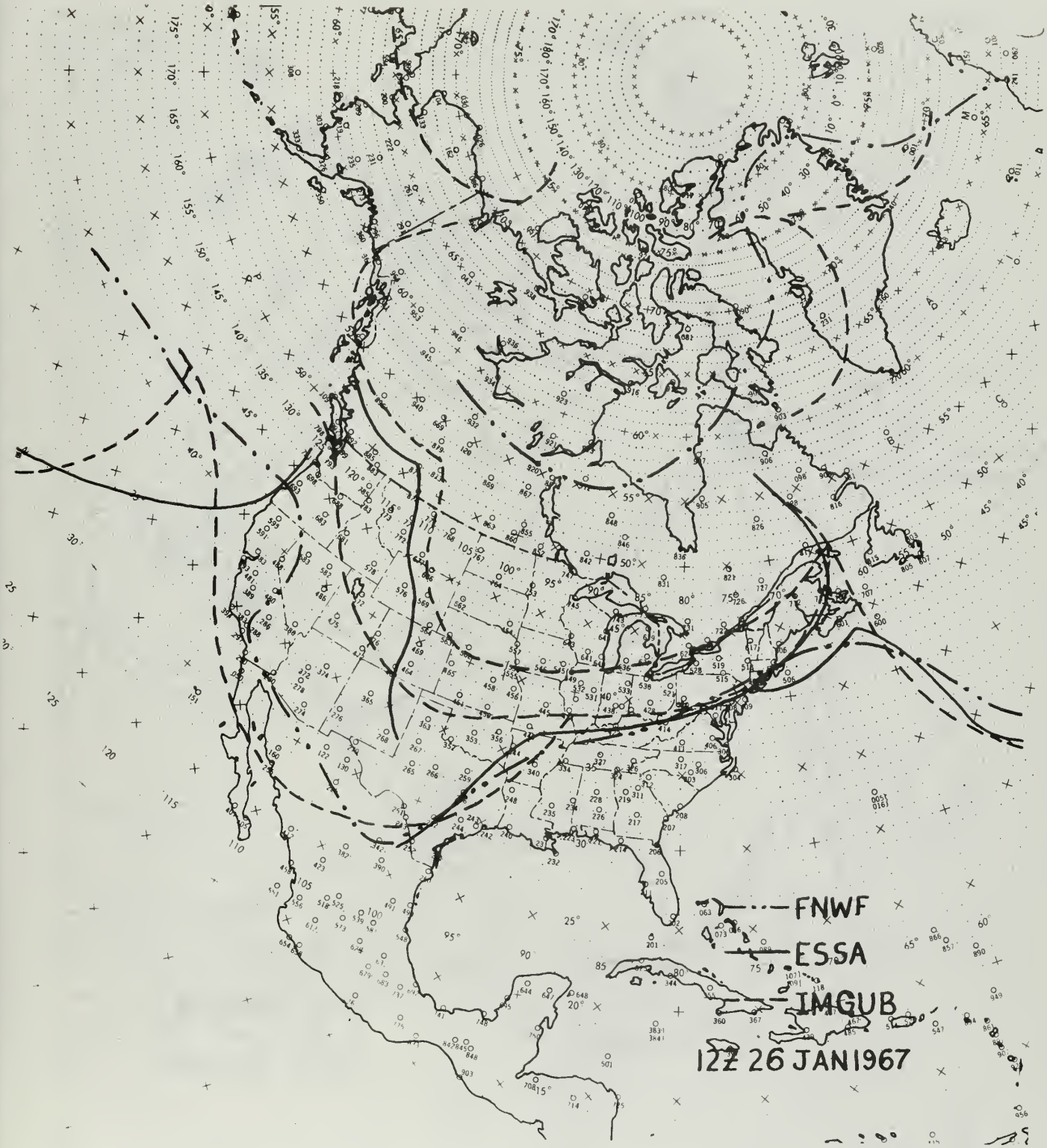

FIG. 9

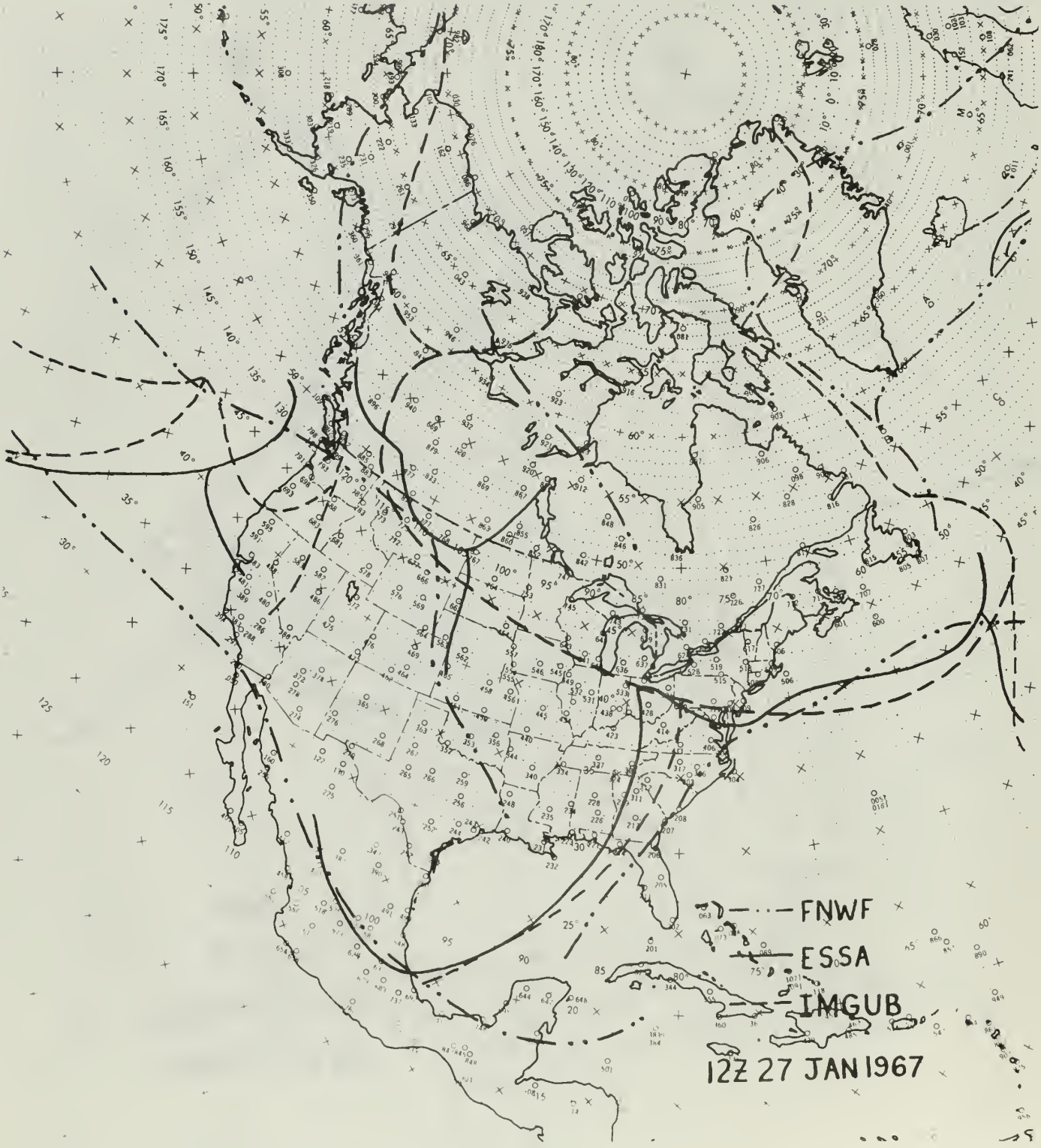

FIG. 10

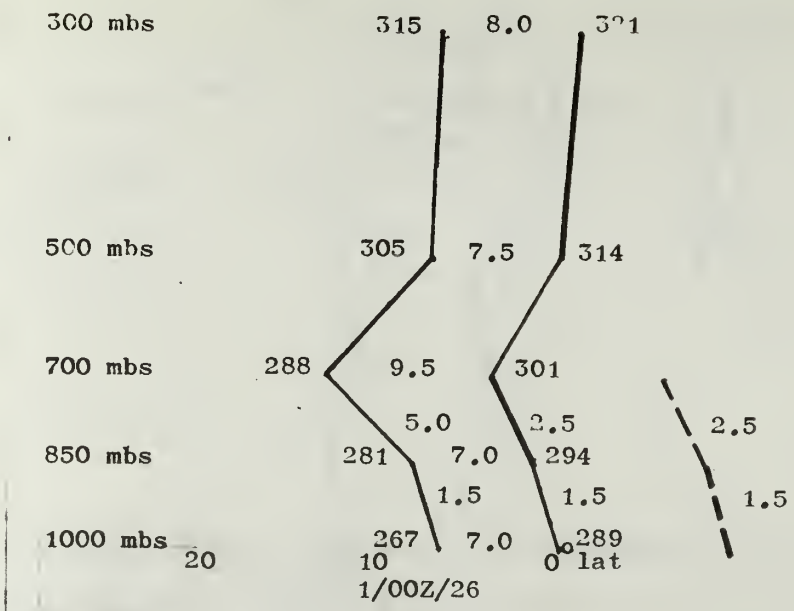

GROUP A

45

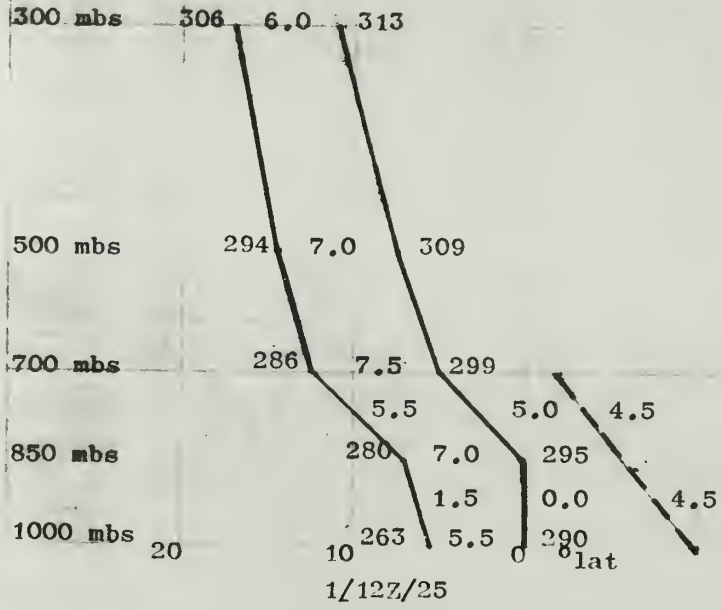

20

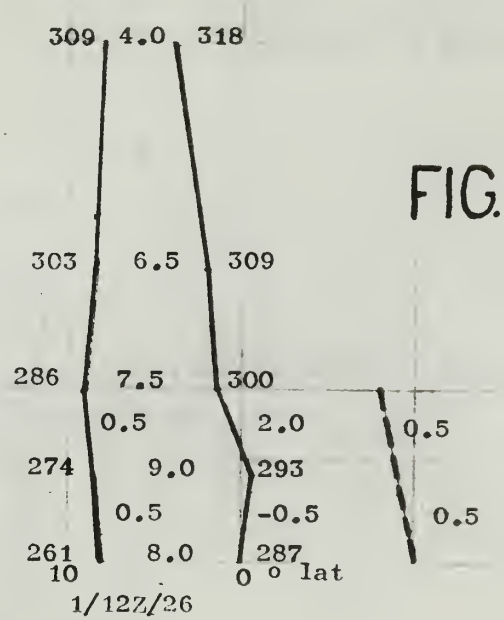

FIG. 11

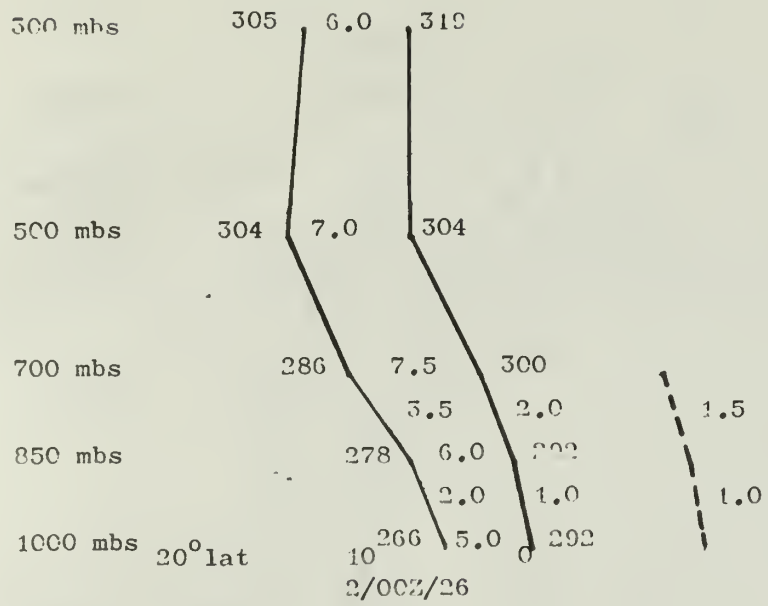

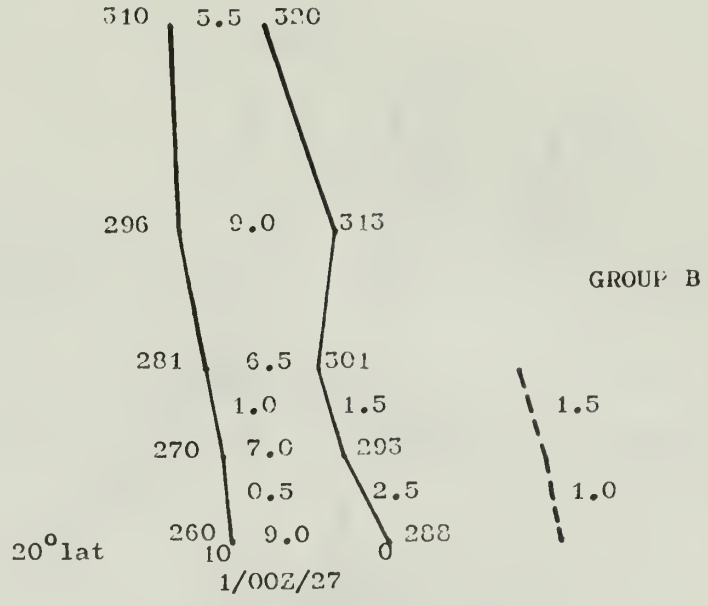

GROUP B

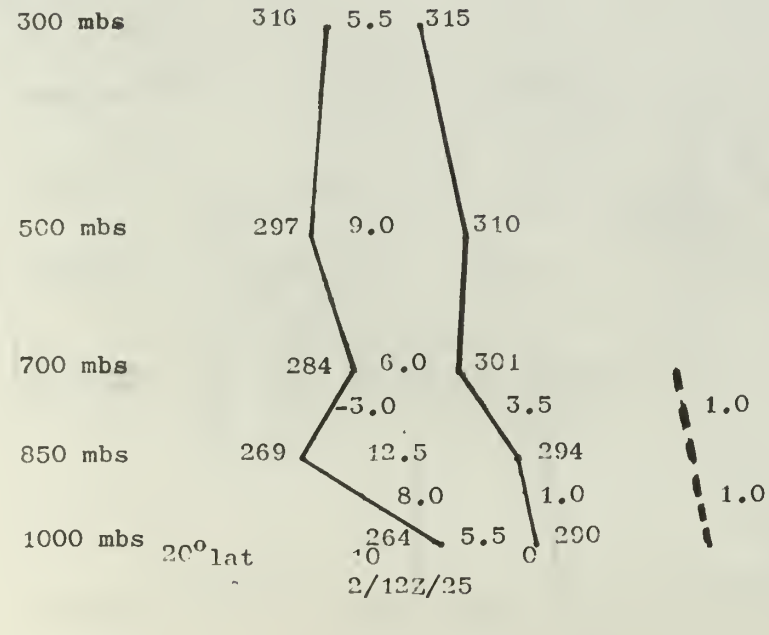

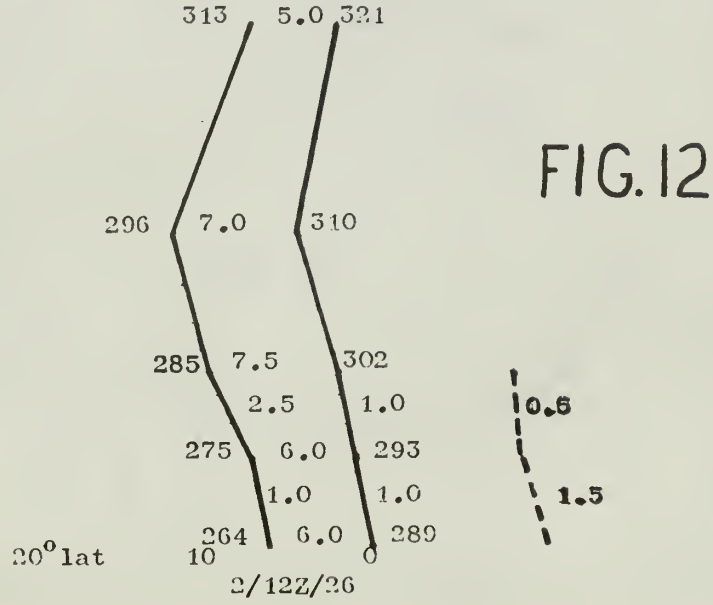

FIG. 12

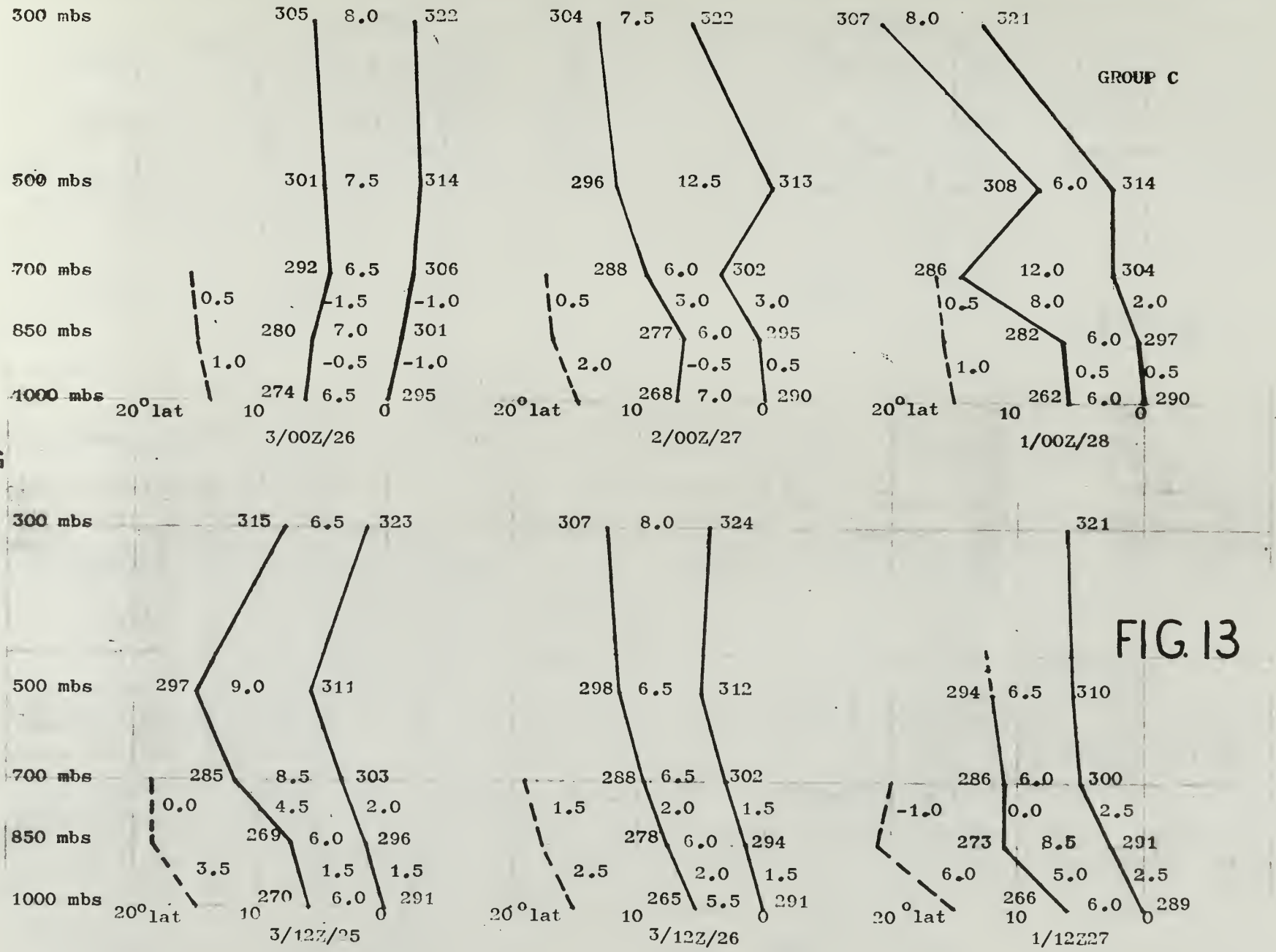
GROUP C
300 mbs
500 mbs
700 mbs
850 mbs
1000 mbs
305 8.0 322
301 7.5 314
292 6.5 306
0.5
-1.5 -1.0
280 7.0 301
1.0
-0.5 -1.0
274 6.5 295
20°lat 10 0
3/00Z/26
304 7.5 322
296 12.5 313
288 6.0 302
0.5
3.0 3.0
277 6.0 295
2.0
-0.5 0.5
268 7.0 290
20°lat 10 0
2/00Z/27
307 8.0 321
308 6.0 314
286 12.0 304
0.5
8.0 2.0
282 6.0 297
1.0
0.5 0.5
262 6.0 290
20°lat 10 0
1/00Z/28
300 mbs
500 mbs
700 mbs
850 mbs
1000 mbs
315 6.5 323
297 9.0 311
285 8.5 303
0.0
4.5 2.0
269 6.0 296
3.5
1.5 1.5
270 6.0 291
20°lat 10 0
3/12Z/25
307 8.0 324
298 6.5 312
288 6.5 302
1.5
2.0 1.5
278 6.0 294
2.5
2.0 1.5
265 5.5 291
20°lat 10 0
3/12Z/26
321
294 6.5 310
286 6.0 300
-1.0
0.0 2.5
273 8.5 291
6.0
5.0 2.5
266 6.0 289
20°lat 10 0
1/12Z27

FIG. 13

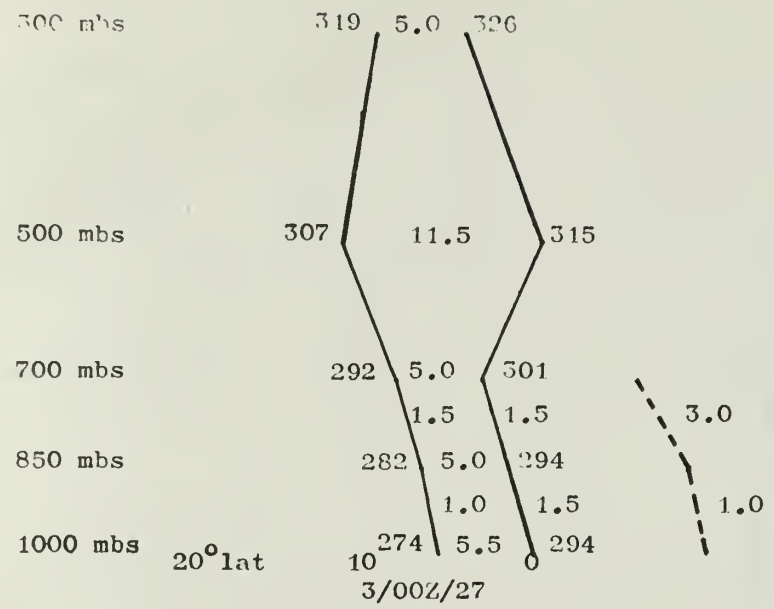

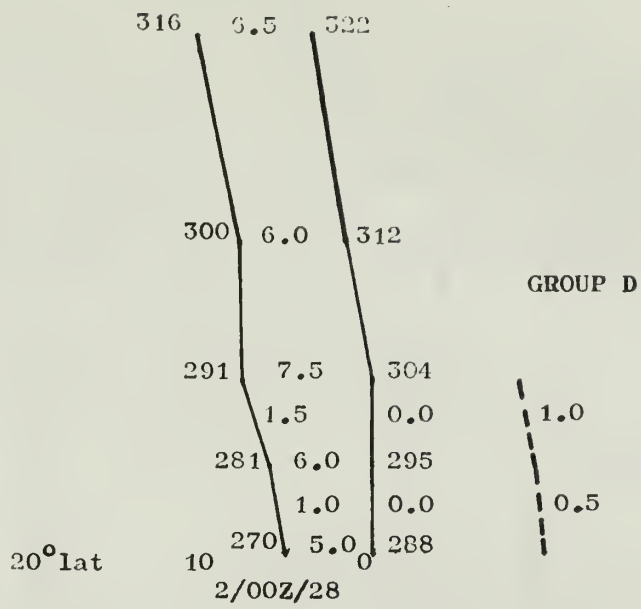

GROUP D

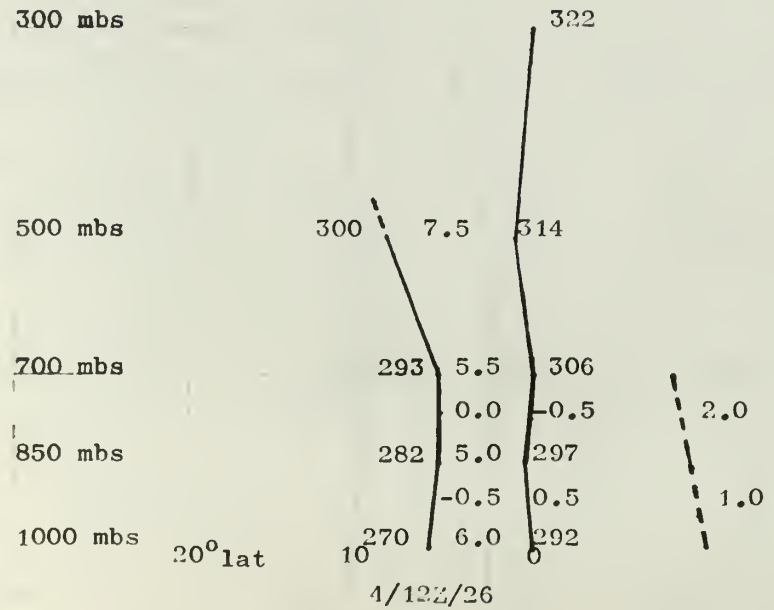

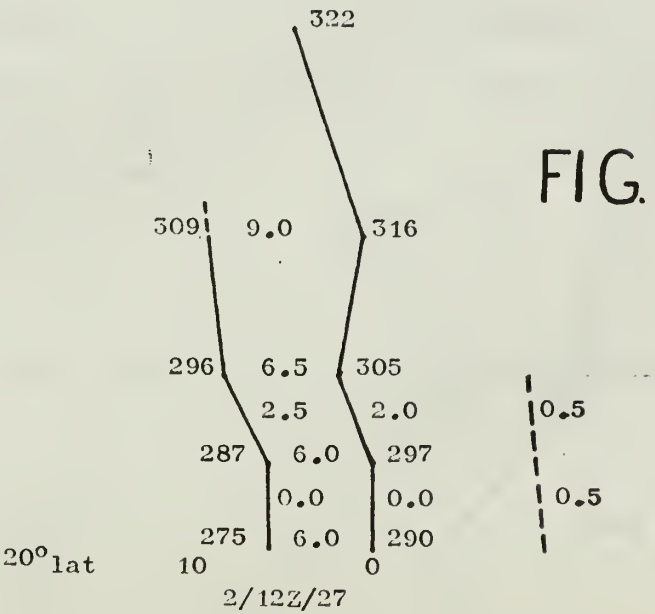

FIG. 14

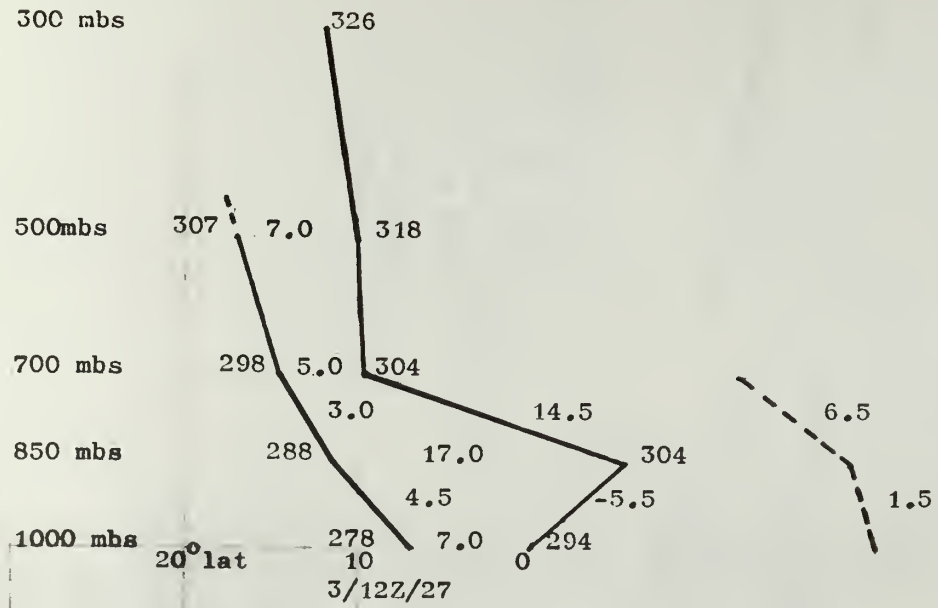

GROUP E

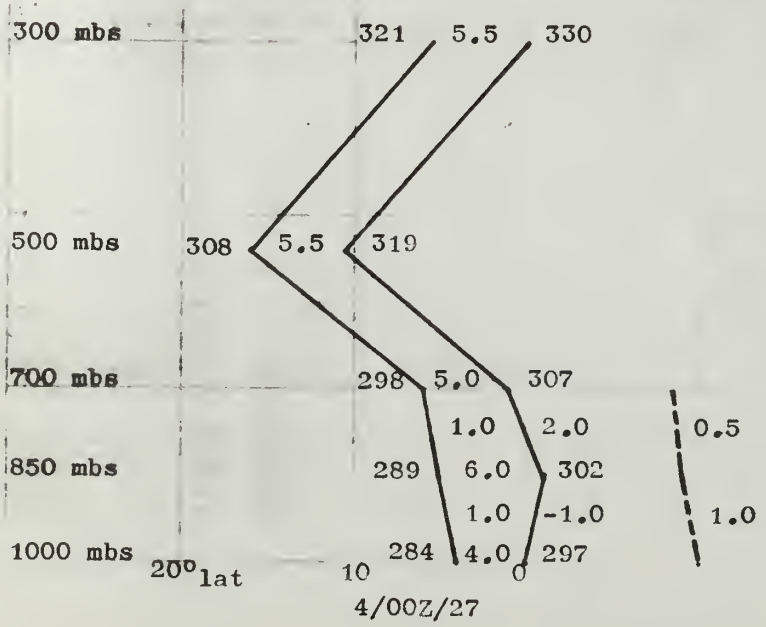

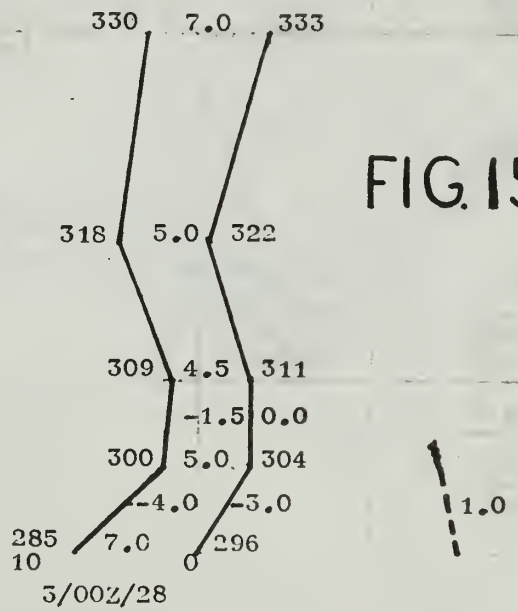

FIG. 15

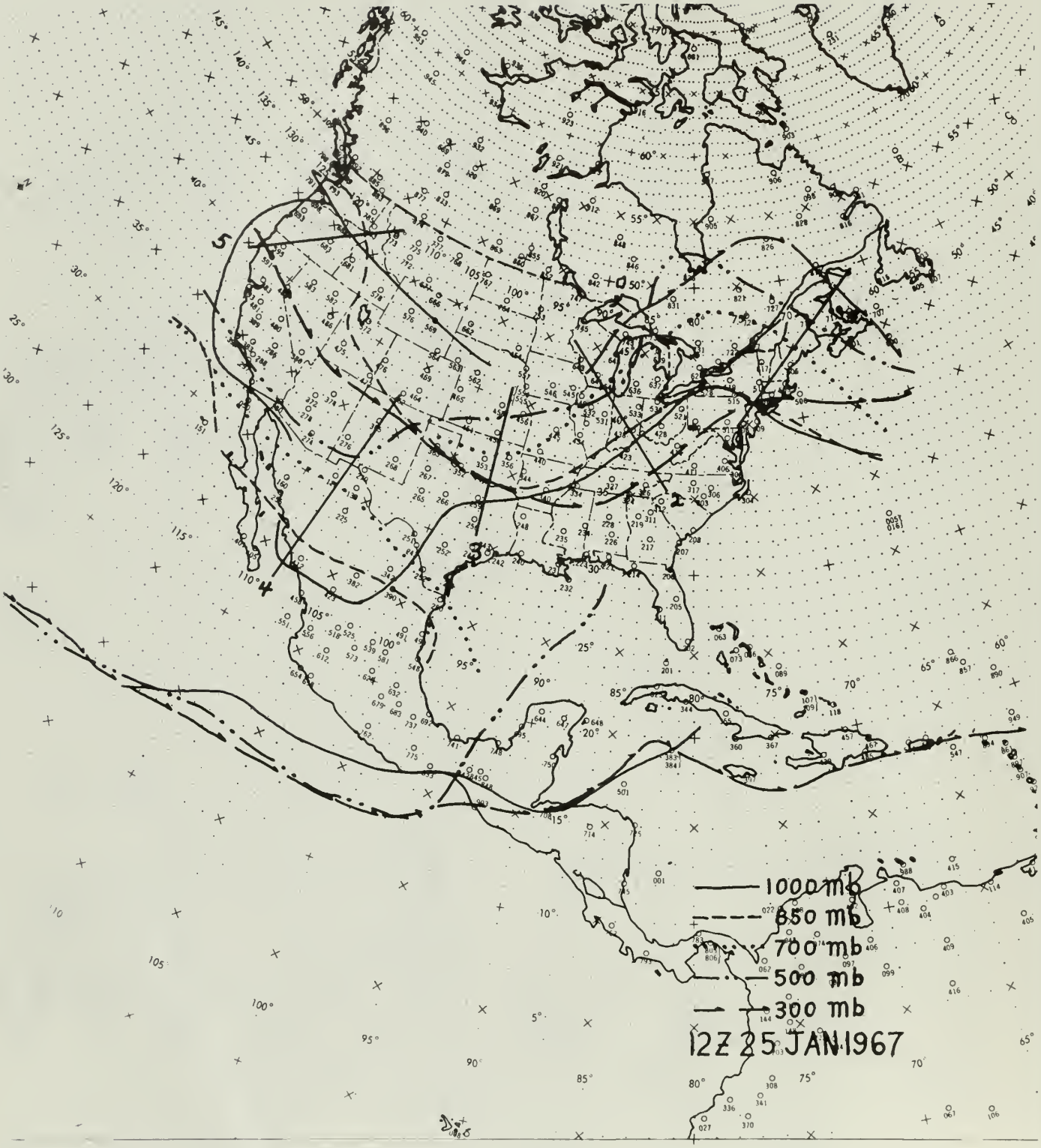

FIG. 16

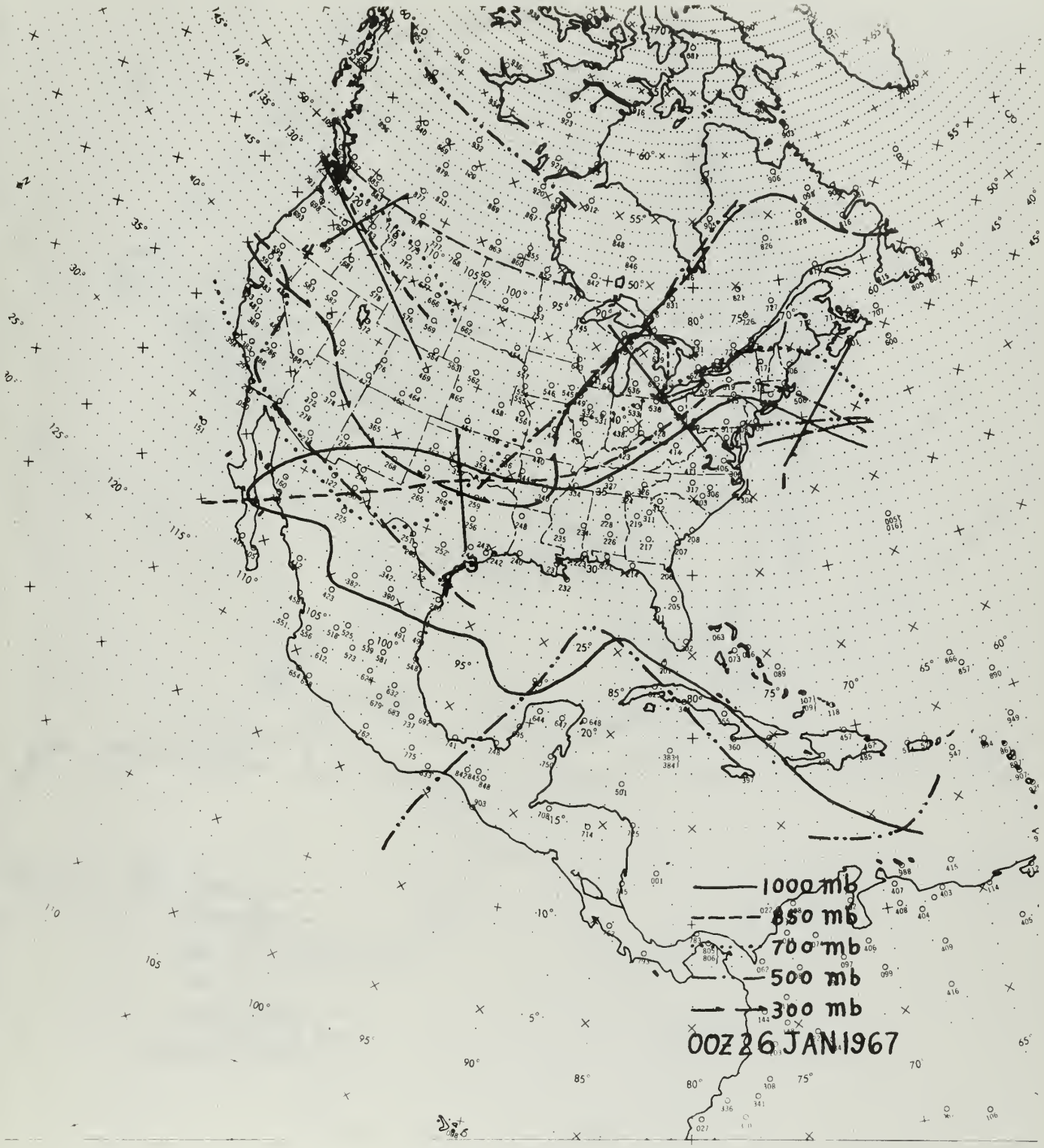

FIG. 17

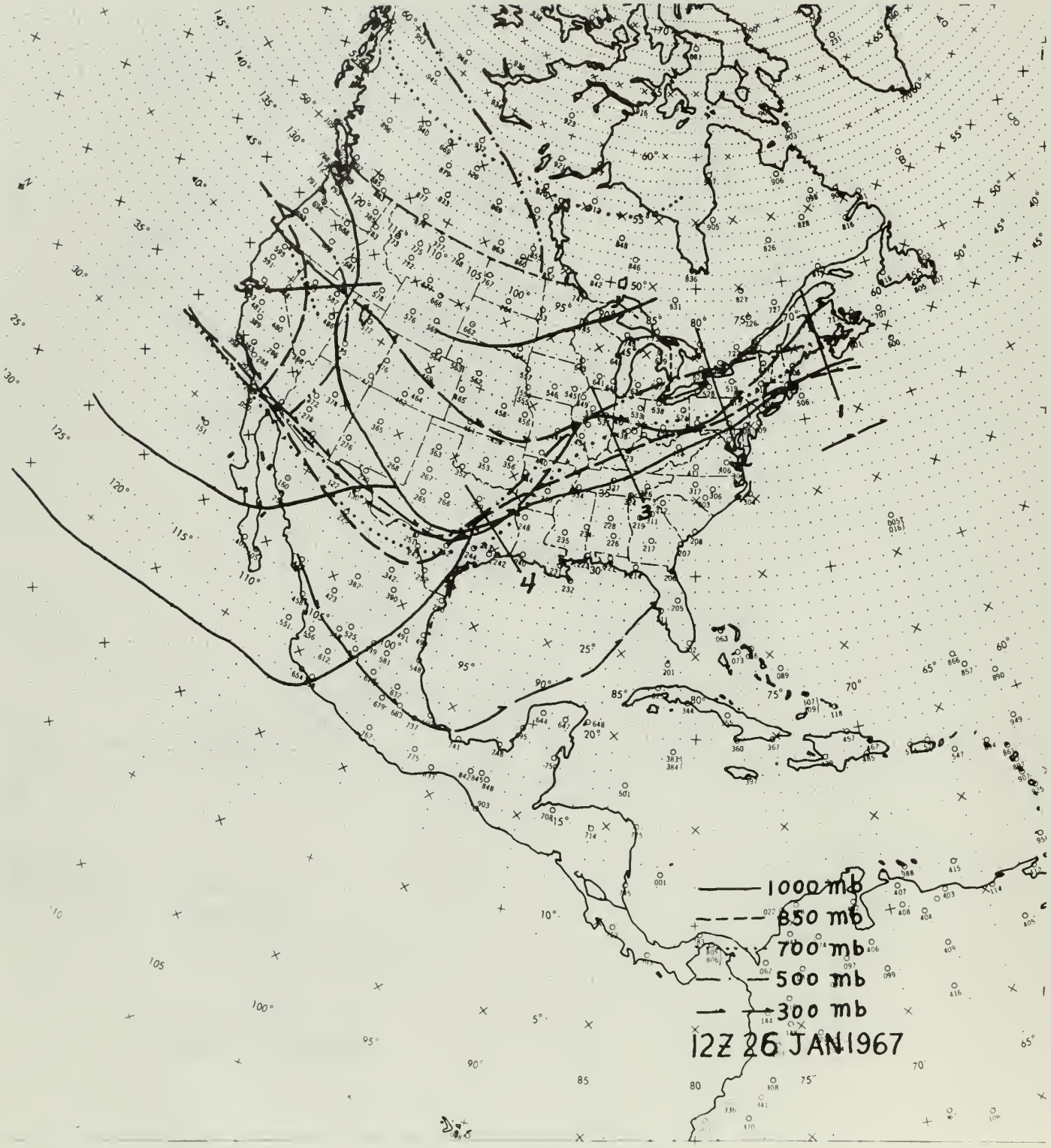

FIG. 18

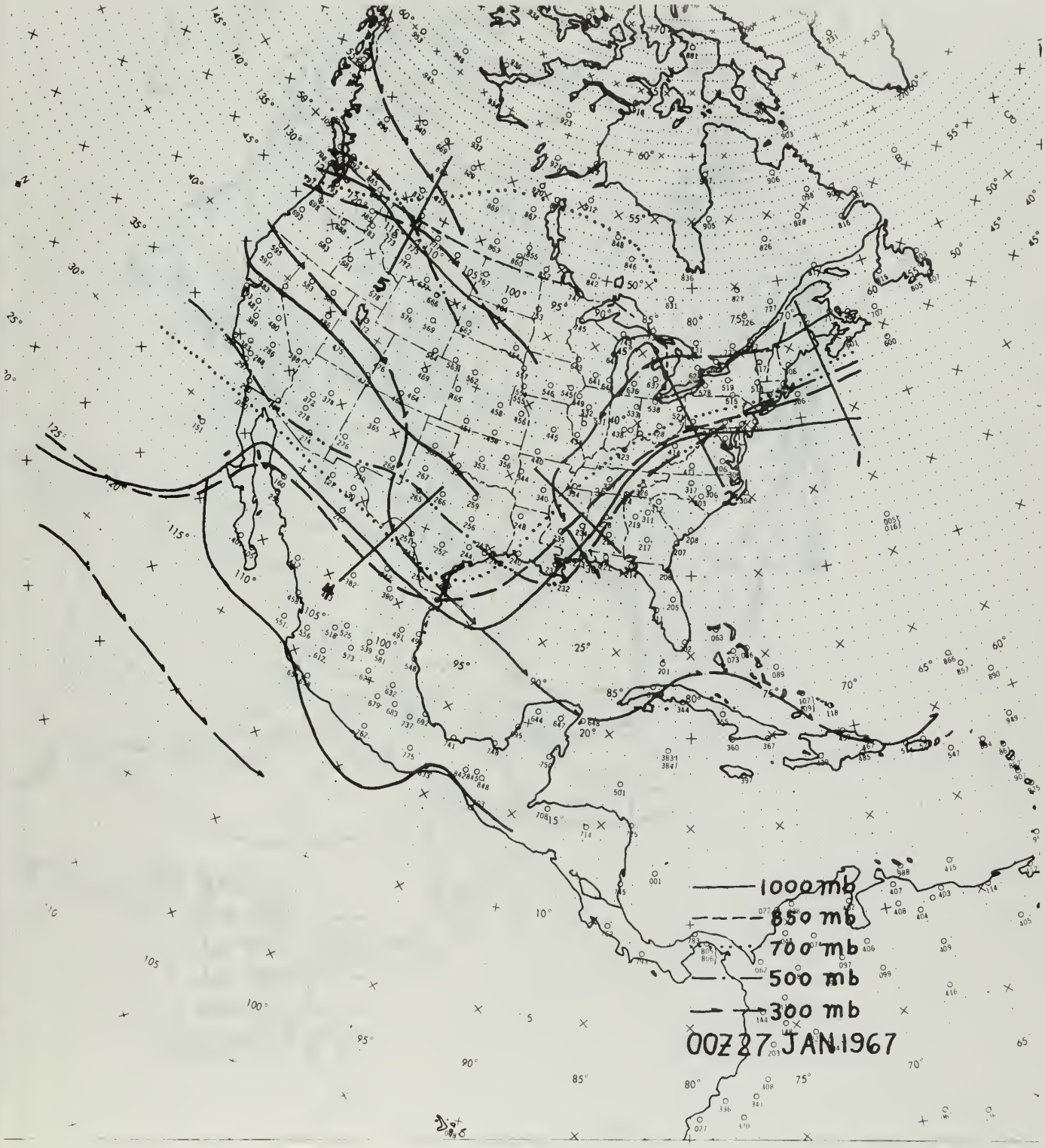

FIG. 19

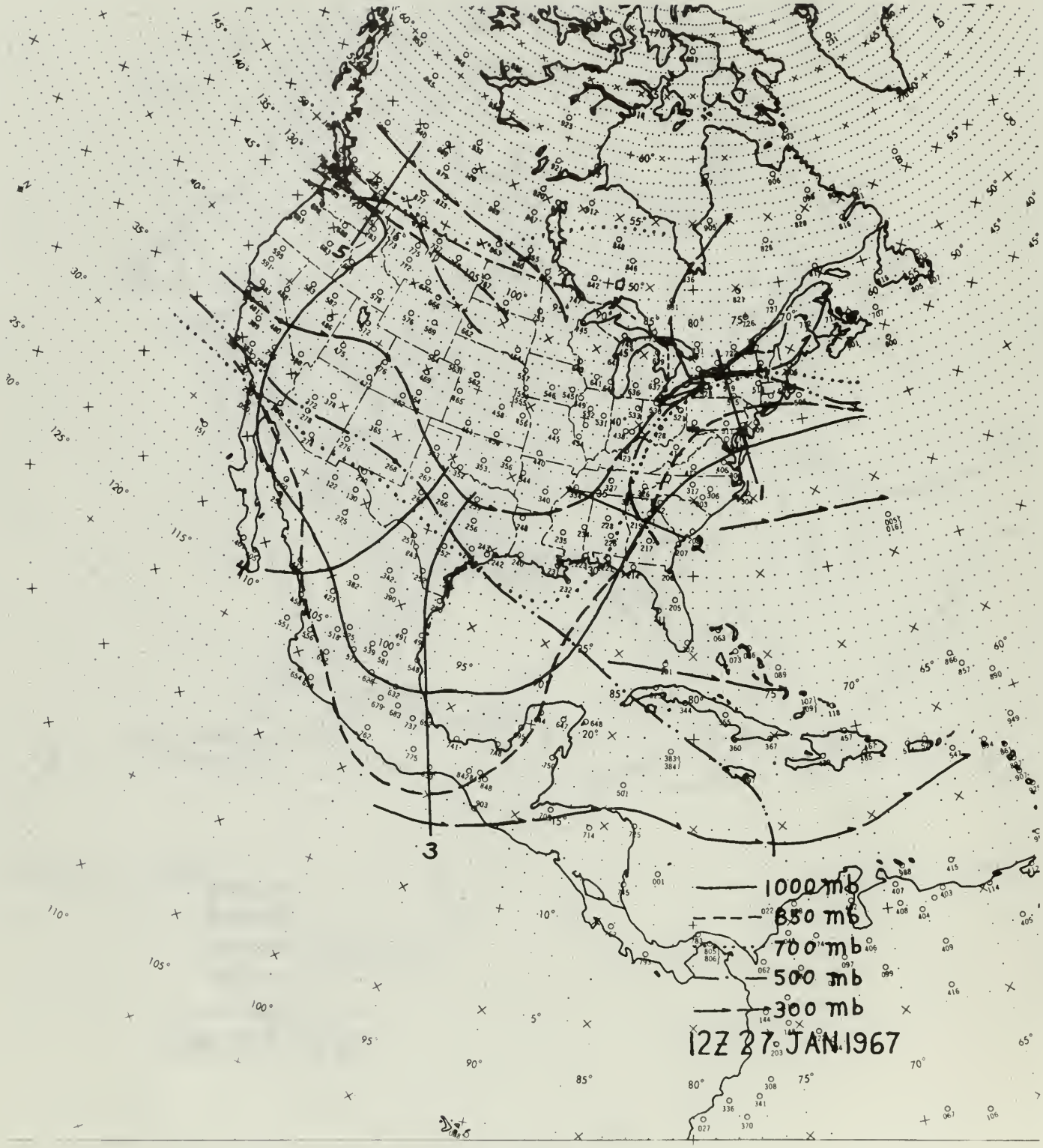

FIG. 20

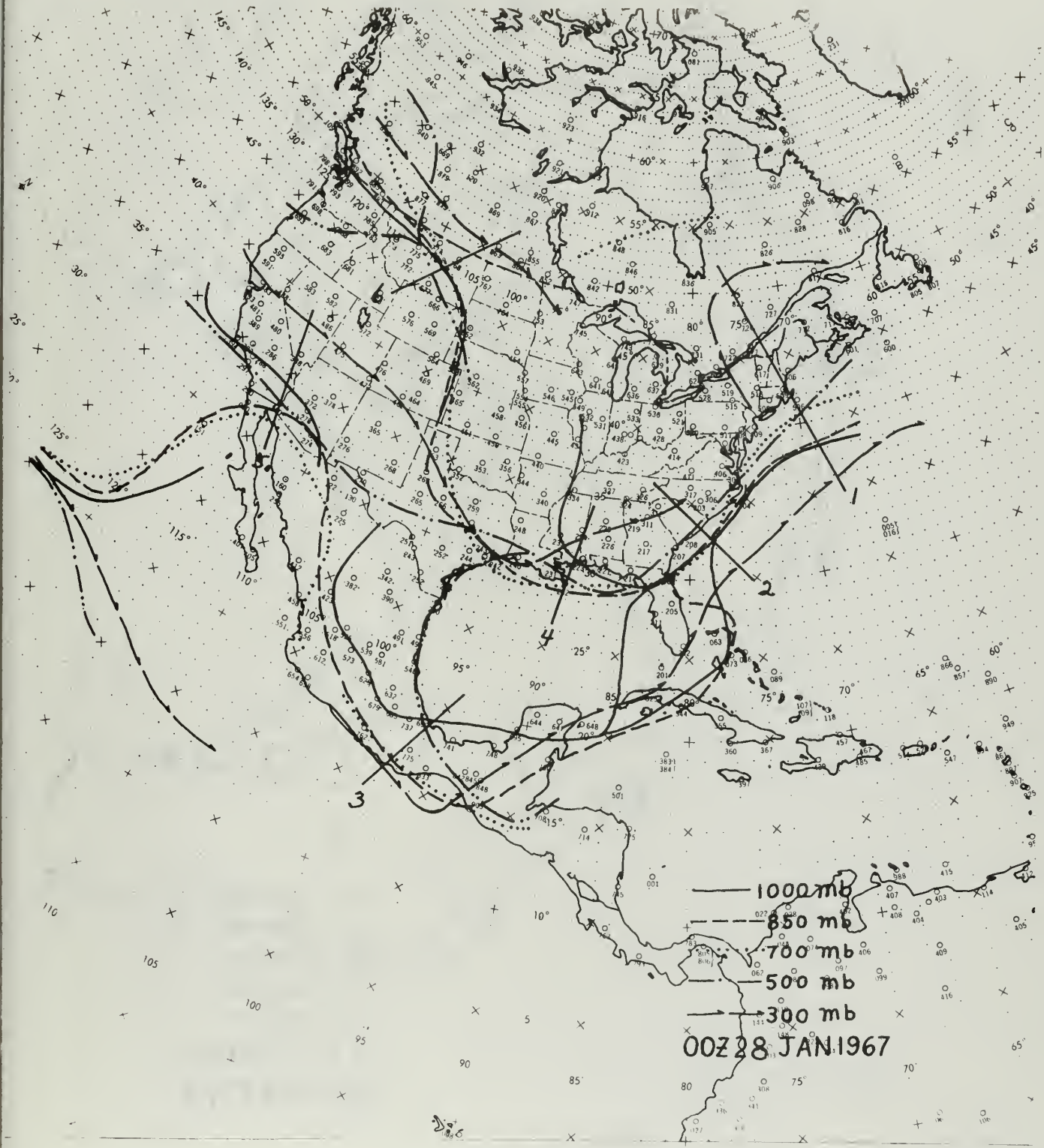

FIG. 21

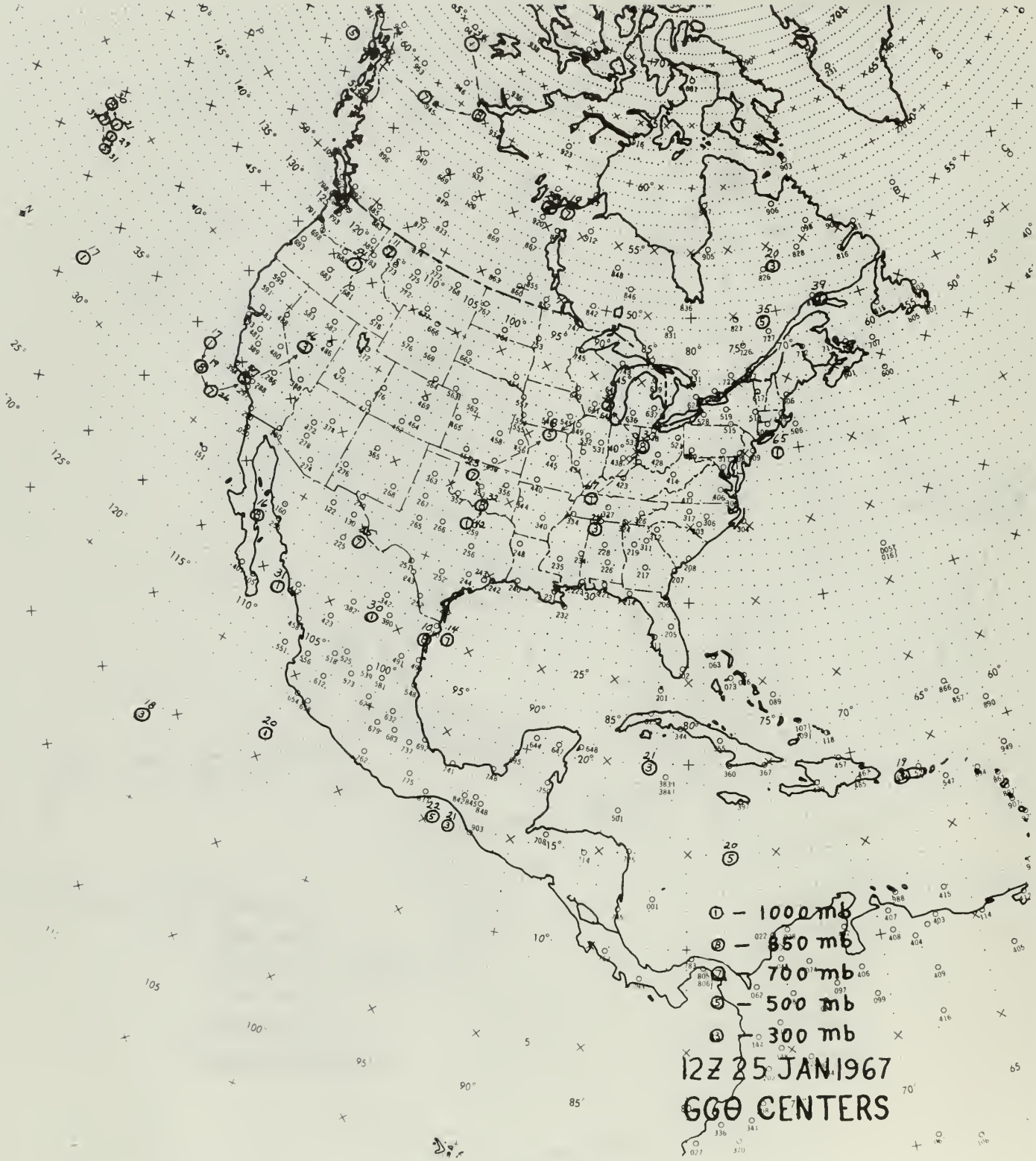
① – 1000 mb
② – 850 mb
③ – 700 mb
⑤ – 500 mb
⑧ – 300 mb
12Z 25 JAN 1967
GGθ CENTERS

FIG. 22

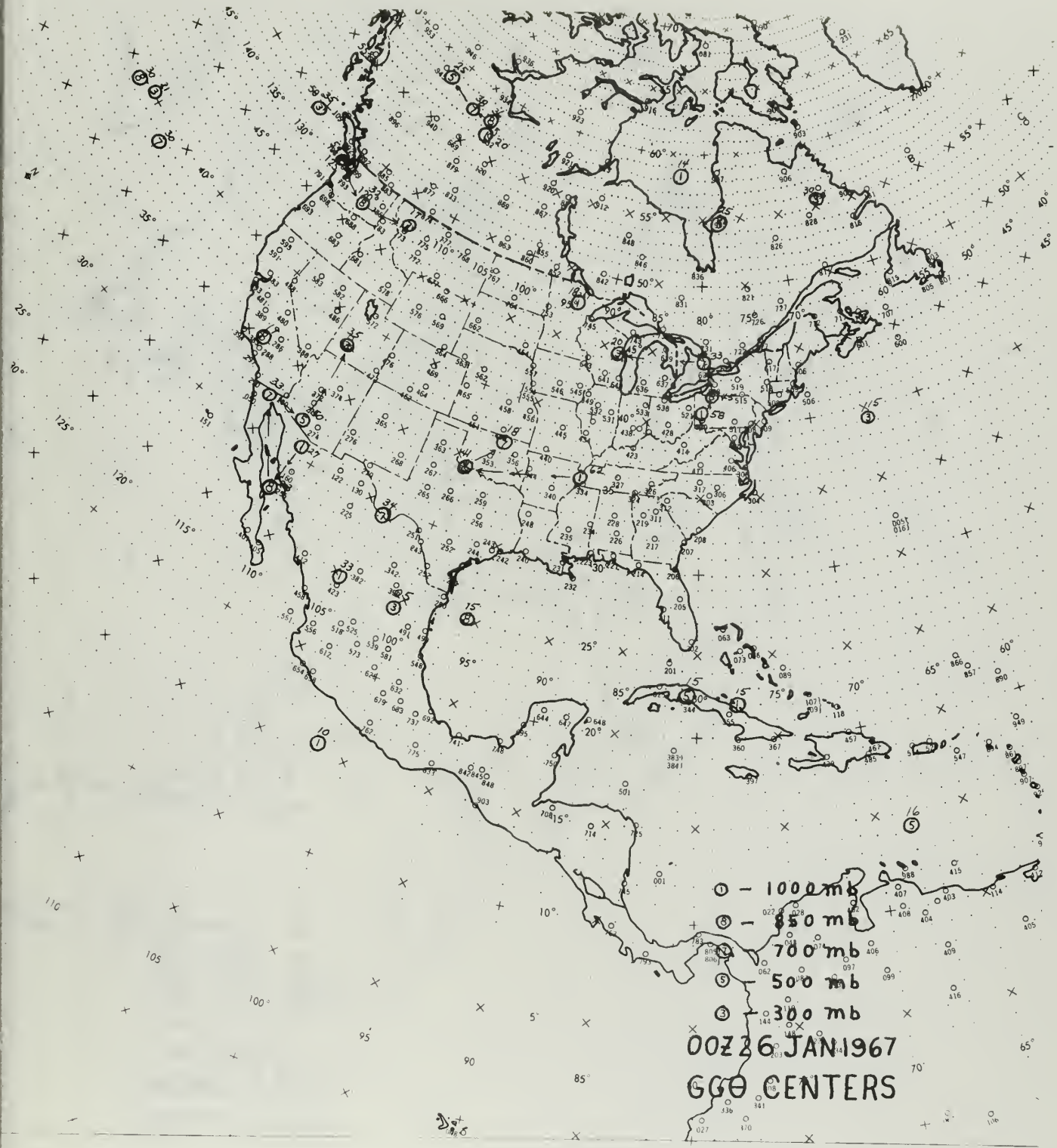
① – 1000 mb
② – 850 mb
③ – 700 mb
⑤ – 500 mb
③ – 300 mb
00Z 26 JAN 1967
GGO CENTERS

FIG. 23

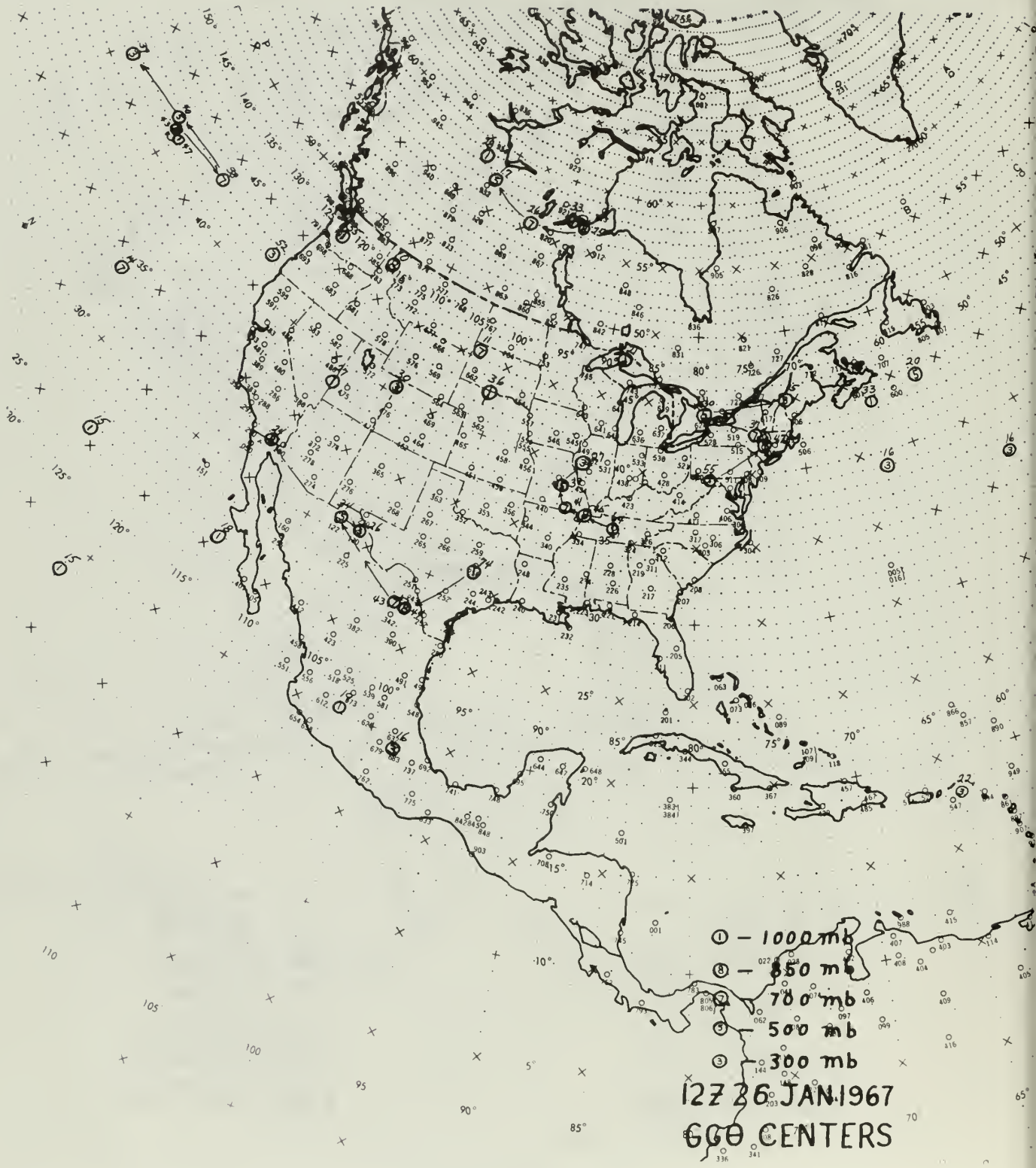
① – 1000 mb
② – 850 mb
④ – 700 mb
⑤ – 500 mb
③ – 300 mb
12Z 26 JAN 1967
GGO CENTERS

FIG. 24

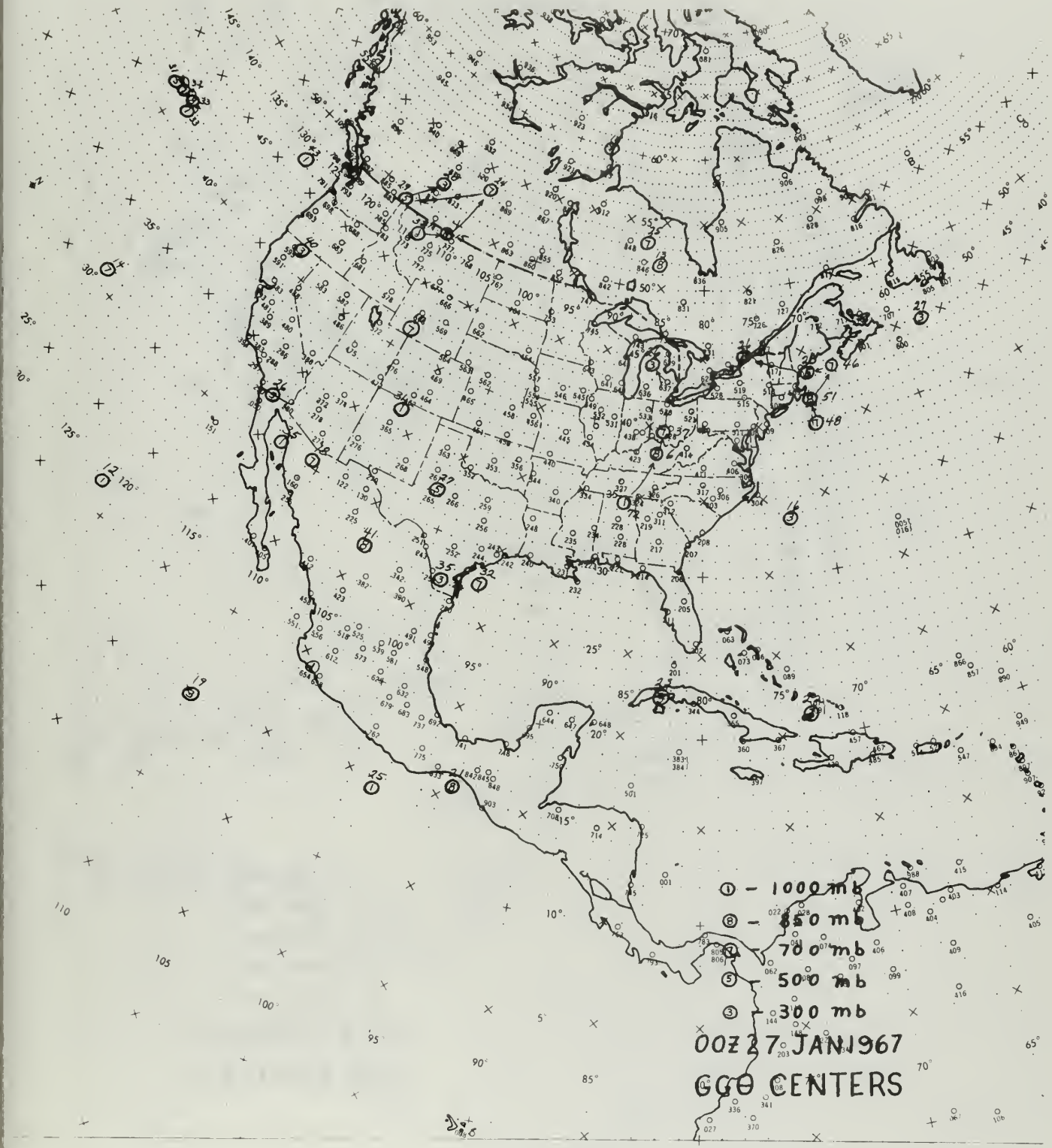
① - 1000 mb
② - 850 mb
④ - 700 mb
⑤ - 500 mb
③ - 300 mb
00Z 27 JAN 1967
GGO CENTERS

FIG. 25

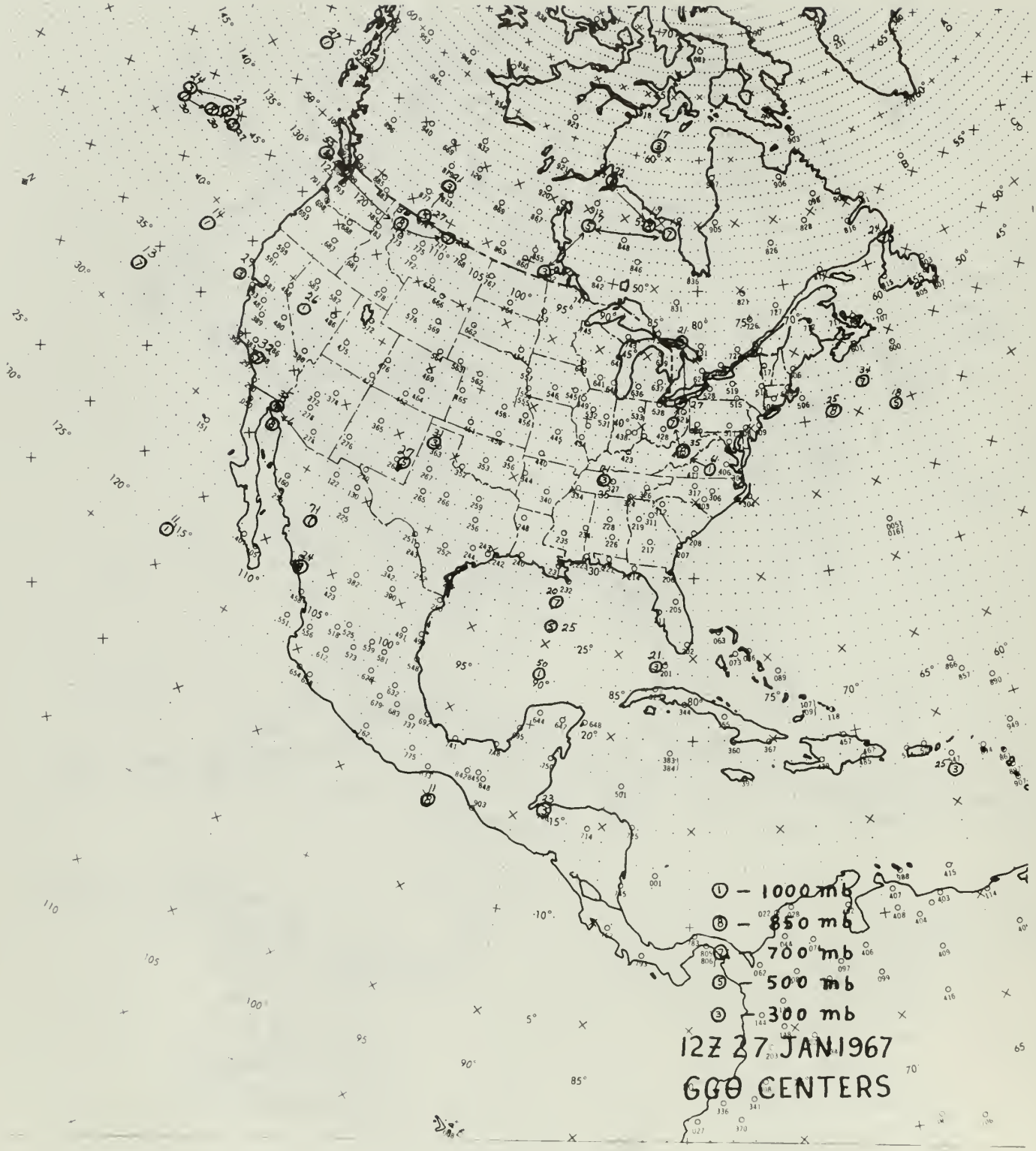
① – 1000 mb
⑧ – 850 mb
7 – 700 mb
⑤ – 500 mb
③ – 300 mb
12Z 27 JAN 1967
GGO CENTERS

FIG. 26

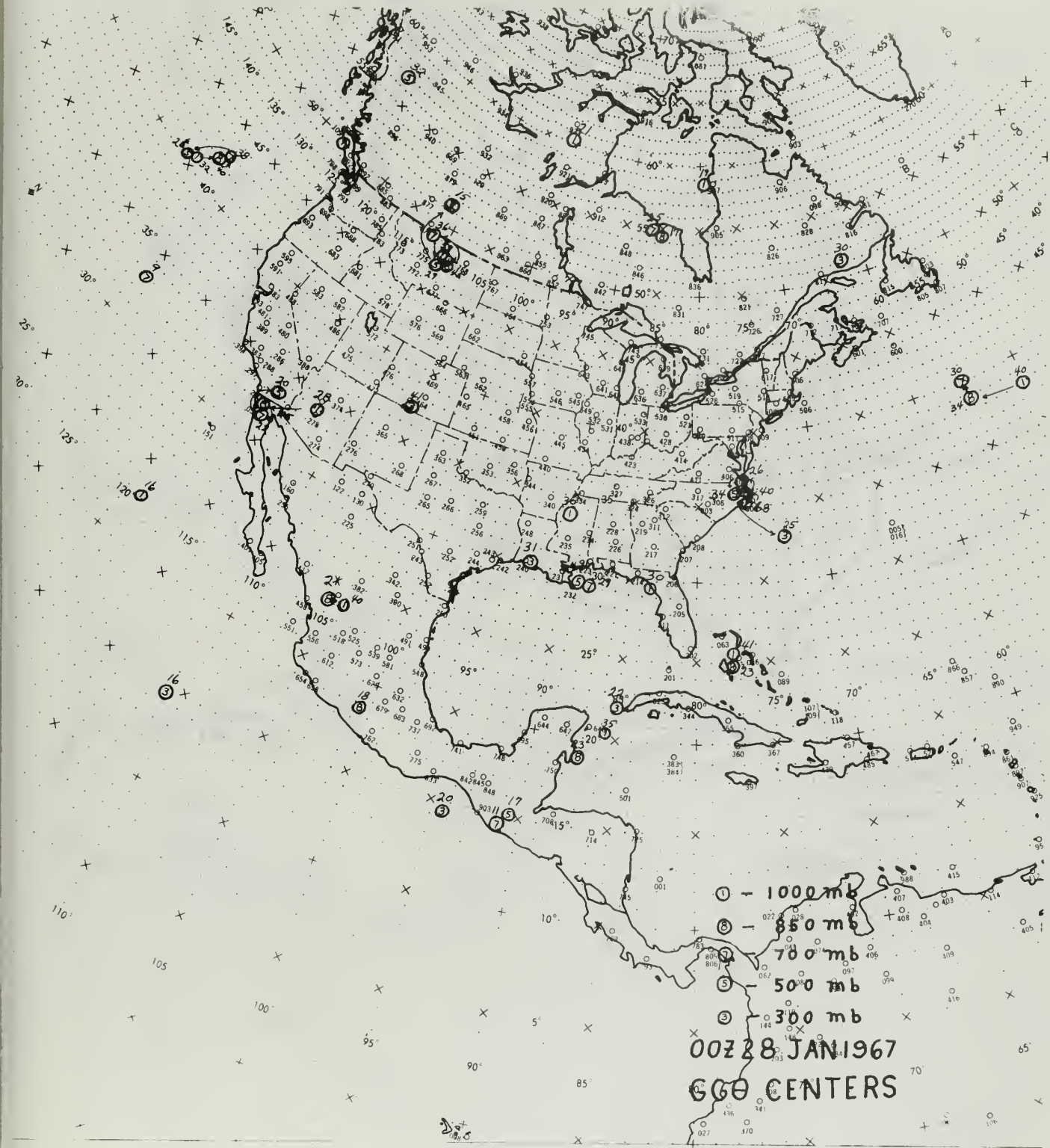
① - 1000 mb
⑧ - 850 mb
⑦ - 700 mb
⑤ - 500 mb
③ - 300 mb
00Z 28 JAN 1967
GGO CENTERS

FIG. 27

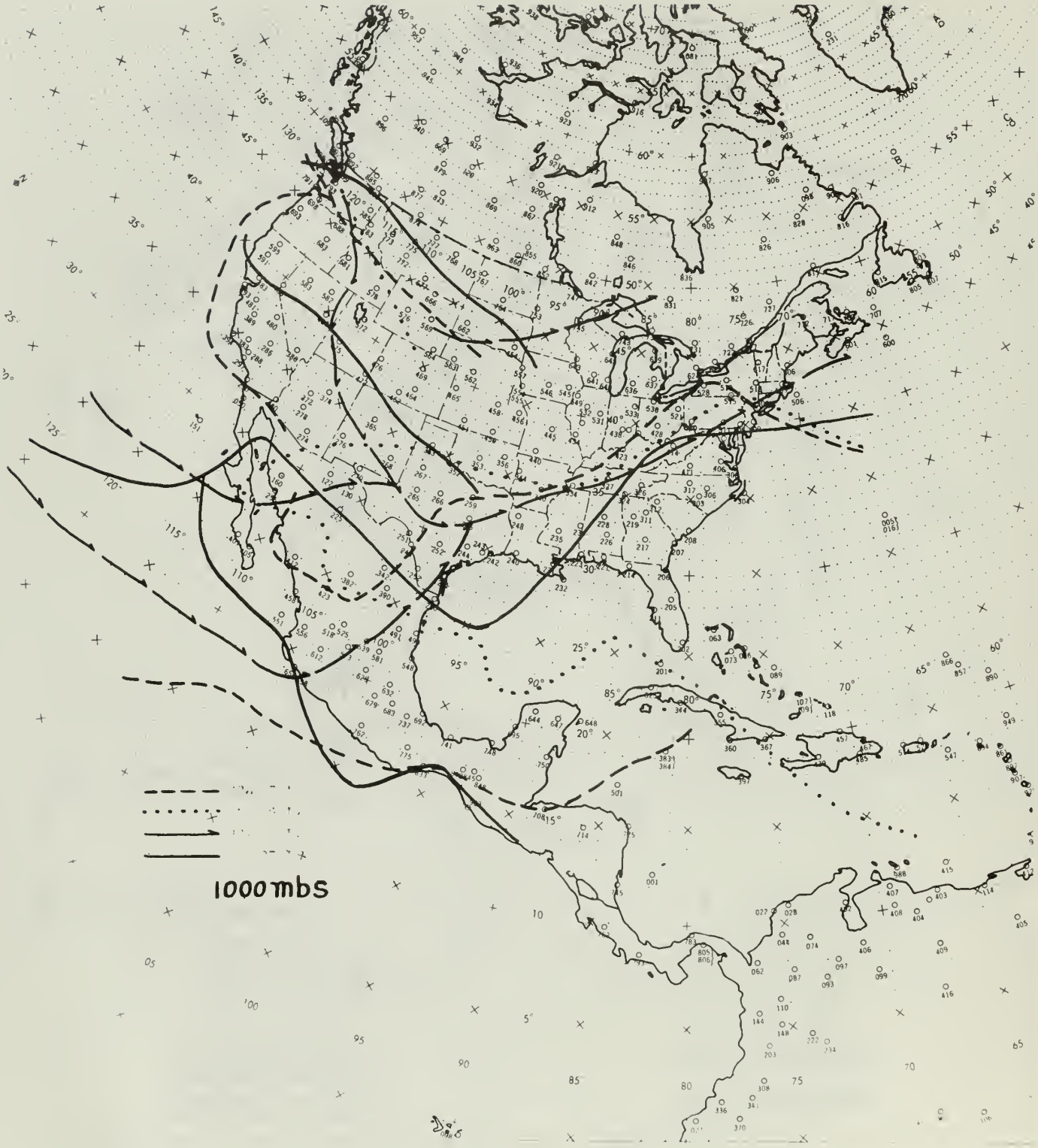

FIG. 28

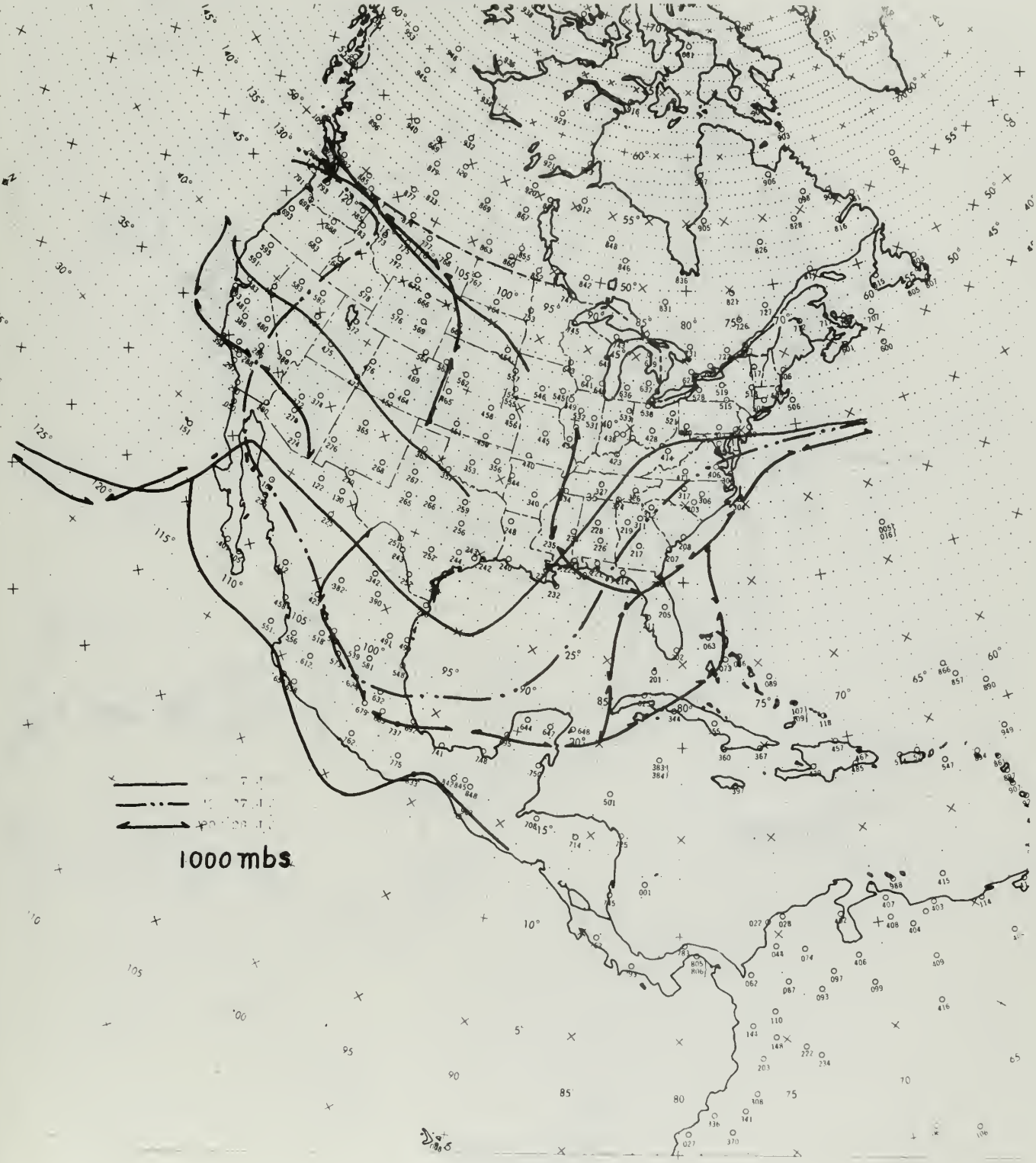

FIG. 29

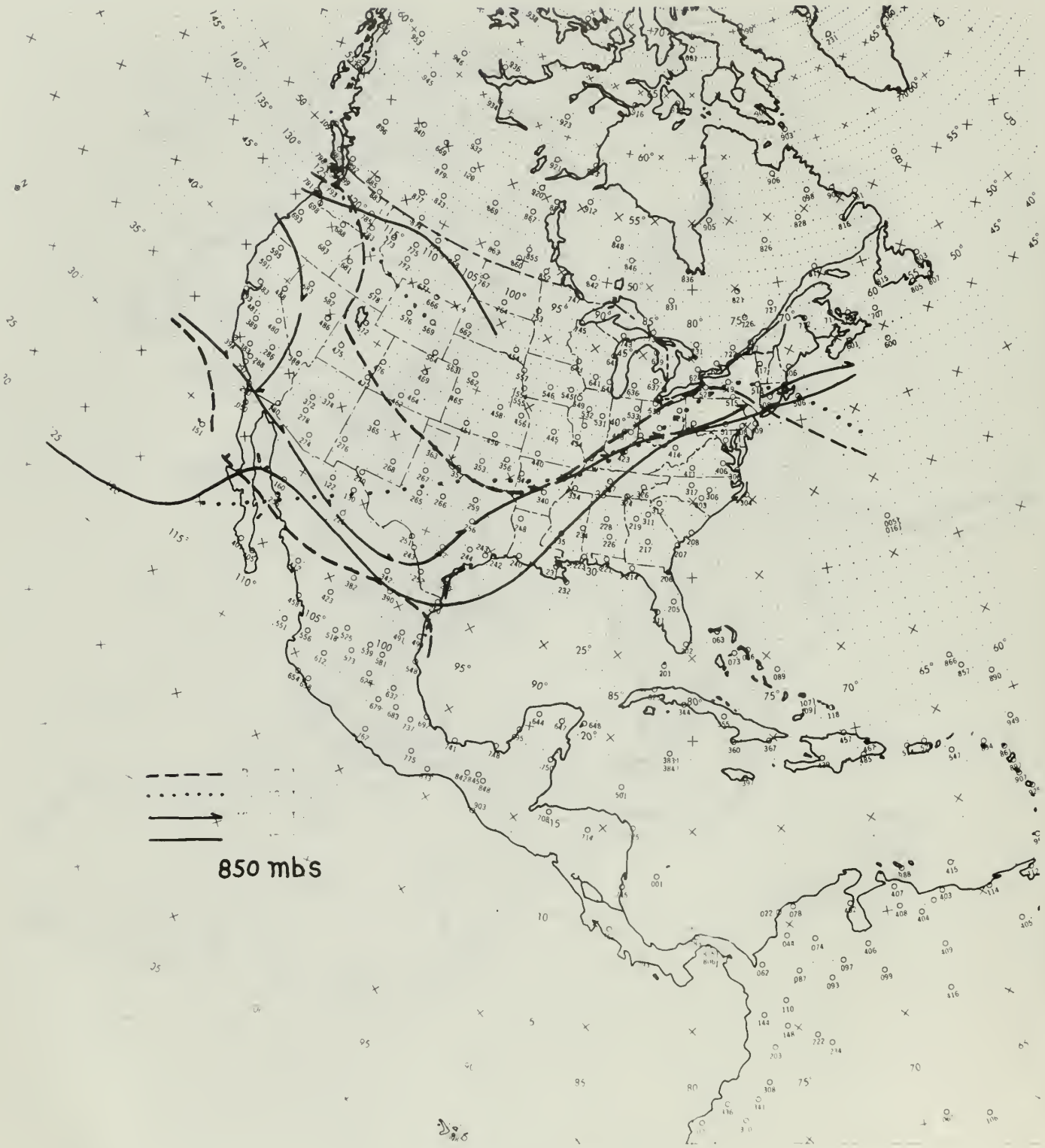

FIG. 30

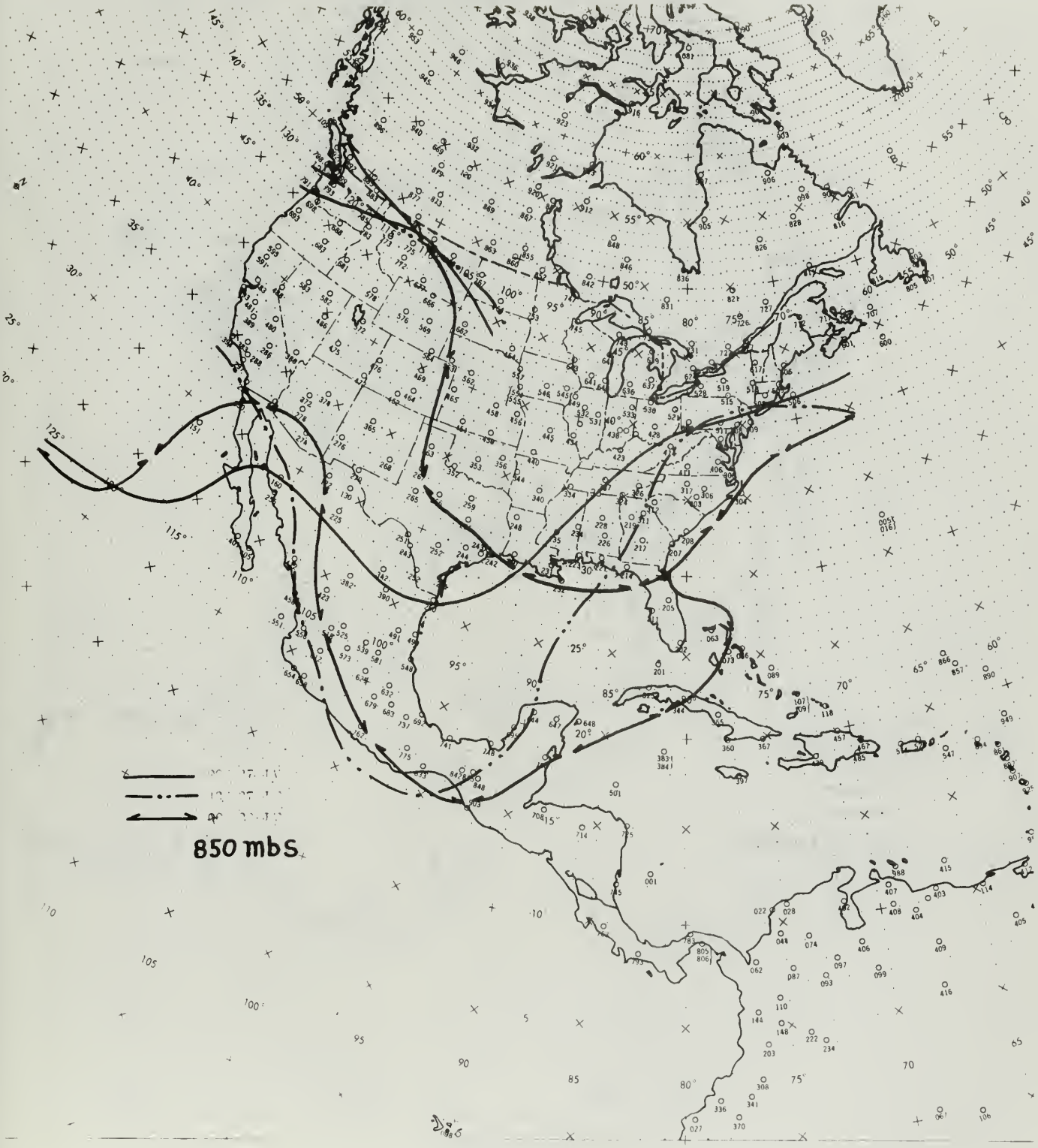

FIG. 31

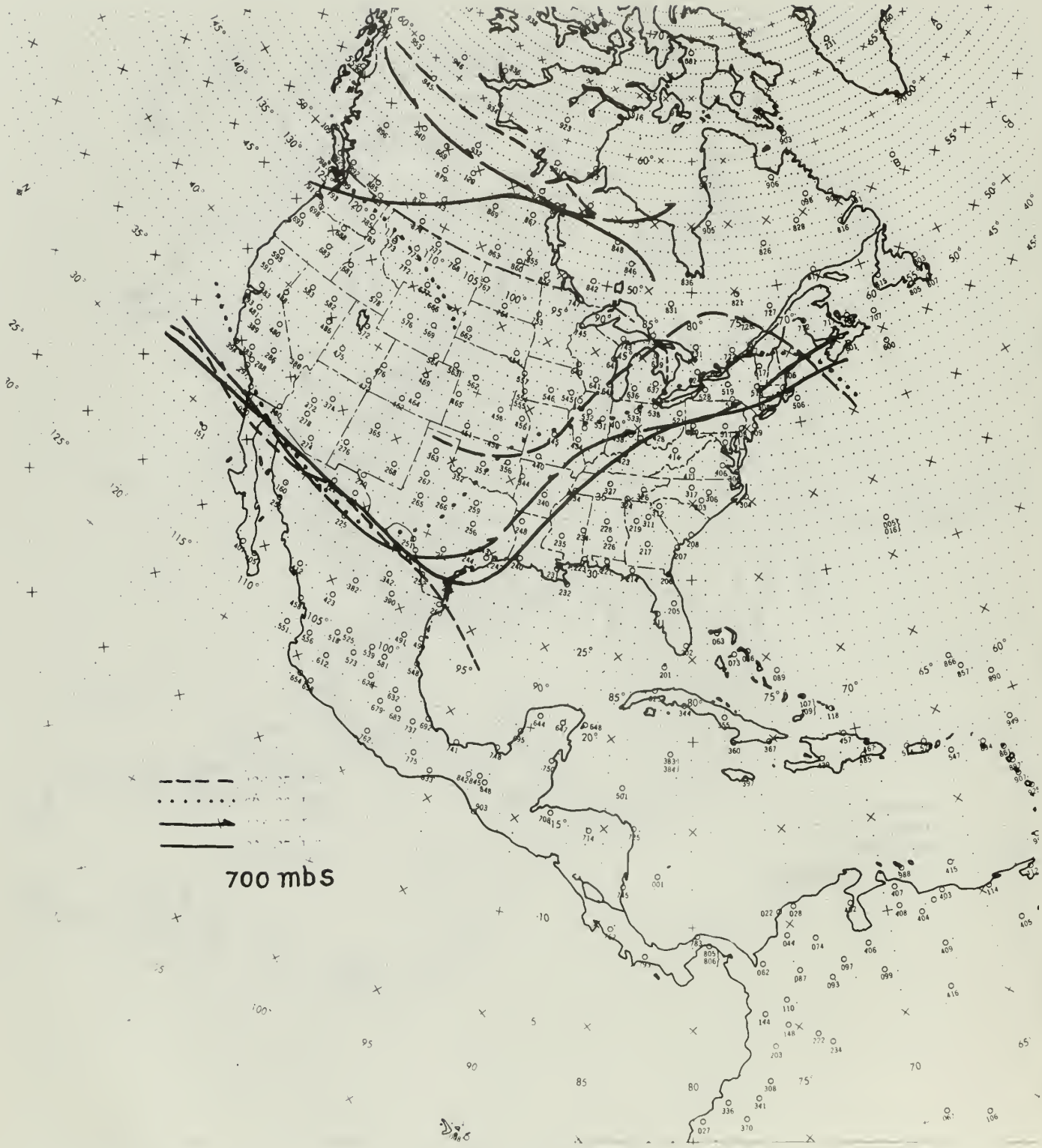

FIG. 32

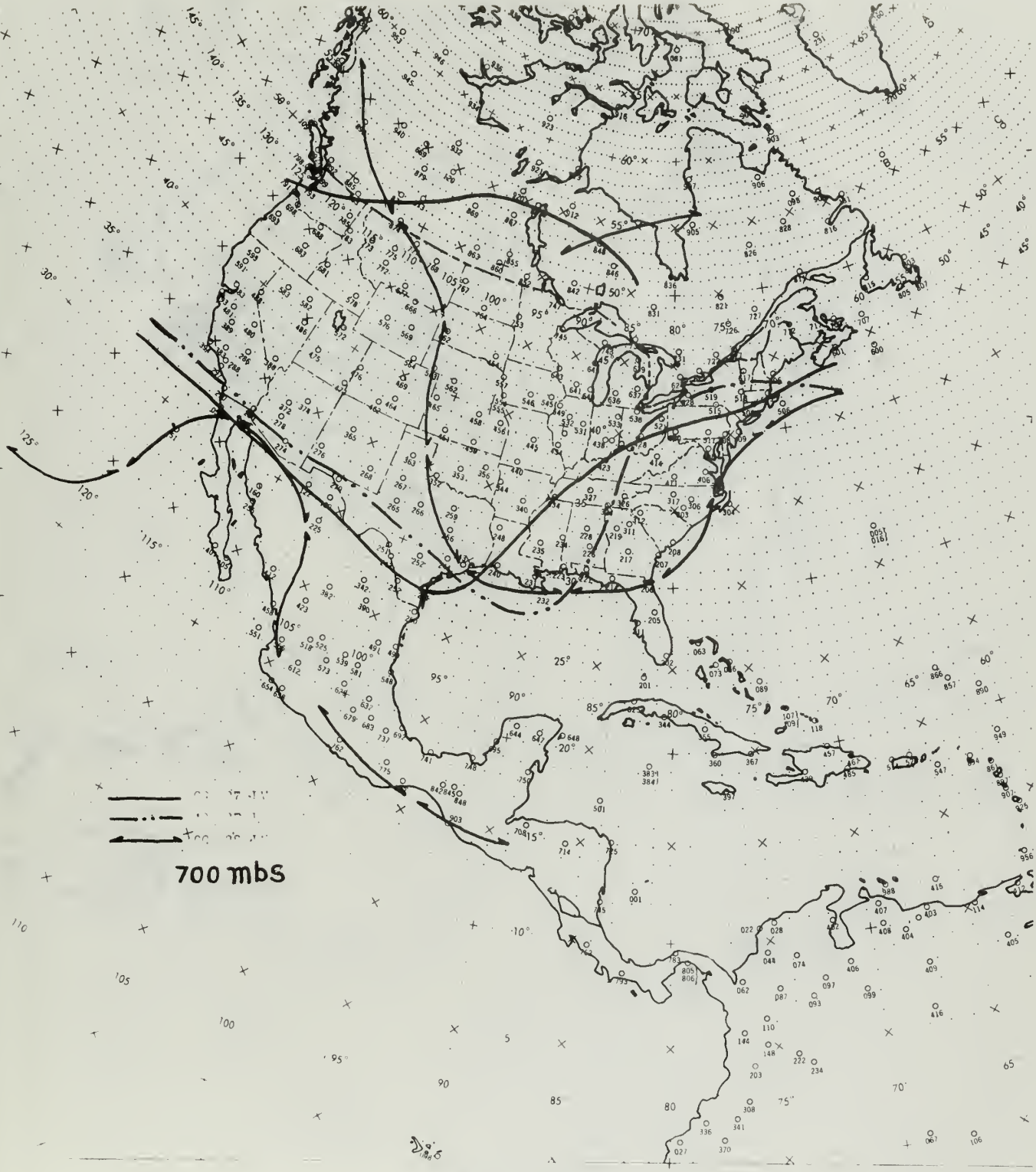

FIG. 33

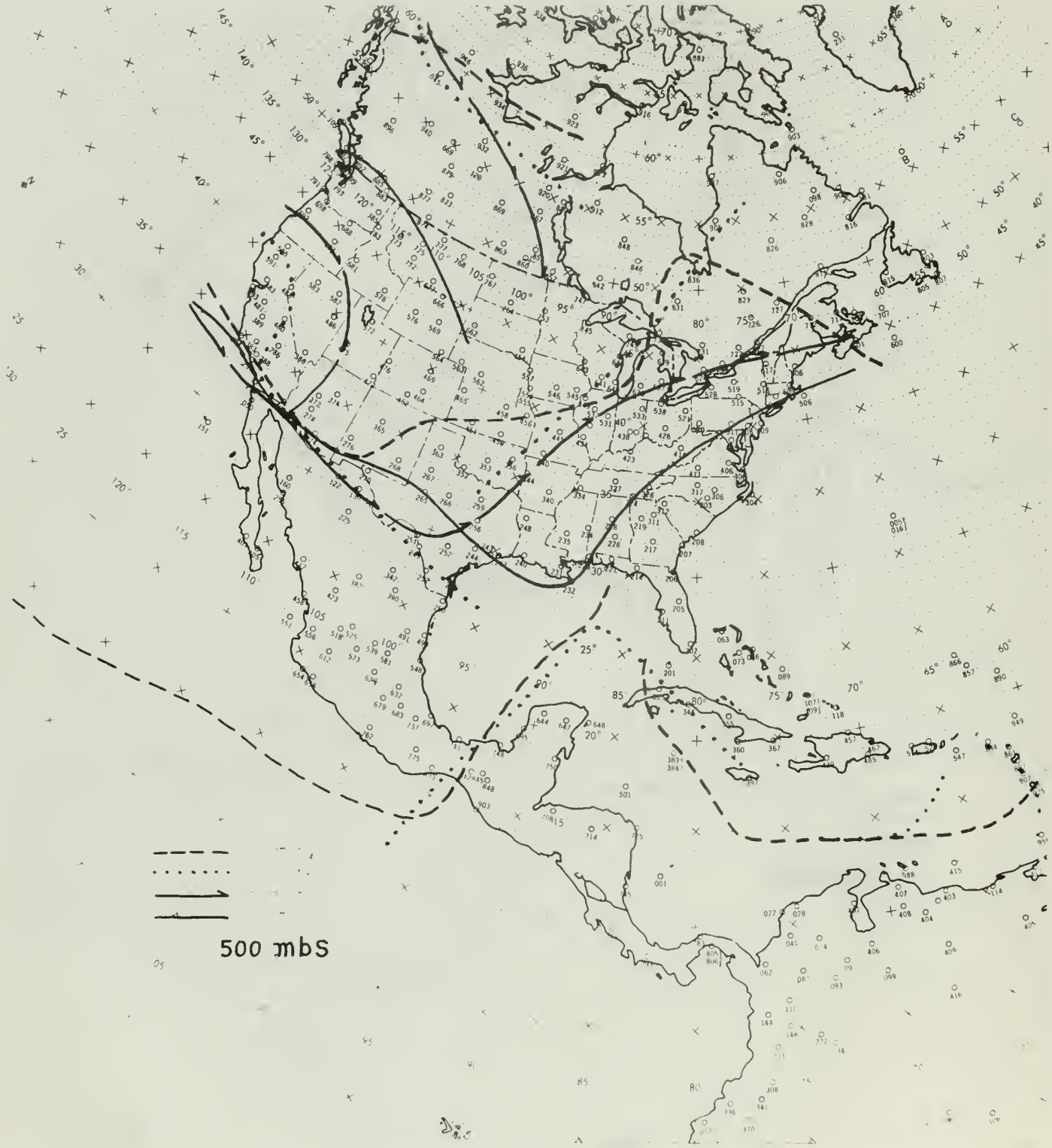

FIG. 34

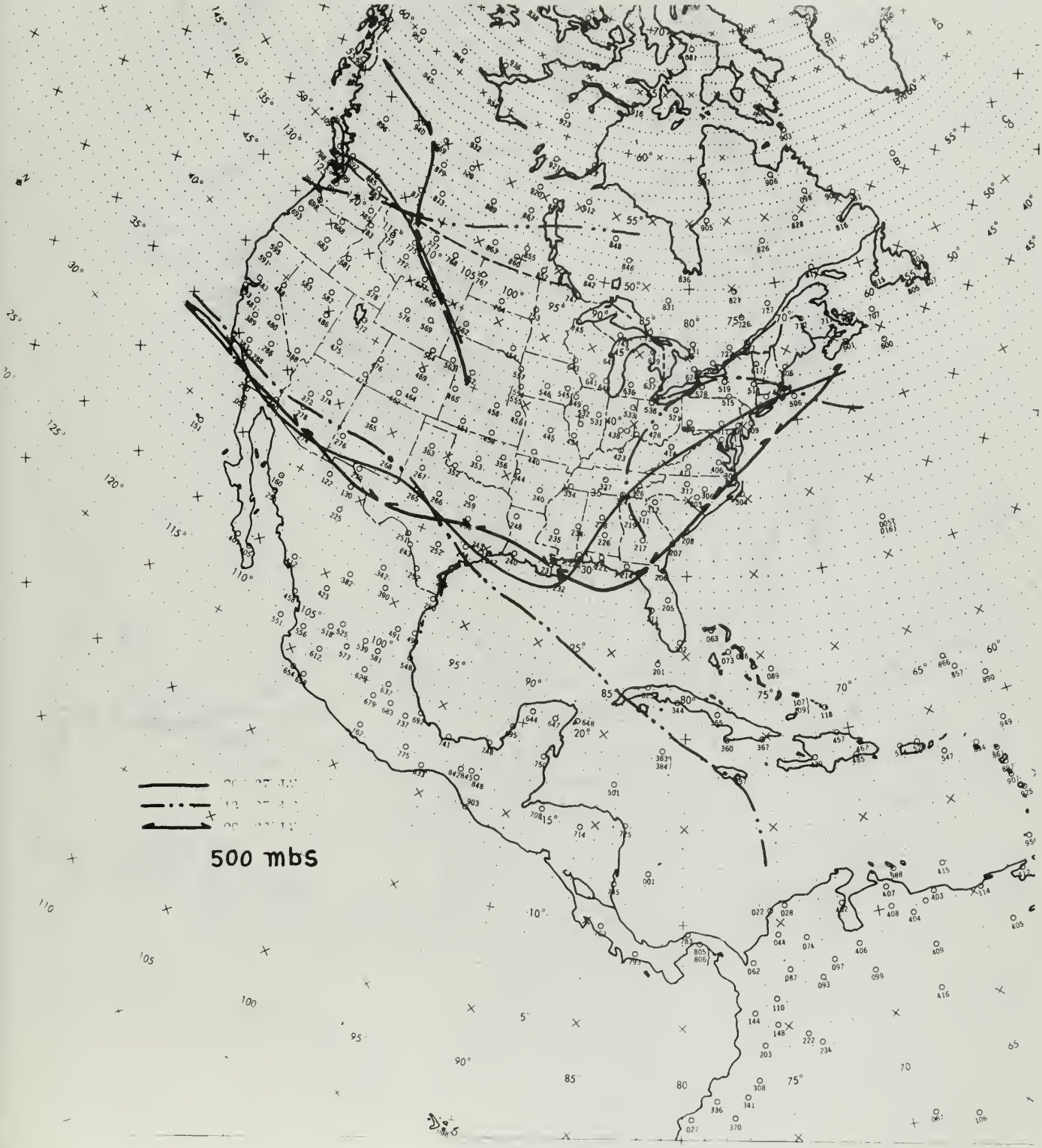

FIG. 35

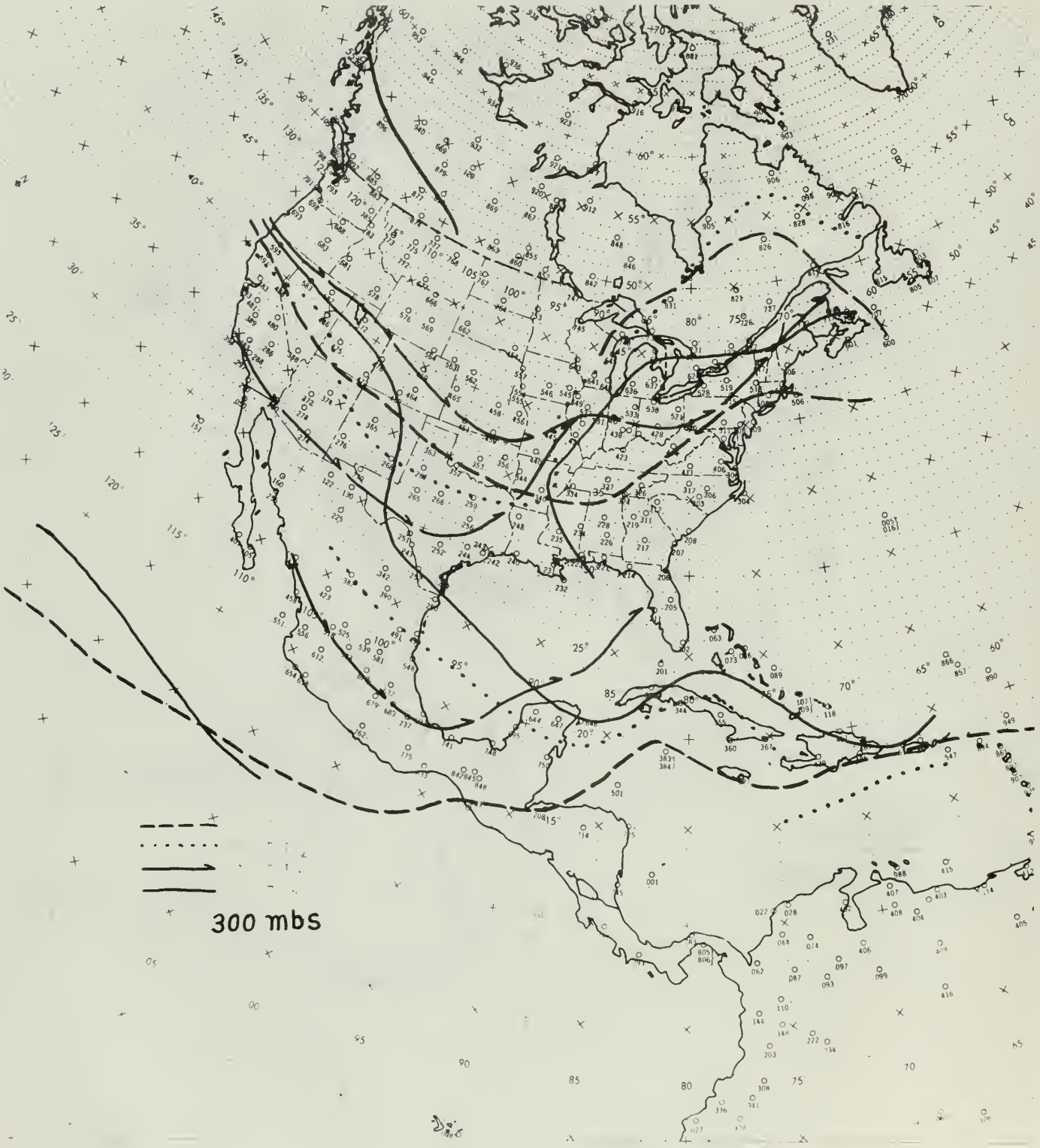

FIG. 36

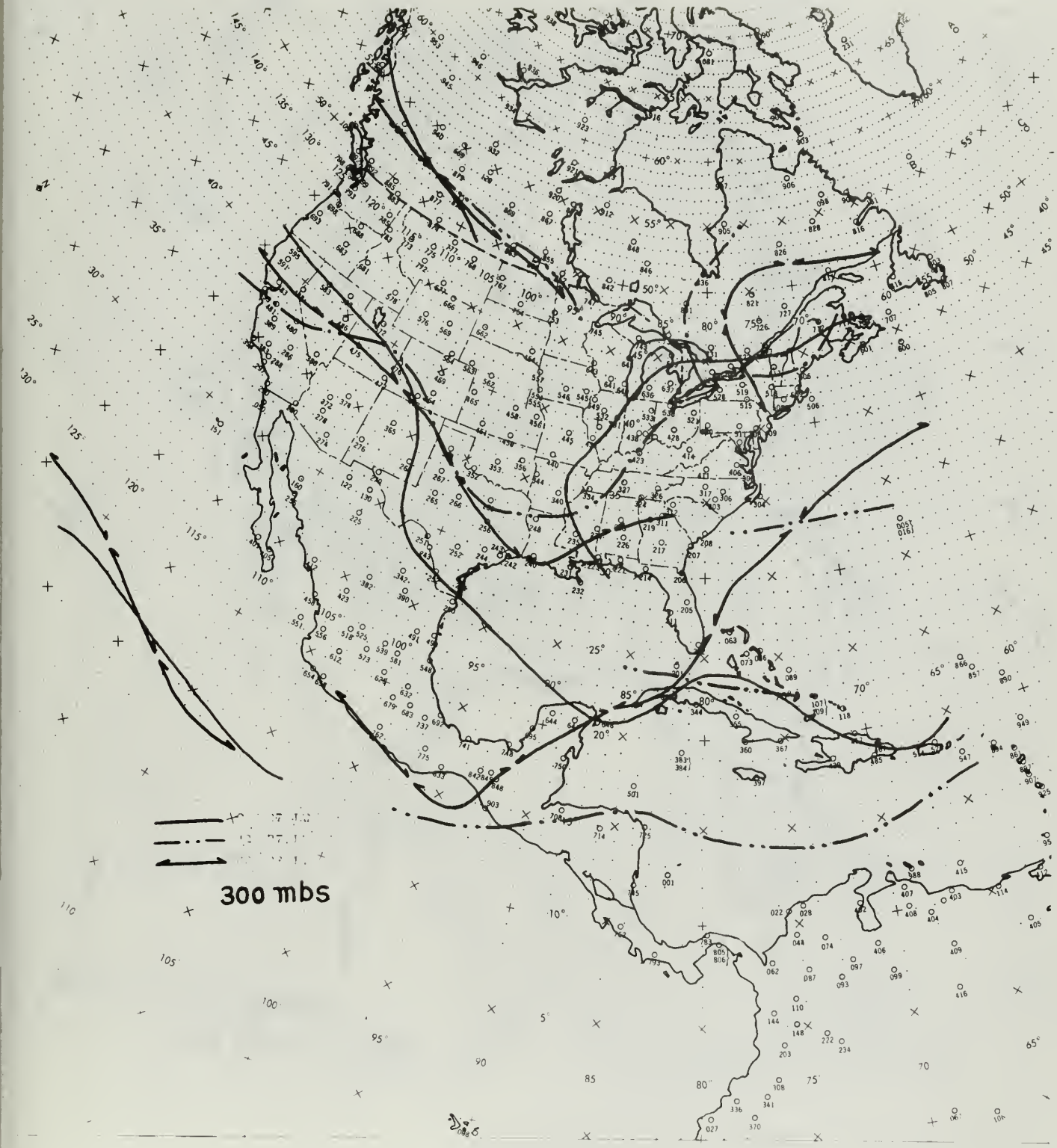

FIG. 37

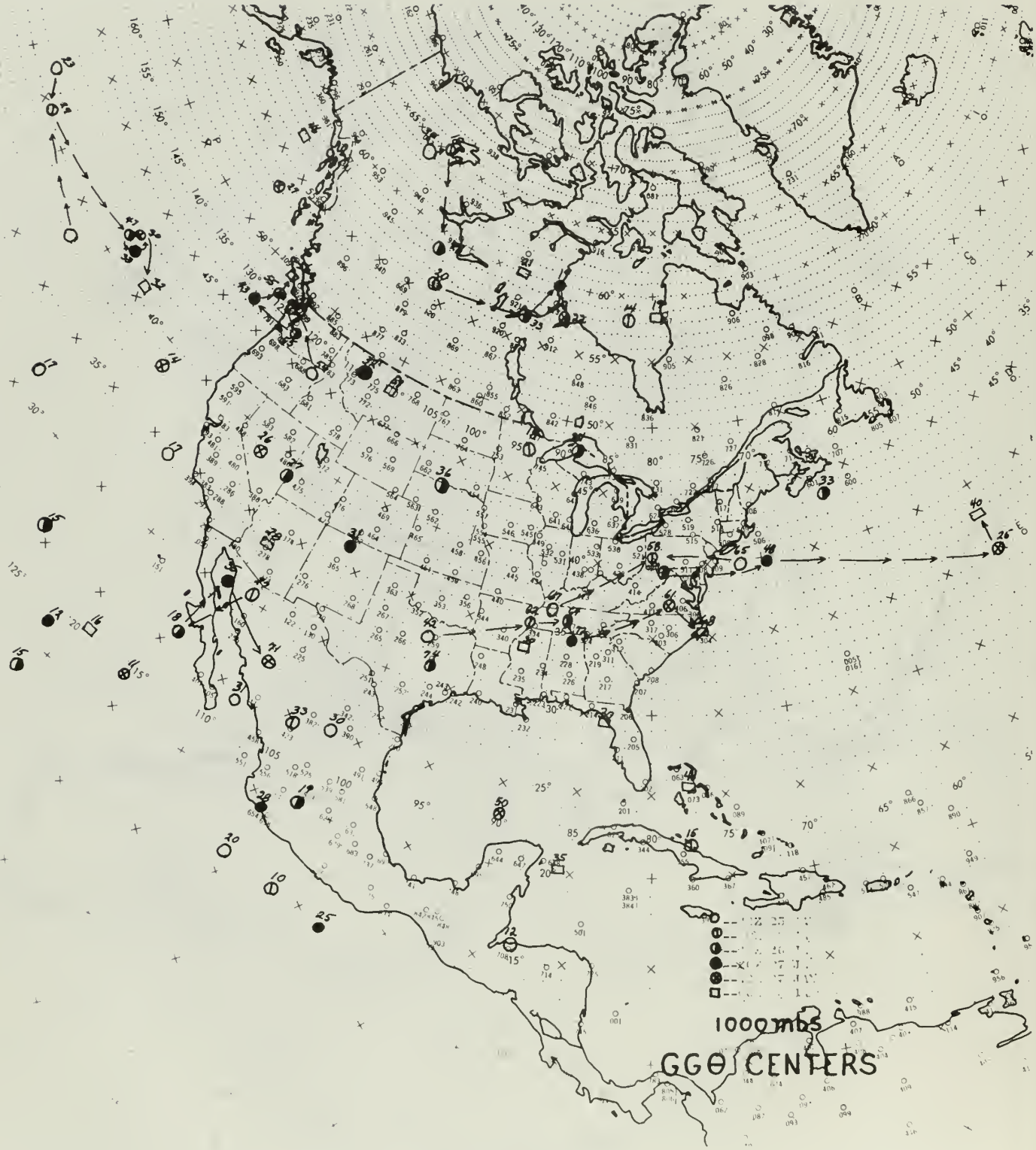

FIG. 38

FIG. 39

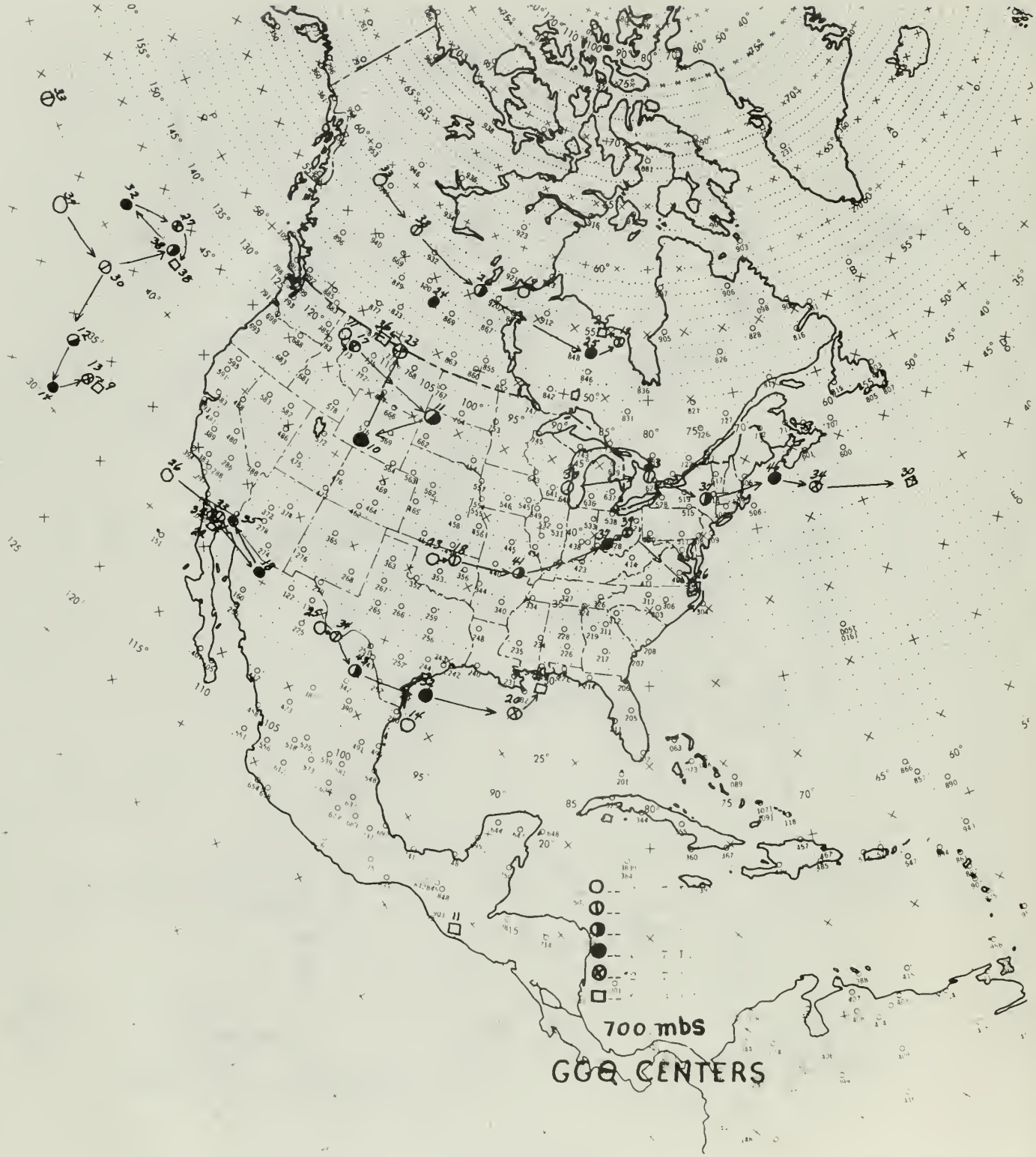

FIG. 40

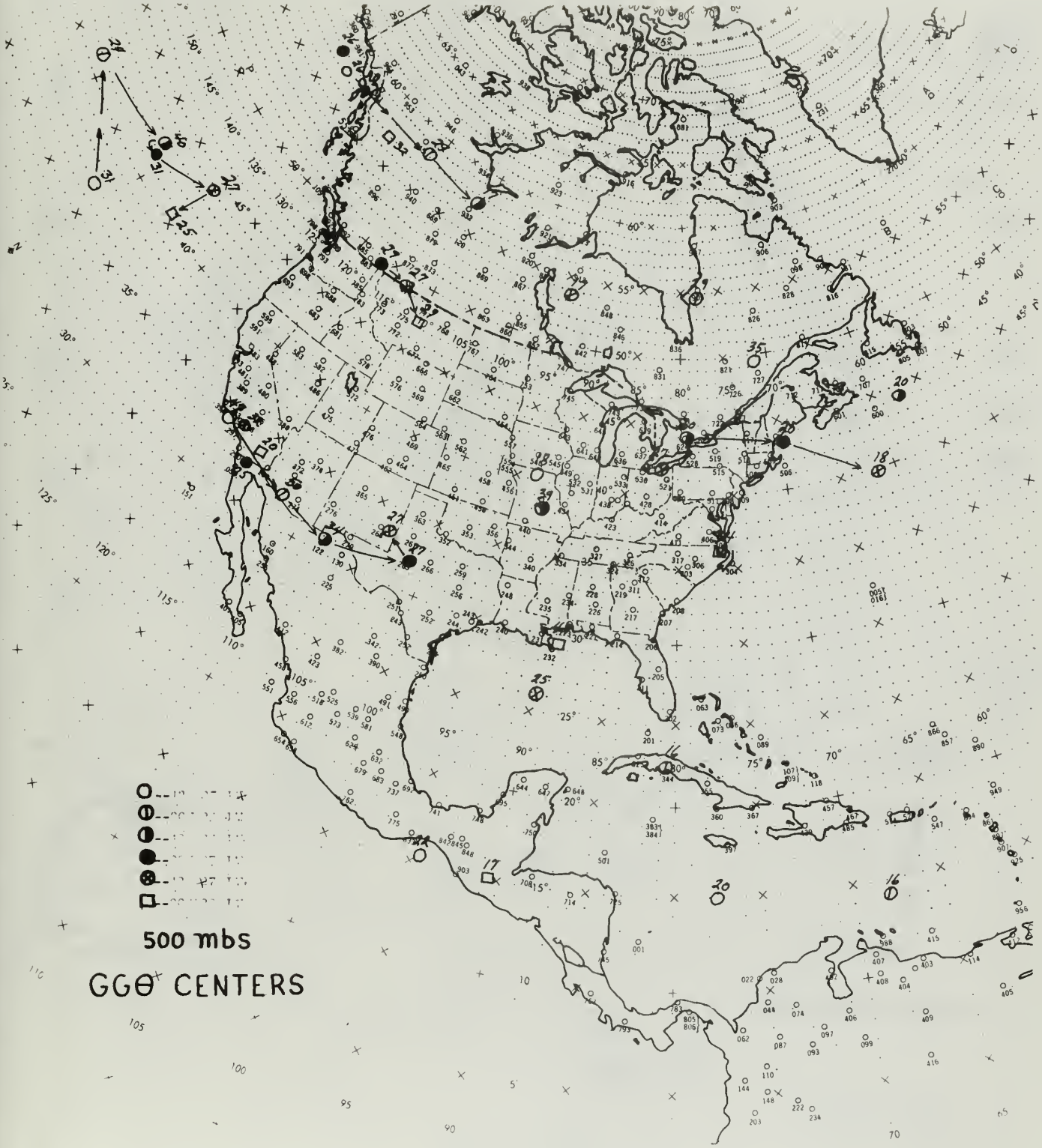

FIG 41

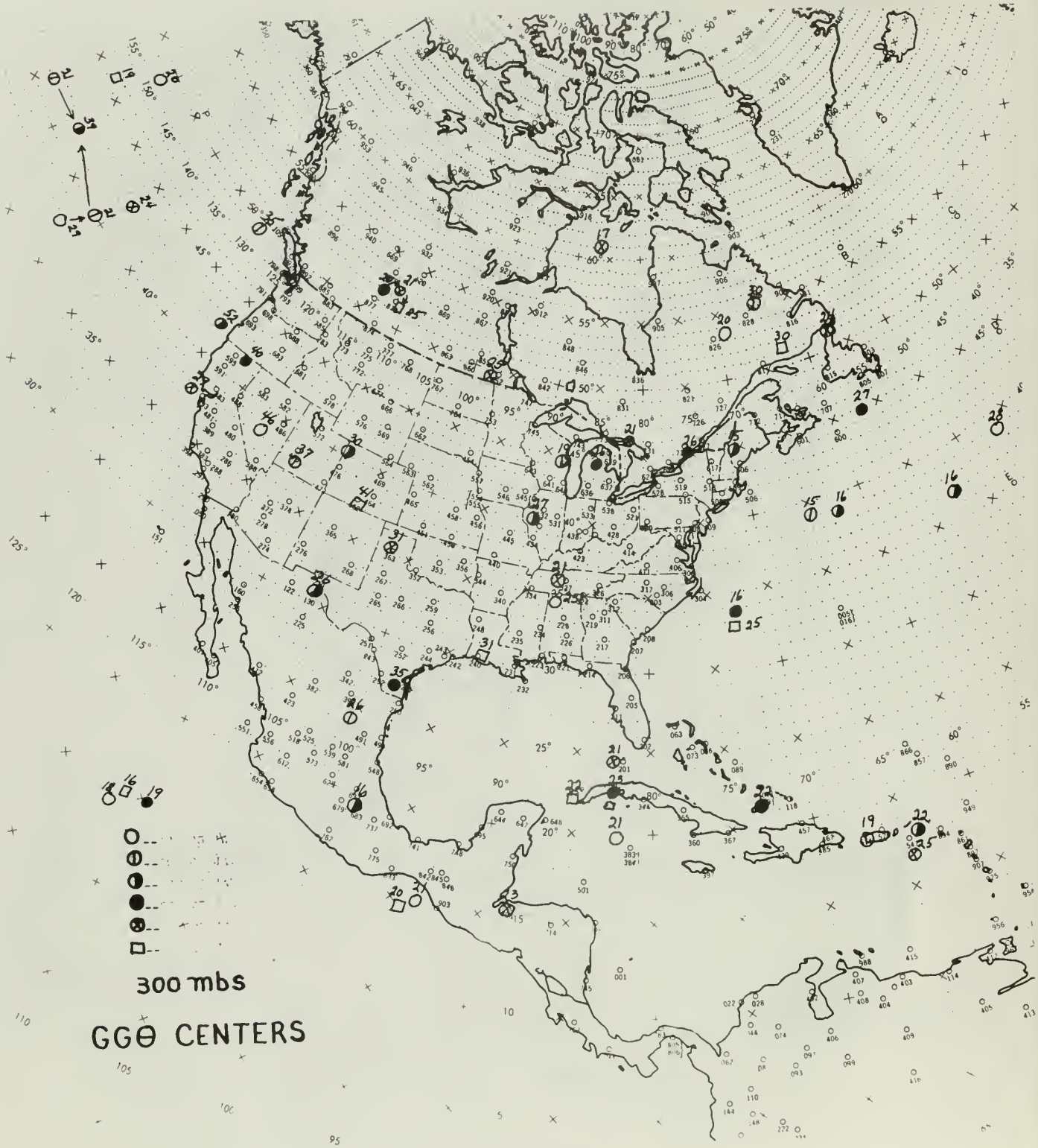

FIG. 42

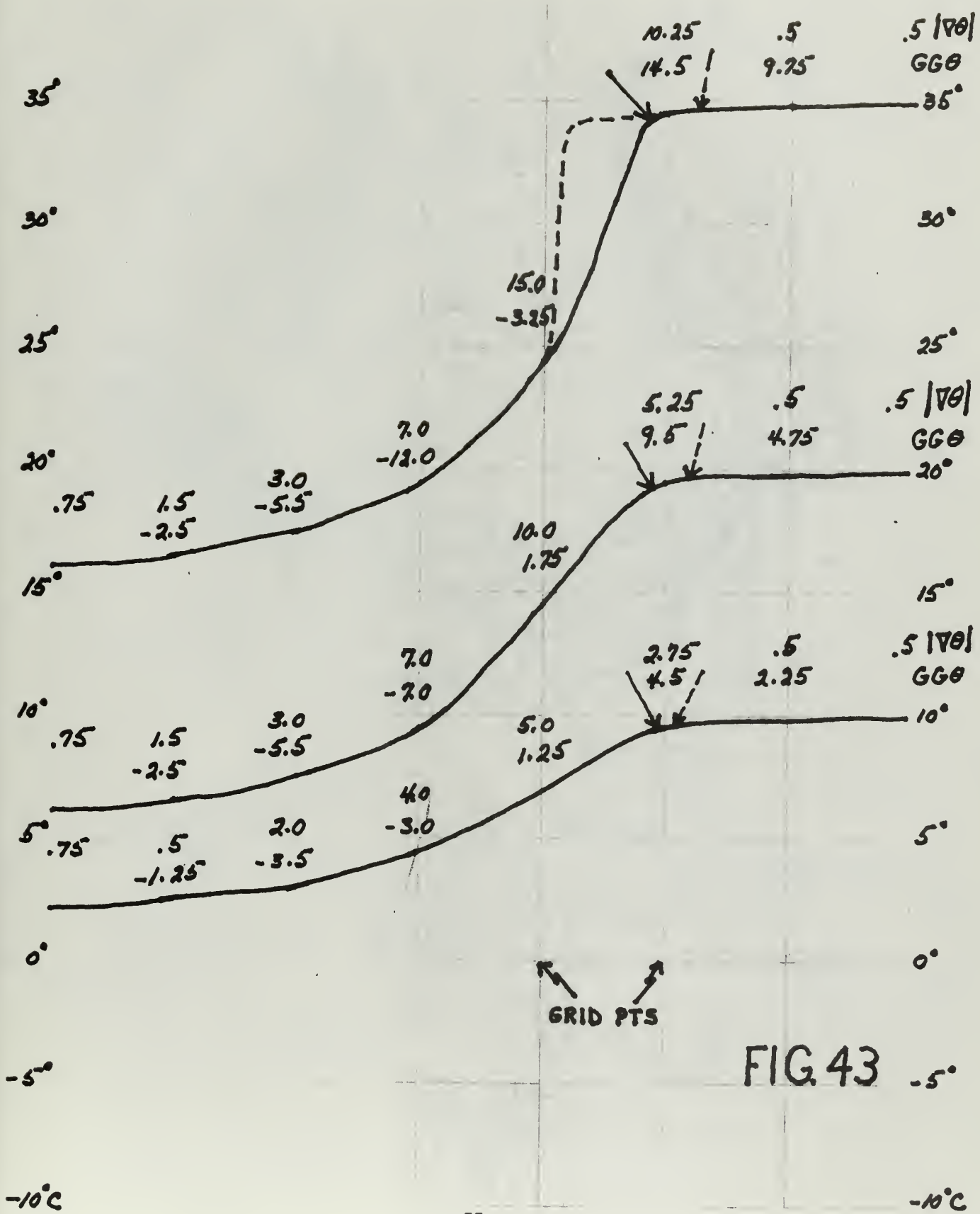
10.25
14.5
.5
9.25
.5 |∇θ|
GGθ
35°
30°
25°
20°
15°
10°
5°
0°
-5°
-10°C
15.0
-3.25
7.0
-12.0
3.0
-5.5
1.5
-2.5
.75
5.25
9.5
.5
4.75
10.0
1.75
7.0
-7.0
5.0
1.25
4.0
-3.0
2.0
-3.5
.5
-1.25
2.75
4.5
.5
2.25
GRID PTS

FIG. 43

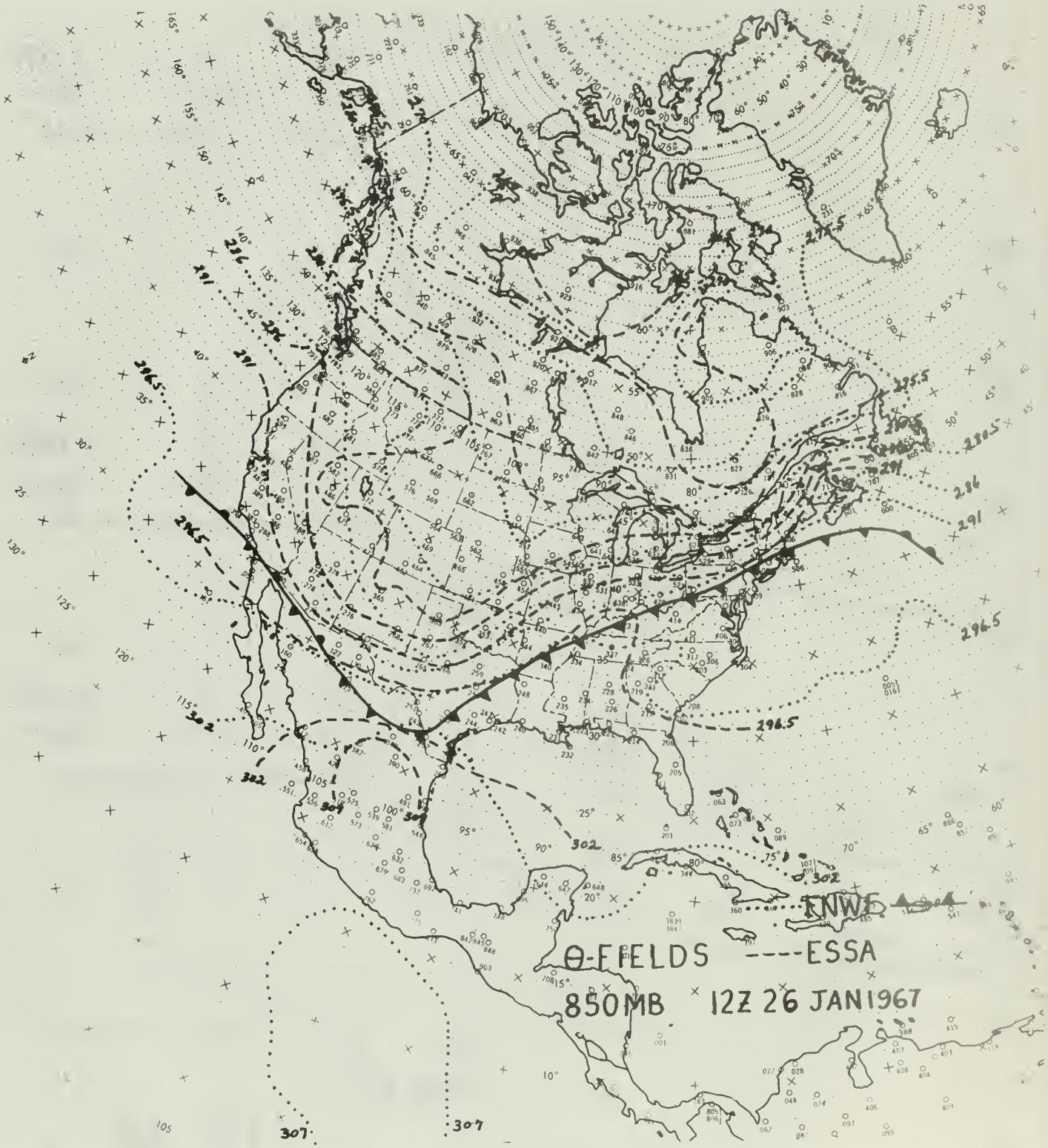

FIG. 44

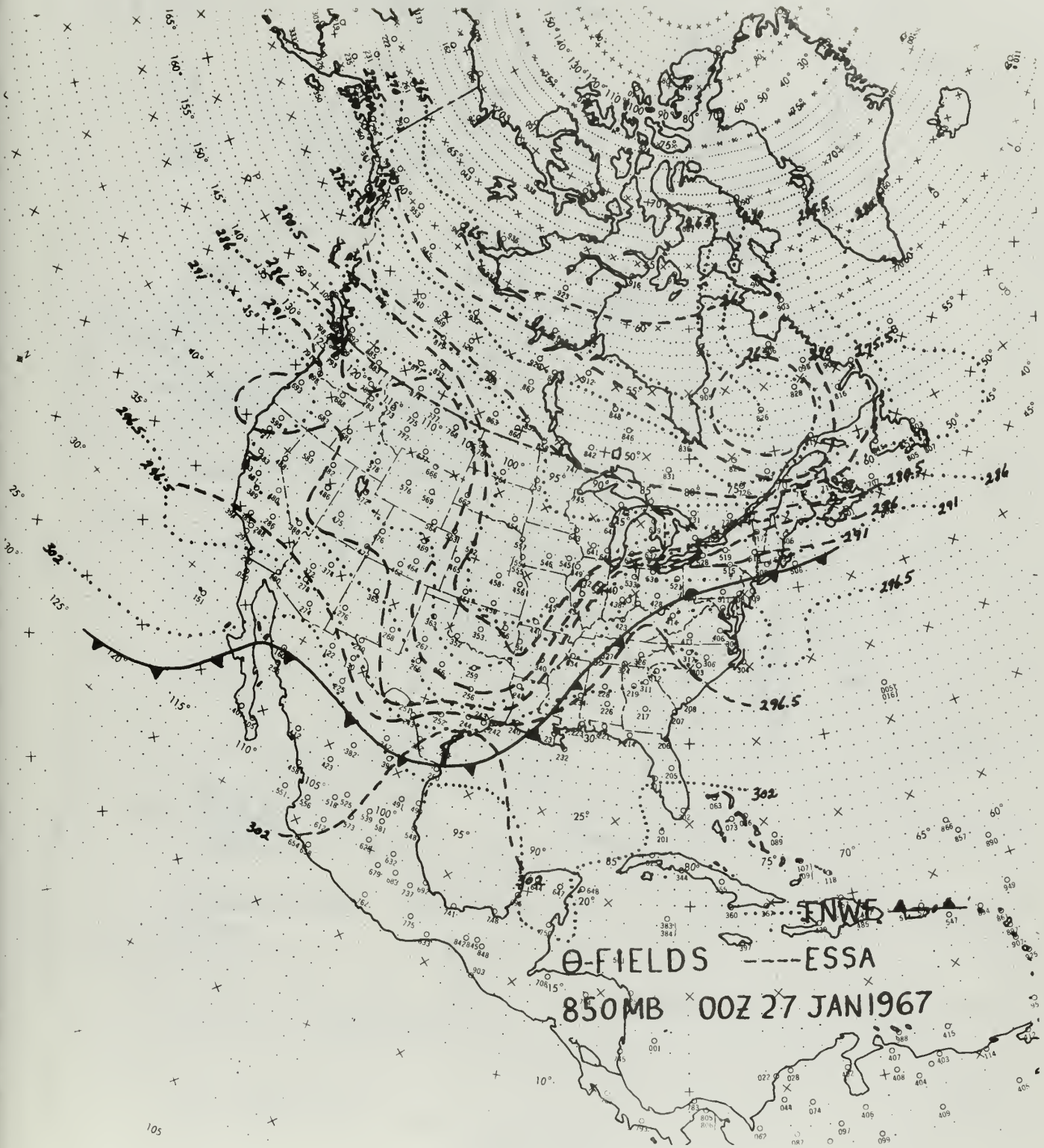

FIG. 45

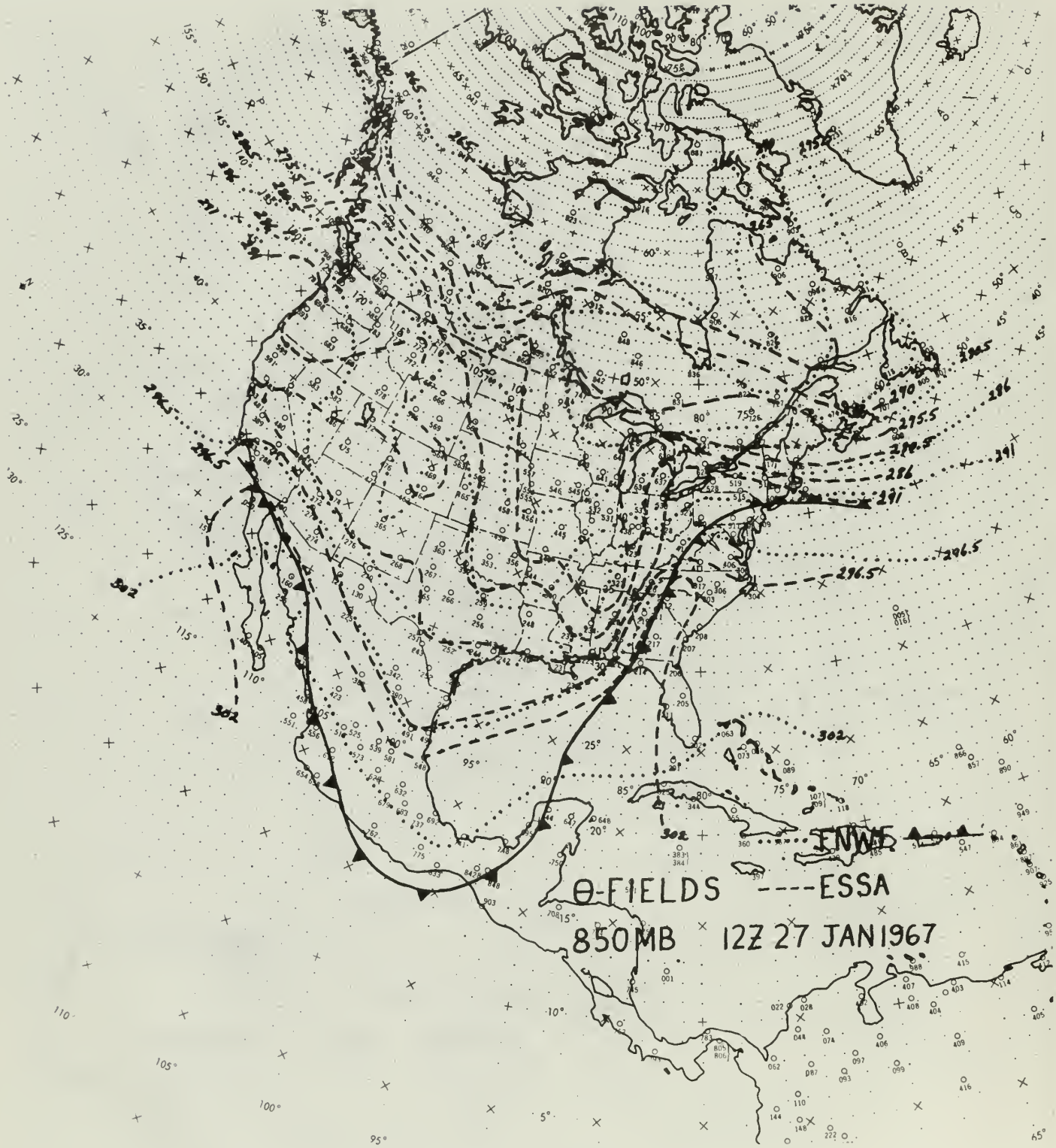
θ-FIELDS ----ESSA
850MB 12Z 27 JAN 1967
ENW
270
275.5
286
291
296.5
302

FIG. 46

INITIAL DISTRIBUTION LIST

		No. Copies
1.	Defense Documentation Center Cameron Station Alexandria, Virginia 22314	20
2.	Library Naval Postgraduate School, Monterey, California	2
3.	Naval Weather Service Command Naval Station (Washington Navy Yard Annex) Washington, D. C. 20390	1
4.	Prof. Robert J. Renard Department of Meteorology & Oceanography Naval Postgraduate School, Monterey, California	10
5.	Department of Meteorology & Oceanography Naval Postgraduate School, Monterey, California	3
6.	LCDR William Carroll Kaag, USN Department of Meteorology & Oceanography Naval Postgraduate School, Monterey, California	2
7.	Officer in Charge, Naval Weather Research Facility Naval Air Station, Building R-48 Norfolk, Virginia 23511	1
8.	Commanding Officer, U. S. Fleet Weather Central Box 12, COMNAVMARIANAS FPO, San Francisco, California 96601	1 (GUAM)
9.	Commanding Officer, U.S. Fleet Weather Central FPO Seattle, Washington 98790	1 (Kodiak)
10.	Commanding Officer, U. S. Fleet Weather Central Box 10 FPO San Francisco, California 96610	1 (Pearl Harbor)
11.	Commanding Officer, U. S. Fleet Weather Central FPO New York, New York 09540	1 (Rota)
12.	Commanding Officer, Fleet Weather Central Navy Department Washington, D. C. 20390	1 (Suitland)
13.	Commanding Officer, Fleet Weather Central Naval Air Station Alameda, California 94501	1

14. Officer in Charge, U. S. Fleet Weather Facility — 1
FPO New York, New York 09597 (Argentia)

15. Officer in Charge, U. S. Fleet Weather Facility — 1
Box 72 (London)
FPO New York, New York 09510

16. Officer in Charge, U. S. Fleet Weather Facility — 1
FPO New York, New York 09571 (Keflavik)

17. Officer in Charge, U. S. Fleet Weather Facility — 1
FPO San Francisco, California 96662 (Yokosuka)

18. Officer in Charge, U. S. Fleet Weather Facility — 1
FPO San Francisco, California 96652 (Sangley Point)

19. Officer in Charge, Fleet Weather Facility — 1
Naval Air Station
San Diego, California 92135

20. Officer in Charge, Fleet Weather Facility — 1
Naval Air Station
Quonset Point, Rhode Island 02819

21. Officer in Charge, Fleet Weather Facility — 1
P. O. Box 85
Naval Air Station
Jacksonville, Florida 32212

22. Officer in Charge, Fleet Numerical Weather Facility — 1
Naval Postgraduate School, Monterey, California 93940

23. Director, Naval Research Laboratory — 1
Attn: Tech. Services Information Officer
Washington, D. C. 20390

24. Commander, Air Weather Service — 2
Military Airlift Command
U. S. Air Force
Scott Air Force Base, Illinois 62226

25. Department of Commerce, ESSA — 2
Weather Bureau
Washington, D. C. 20235

DOCUMENT CONTROL DATA - R&D

(Security classification of title, body of abstract and indexing annotation must be entered when the overall report is classified)

1. ORIGINATING ACTIVITY (Corporate author)	2a. REPORT SECURITY CLASSIFICATION
Naval Postgraduate School Monterey, California	UNCLASSIFIED
	2b. GROUP

3. REPORT TITLE

A CASE STUDY OF THE SPACE AND TIME CONTINUITY OF NUMERICAL FRONTAL ANALYSIS

4. DESCRIPTIVE NOTES *(Type of report and inclusive dates)*

THESIS

5. AUTHOR(S) *(Last name, first name, initial)*

William C. KAAG

6. REPORT DATE	7a. TOTAL NO. OF PAGES	7b. NO. OF REFS
September 1967	83	13

8a. CONTRACT OR GRANT NO.	9a. ORIGINATOR'S REPORT NUMBER(S)
b. PROJECT NO.	
c.	9b. OTHER REPORT NO(S) *(Any other numbers that may be assigned this report)*
d.	

10. AVAILABILITY/LIMITATION NOTICES

Distribution of this document is unlimited.

11. SUPPLEMENTARY NOTES	12. SPONSORING MILITARY ACTIVITY
	NAVAL POSTGRADUATE SCHOOL MONTEREY, CALIFORNIA 93940

13. ABSTRACT

The space and time continuity of numerical fronts as operationally produced by the Fleet Numerical Weather Facility, Monterey, California (FNWF), are investigated at 1000, 850, 700, 500, and 300 mbs for the four-day period January 25-28, 1967. Front locations, intensities, movements and slopes are examined over North America and compared with those from other analysis centers. Vertical structures of baroclinic zones and their changes with time are also investigated. Finally, a study is made of the FNWF computer processed temperature fields compared to manually analyzed temperatures.

Results indicate reasonable vertical consistency of frontal information in the central and eastern United States below the 700-mb level. Time continuity is best maintained at the 700-mb surface. A fictitious displacement of numerical fronts toward the warm air is observed at each of the mandatory pressure levels considered. The temperature fields of FNWF are found to produce smoothing of thermal perturbations associated with open frontal waves while relaxing the thermal gradient which leads to widening and weakening of baroclinic zones.

DD FORM 1 JAN 64 1473

14. KEY WORDS	LINK A		LINK B		LINK C	
	ROLE	WT	ROLE	WT	ROLE	WT
Numerical						
Fronts						
Baroclinic zone						
Analysis						

thesK104
A case study of the space and time conti
3 2768 002 11356 5
DUDLEY KNOX LIBRARY